Aus der Inneren Medizin V, Pneumologie, Allergologie, Beatmungsmedizin-Klinik,
Universitätsklinikum des Saarlandes, Homburg/Saar
Direktor: Prof. Dr. Dr. Robert Bals
der Universität des Saarlandes, Homburg/Saar

Mutual regulation of transcriptomes between alveolar epithelial cells and fibroblasts during alveolar regeneration and pulmonary fibrosis

Dissertation zur Erlangung des Grades eines Doktors der Naturwissenschaften
der Medizinischen Fakultät
der UNIVERSITÄT DES SAARLANDES
2023

vorgelegt von: Yiwen Yao
geb. am: 09.12.1983 in Shanghai, PR China

Tag der Promotion: 10. Apirl 2024

Dekan: Univ.-Prof. Dr. Med. Michael D. Menger

Berichterstatter: Prof. Dr. Bals

Prof. Dr. Krasteva-Christ

Prof. Dr. Taube

To

My Dear Parents

&

Dear Myself

Declaration

I hereby declare that this thesis is my own original work and effort. All experiments, except for those specified, were exclusively performed by me. Except for the publications written by myself listed in the publication list, the data presented here have not been submitted anywhere else for any award. Where other sources of information and help have been used, they have been indicated and acknowledged.

Homburg/Saar,

_____

Yiwen Yao

CONTENTS

SUMMARY

Lung epithelial progenitor/stem cells play an important role in pulmonary homeostasis and regeneration. A disturbed crosstalk between fibroblasts and epithelial cells contributes to the loss of lung structure in chronic lung diseases, such as chronic obstructive pulmonary disease (COPD) and idiopathic pulmonary fibrosis (IPF). It is therefore important to understand how fibroblasts and lung epithelial cells interact with each other during regeneration and disease progression. DKK3, secreted by renal tubular epithelial cells, is closely associated with renal fibrosis. Single-cell data indicate that both airway epithelial cells and (alveolar) fibroblasts express DKK3 in the lungs. However, the role of DKK3 in pulmonary fibrosis is unclear.

The aim of this work was to establish suitable *in vitro* culture models to study the interaction between fibroblasts and pneumocytes in regeneration and pathological states. Additionally, the function of DKK3 in lung regeneration and disease states was investigated using an air liquid interface culture (ALI) model and a mouse model for pulmonary fibrosis.

Alveolar type 2 cells (AT2) derived from human lungs were differentiated in Matrigel to alveolar organoids which showed a grape-like structure consisting of AT2 cells. Co-culturing with fibroblasts isolated from human lung tissue of different donors during the differentiation phase resulted in a secretory, cystic phenotype of the organoids. Single-cell analysis, histology, and qRT-PCR revealed that such cystic organoids show reduced expression of surfactant protein C (*SFTPC*) but increased expression of Mucin 5B (*MUC5B*). There was no expression of the airway epithelial markers keratin 5 (*KRT5*) and secretoglobin family 1A member 1 (*SCGB1A1*). Single-cell transcriptomics further showed that the patient-derived fibroblasts co-cultured with pneumocytes were highly activated as seen in murine lung fibrosis models and in IPF patients. Bleomycin treatment further increased the expression of *MUC5B*, fibrosis markers (e.g. *CTHRC1*, *ACTA2*) and *DKK3* in organoids co-cultured with fibroblasts.

ALI cultures were established with lung epithelial cells and fibroblasts isolated from murine lung tissue. For this purpose, the lung epithelial cells were seeded apically on

the filter membrane and the fibroblasts in the basolateral compartment. Single-cell transcriptomics showed that co-cultivation with fibroblasts led to increased expression of AT2 markers in pneumocytes and club cell populations and trans-differentiation of club cells towards pneumocytes. This maintenance of AT2 cells was likely mediated through activation of regulons, such as the Etv5 regulon. The co-culture with fibroblasts led to an increased transepithelial barrier. Conversely, lung epithelial cells induced increased expression of IL-6 and other differentiation factors (e.g. FGFs) in fibroblasts, mediated by activation of signalling pathways (e.g. JAK-STAT3, NF-κB) and the Cebpb regulon. Stimulation with low concentrations of recombinant IL-6 enhanced epithelial barrier formation and expression of AT2 and club cell markers.

Lung epithelial cells and fibroblasts isolated from *Dkk3* knockout- and wildtype-mice were cultured in the ALI model and 24-well plate, respectively. Single-cell transcriptomics showed that *Dkk3* was expressed in basal cells and fibroblasts. Epithetical cells isolated from *Dkk3*$^{-/-}$ mice developed a significantly reduced transepithelial electrical resistance (TEER). qRT-PCR showed a reduced expression of pneumocyte markers (e.g. *Sftpc*, *Hopx* and *Aqp5*) in *Dkk3*$^{-/-}$ cultures. The single-cell data showed that the proportion of pneumocytes (AT2, AT1 and AT1 immature cells) was higher in WT cultures than in *Dkk3*$^{-/-}$ cultures, while the proportion of airway epithelial cells was increased in knockout cultures. qRT-PCR results showed a decreased expression of *Sftpc* and increased expression of type 1 markers (e.g. *Hopx, Aqp5*) in wildtype epithelial cells after 4 days of ALI culture, whereas there was no increase in type 1 markers in knockout epithelial cells after 4 days of ALI culture. DKK3-expressing cells were significantly more abundant in fibrotic lesions of IPF patient and in mice with bleomycin-induced pulmonary fibrosis. The lung damage induced by bleomycin was dramatically decreased in *Dkk3* knockout mice, as shown by invasive lung function and fibrosis scores.

This work shows that overly activated fibroblasts induce aberrant differentiation of alveolar organoids, as observed in chronic lung disease. Alveolar AT2-derived organoids transdifferentiate into MUC5B+ secretory AT2 cells, which have been

described in honeycomb structures in IPF. The obtained results suggest that the interaction between fibroblasts and AT2 cells leads to a vicious cycle in IPF progression. The model can be used to further elucidate the interaction between fibroblasts and AT2 cells in IPF and for drug development. In the ALI co-culture model, regulatory loops were identified that mediate regeneration and differentiation of the alveolar epithelium in a cooperative manner with the mesenchymal compartment. DKK3 expressed by epithelial cells or fibroblasts may have a regulatory role in the differentiation of AT2 cells to AT1 cells during lung regeneration. DKK3 has been shown to have a role in promoting lung fibrosis in the bleomycin-dependent mouse model. Thus, the above results suggest that the interaction between alveolar epithelial cells and fibroblasts is important for regeneration and disease progression.

ZUSAMMENFASSUNG

Progenitor-/Stammzellen des Lungenepithels spielen eine wichtige Rolle bei der Homöostase und Regeneration der Lunge. Eine gestörte Wechselwirkung zwischen Fibroblasten und Epithelzellen trägt zum Verlust der Lungenstruktur bei chronischen Lungenerkrankungen wie der chronisch obstruktiven Lungenerkrankung (COPD) und der idiopathischen Lungenfibrose (IPF) bei. Daher ist es wichtig zu verstehen, auf welche Weise Fibroblasten und Lungenepithelzellen bei der Regeneration der Lunge und Krankheitsverläufen miteinander interagieren. DKK3, das von renalen Tubulusepithelzellen sezerniert wird, ist eng mit der Nierenfibrose verbunden. Einzelzelldaten deuten darauf hin, dass sowohl Epithelzellen der Atemwege als auch (alveoläre) Fibroblastenzellen in der Lunge DKK3 exprimieren. Die Rolle von DKK3 bei der Lungenfibrose ist jedoch unklar.

Ziel dieser Arbeit war es, geeignete *in-vitro*-Kulturmodelle zu etablieren, um die Interaktion zwischen Fibroblasten und Pneumozyten bei der Regeneration der Lunge und bei pathologischen Zuständen zu untersuchen. Darüber hinaus wurde die Funktion von DKK3 bei der Lungenregeneration und Krankheitszuständen mithilfe von Air Liquid Interface (ALI)-Kulturen und murinen Lungenfibrose-Modellen untersucht.

Aus menschlichen Lungen stammende alveoläre Typ-2-Zellen (AT2) wurden in Matrigel zu alveolären Organoiden differenziert, die eine traubenartige Struktur aufwiesen. Während der Differenzierungsphase führte die Co-Kultur mit Fibroblasten, die aus menschlichem Lungengewebe verschiedener Spender isoliert wurden, zu einem sekretorischen, zystischen Phänotyp der Organoide. Einzelzellanalyse, Histologie und qRT-PCR ergaben, dass solche zystischen Organoide eine verminderte Expression des Surfactant-Proteins C (*SFTPC*), aber eine erhöhte Expression von Mucin 5B (*MUC5B*) aufwiesen. Es zeigte sich keine Expression für Maker von Atemwegsepithelzellen wie Keratin 5 (KRT5) und Sekretoglobin Familie 1A Mitglied 1(SCGB1A1). Einzelzell-Analysen zeigten außerdem, dass die von Patienten stammenden Fibroblasten, die zusammen mit Pneumozyten kultiviert wurden, stark aktiviert waren, wie es auch in murinen Lungenfibrosemodellen und bei IPF-Patienten der Fall ist. Die

Behandlung mit Bleomycin erhöhte die Expression von *MUC5B*, Fibrosemarkern (z. B. *CTHRC1*, *ACTA2*) und DKK3 in Organoiden, die mit Fibroblasten kultiviert wurden. ALI-Kulturen wurden mit aus murinem Lungengewebe isolierten Lungenepithelzellen und Fibroblasten angelegt. Hierfür wurden die Lungenepithelzellen apikal auf der Filtermembran und die Fibroblasten im basolateralem Kompartiment ausgesät. Einzelzell-Analysen zeigten, dass die gemeinsame Kultivierung mit Fibroblasten zu einer erhöhten Expression von AT2-Markern in Pneumozyten und Keulenzellpopulationen sowie zur Transdifferenzierung von Keulenzellen in Richtung Pneumozyten führte. Diese Aufrechterhaltung der AT2-Zellen wurde wahrscheinlich durch die Aktivierung von Regulons wie dem Evt5-Regulon vermittelt. Die Ko-Kultur mit Fibroblasten führte zu einer verstärkten transepithelialen Barriere. Umgekehrt induzierten Lungenepithelzellen eine erhöhte Expression von IL-6 und anderen Differenzierungsfaktoren (z. B. FGFs) in Fibroblasten, was durch die Aktivierung von Signalwegen (z.B. JAK-STAT3, NF-κB) und dem Cebpb-Regulon vermittelt wurde. Die Stimulation mit niedrigen Konzentrationen von rekombinantem IL-6 verstärkte die Bildung der epithelialen Barriere und die Expression von AT2- und Keulenzellmarkern. Lungenepithelzellen und Fibroblasten, aus *Dkk3*-Knockout- und Wildtyp-Mäusen isoliert, wurden im ALI-Modell bzw. in 24-Well-Platten kultiviert. Einzelzell-Analysen zeigten, dass *Dkk3* in Basalzellen und Fibroblasten exprimiert wurde. Epitheliale Lungenzellen, die aus *Dkk3*$^{-/-}$ Mäusen isoliert wurden, entwickelten einen signifikant reduzierten transepithelialen Widerstand. qRT-PCR-Analysen zeigten eine reduzierte Expression von Pneumozytenmarkern (z.B. *Sftpc*, *Hopx* und *Aqp5*) in *Dkk3*$^{-/-}$ Kulturen. Einzelzell-Anaylsen zeigten, dass der Anteil der Pneumozyten (AT2, AT1 und AT1 unreife Zellen) in WT-Kulturen höher war als in *Dkk3*$^{-/-}$-Kulturen, während der Anteil der Epithelzellen der Atemwege in den Knockout-Kulturen erhöht war. Die qRT-PCR-Ergebnisse zeigten eine verringerte Expression von Sftpc und eine erhöhte Expression von Typ-1-Markern (z. B. *Hopx*, *Aqp5*) in Wildtyp-Epithelzellen nach 4 Tagen ALI-Kultur, während es in Knockout-Epithelzellen nach 4 Tagen ALI-Kultur keinen Anstieg der Typ-1-Marker gab. DKK3-exprimierende Zellen waren in fibrotischen

Läsionen von IPF-Patienten und in Mäusen mit Bleomycin-induzierter Lungenfibrose signifikant erhöht. Die Bleomycin-induzierte Lungenschädigung war bei *Dkk3*-Knockout-Mäusen drastisch reduziert, was durch invasive Lungenfunktion und Fibrose-Scores belegt wurde.

Die vorliegende Arbeit zeigt, dass aktivierte Fibroblasten eine pathologische Differenzierung von alveolären Organoiden hervorruft, wie sie bei chronischen Lungenerkrankungen beobachtet wird. Die alveolären AT2-abgeleiteten Organoide transdifferenzieren zu MUC5B+ sekretorische AT2-Zellen, wie sie für honeycomb Strukturen bei IPF beschrieben wurden. Die erzielten Ergebnisse deuten darauf hin, dass die Interaktion von Fibroblasten mit AT2-Zellen zu einem Teufelskreis in der IPF-Progression führt. Das Modell kann zur weiteren Aufklärung der Interaktion zwischen Fibroblasten und AT2-Zellen bei IPF und zur Entwicklung von Medikamenten verwendet werden. Im ALI-Kokulturmodell wurden Regelkreise identifiziert, die die Regeneration und Differenzierung des Alveolarepithels in Zusammenspiel mit dem mesenchymalen Kompartiment vermitteln. DKK3, das von Epithelzellen oder Fibroblasten exprimiert wird, könnte eine regulierende Rolle bei der Differenzierung von AT2-Zellen zu AT1-Zellen bei der Lungenregeneration spielen. Es hat sich gezeigt, dass DKK3 eine Rolle bei der Förderung der Lungenfibrose im Bleomycin-abhängigen Mausmodell spielt. Diese Ergebnisse legen daher nahe, dass die Interaktion zwischen Alveolarepithelzellen und Fibroblasten für die Regeneration und das Fortschreiten der Krankheit wichtig ist.

1. INTRODUTION

1.1 The anatomical organization of the lung in humans and mice

The lung is a highly complex and dynamic organ. Its main function is to oxygenate the blood and remove carbon dioxide. Mice share many anatomical, histological, and developmental similarities with humans, making them suitably for studying human lung development, function, and disease. However, it is worth noting that these two species still have difference in their structural organization, cellular composition, and connective tissue composition in the lung. In humans, there are multiple intrapulmonary segmental bronchi with cartilaginous and submucosal glands; in mice, however, cartilaginous airways end in lobar bronchi and the lungs are not subdivided into smaller units, which different from humans (Hislop, Wigglesworth, and Desai 1986; Pan et al. 2019) (Fig. 1 A and B).

Based on anatomical and functional features, the lung can be further divided into three epithelial domains with distinct composition of epithelial cell types: the proximal cartilaginous airway (trachea and bronchi), distal bronchioles (bronchioles, terminal bronchioles, and respiratory bronchioles), and gas exchanging airspaces (alveoli). Segmental bronchi in the human lung exhibit an irregular, bifurcated branching pattern, with approximately 16-23 generations of branching from the trachea to the gas exchange region of the lung (Bucher and Reid 1961; Weibel and Gomez 1962). Terminal bronchioles represent the most distal components of the conducting tract. The characteristic human respiratory bronchioles branch from terminal bronchioles for 2 to 3 generations. In mice, airway branching gives rise to ~ 13–17 generations of airways (Irvin and Bates 2003). In contrast, mice do not have respiratory bronchioles. They branch directly from short terminal bronchi to multiple alveolar ducts lined by alveoli (Fig. 1 A and B).

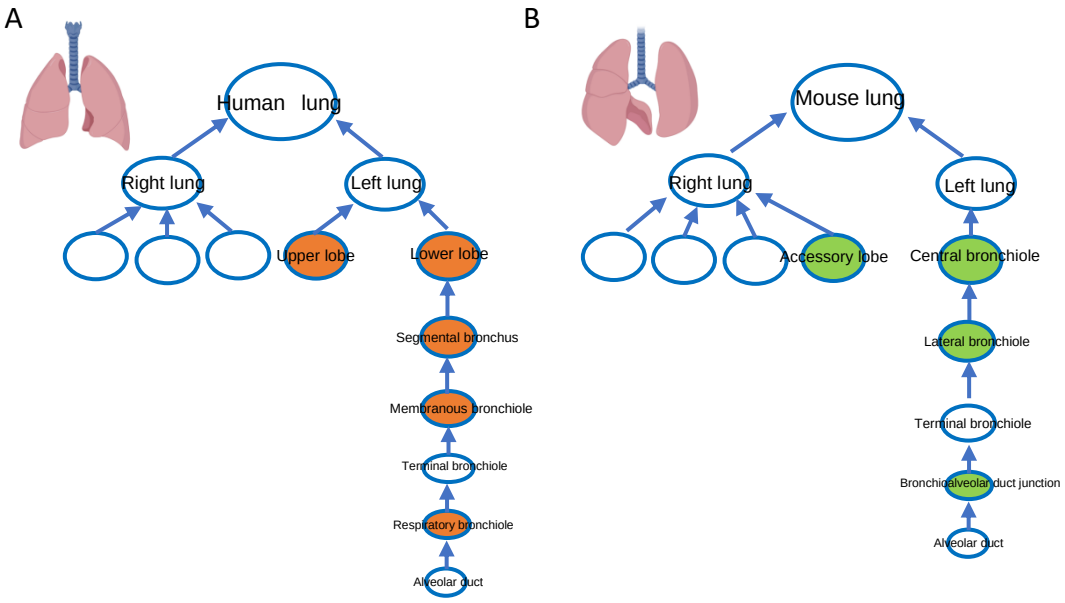

Fig 1. A schematic diagram of simple lung structures in (A) humans and (B) mice. Circles without color indicate similar structural organization between the two species, while those with color indicate different structural organization. The illustration and text have been adapted from Pan et al. 2019.

1.2 Cellular diversity in the adult lungs

The enormously complex lung tissue is comprised of over 40 different unique cell types, including epithelial cells, endothelial cells, immune cells, mesenchymal cells, and so on (Franks et al. 2008). There are important differences in the composition of airway epithelial cell between human and mouse lungs along the proximal-distal axis. The cellular anatomy of the trachea and the most proximal airways in mice and the large airways in humans is very similar. In both species, the epithelium lining the trachea and bronchi is pseudostratified, primarily consisting of three types of epithelial cells: basal cells, club cells, and ciliated cells, as well as a small number of neuroendocrine cells and mucus-secreting goblet cells (Hogan et al. 2014; Morrisey and Hogan 2010). In distal airway (bronchioles), the major cell populations are secretory club cells, ciliated cells, neuroendocrine cells, and goblet cells. Basal cells are still present in the human distal airways, although their numbers gradually decrease, whereas there are no basal or goblet cells in mice. Then, the low cuboidal epithelium is replaced by alveoli

composed of flat squamous alveolar type 1 (AT1) cells and cuboidal alveolar type 2 (AT2) cells in the respiratory bronchioles in the human lung (Basil et al. 2022). Whereas in the mouse, conducting airways terminate into alveolar sacs through bronchioalveolar stem cells (BASCs) at the site of the bronchoalveolar duct junction (BADJ), which is a characteristic of mouse (Wu and Tang 2021) (Fig. 2).

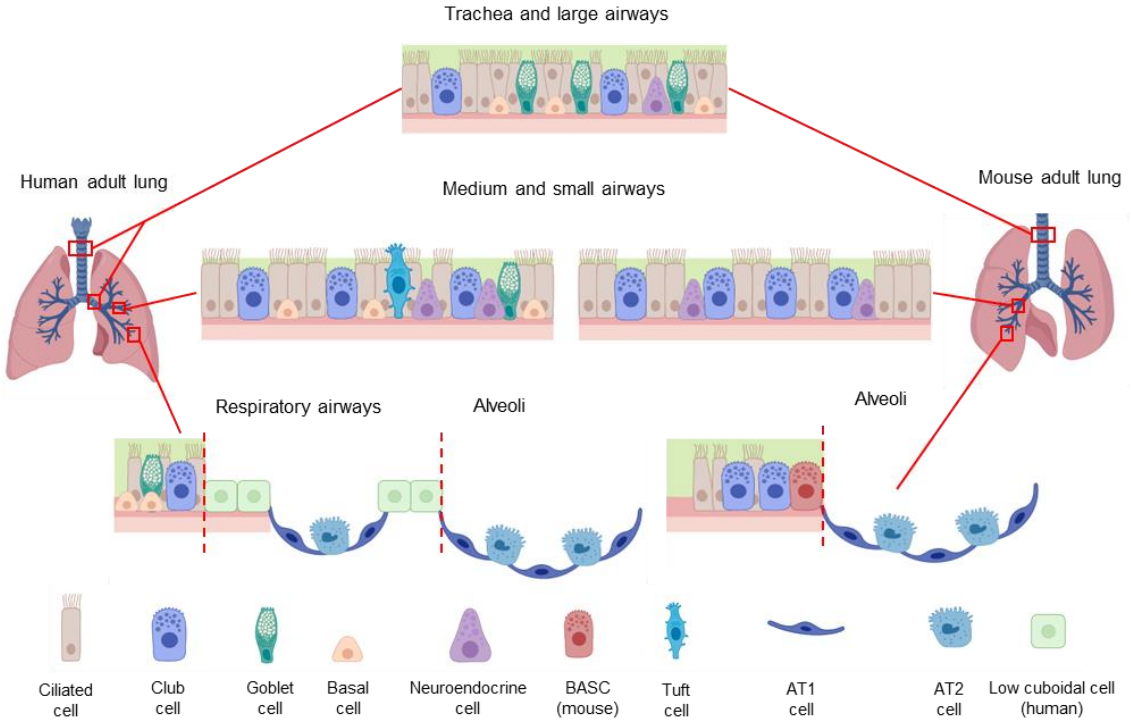

Fig 2. The cellular composition of the lung epithelium in human and mouse lungs. The illustration and text have been adapted from Rackley and Stripp 2012; Wu and Tang 2021.

1.3 Epithelial progenitor/stem cells in the adult lung

The self-renewal, proliferation, and differentiation of different cell types with stem cell capacity is essential for lung homeostasis and regeneration. According to the position within the airway tree, several epithelial cell types in the adult lung have been suggested to act as stem/progenitor cells in response to injury and exert the role in the local injury repair (Li et al. 2015; Parekh et al. 2020) (Fig. 3). In the trachea and bronchi, basal cells expressing keratin 5 (KRT5) or transformation related protein 63 (TRP63) are the dominant stem/progenitor cell populations in the adult lungs of mice and humans,

which can rapidly proliferate and differentiate into club, ciliated, and goblet cells after epithelial injury (Montoro et al. 2018; Plasschaert et al. 2018; Rock and Hogan 2011). In the distal airways, basal (only in humans) and variant club cells expressing Clara cell secretory protein (CCSP) and cytochrome P450 2F2 (CYP2F2) have the potential for self-renewing and give rise to club cells, ciliated cells and goblet cells (Reynolds and Malkinson 2010). Some variant club cells were recently found to differentiate into AT2 cells during bleomycin-induced alveolar injury, although this appears to be limited (Guha et al. 2017). Mouse studies suggest that a small population of club cells co-expressing CCSP and prosurfactant protein C (SPC) at the BADJ serve as BASCs, which possess the ability to generate not only airway cells but also AT2-like cells, and are likely involved in the regeneration of the lung after severe injury (Kim et al. 2005). Single-cell analysis revealed that human respiratory bronchioles also contain secretory airway epithelial cells that are able to differentiate into AT2 cells (Basil et al. 2022). In the alveolar region, self-renewing AT2 cells are the progenitors of AT1 cells (Barkauskas et al. 2013). A sublineage within the AT2 cell population expressing *TM4SF1* plays a dominant role in repairing the lung alveolus after acute injury (Zacharias et al. 2018). Recently, with the development of single-cell RNA sequencing (scRNA-seq) technology, it was found that human AT2 cells in regenerating lungs have the ability to differentiate into either AT1 cells or terminal and respiratory bronchiole secretory cells (Kadur et al. 2022).

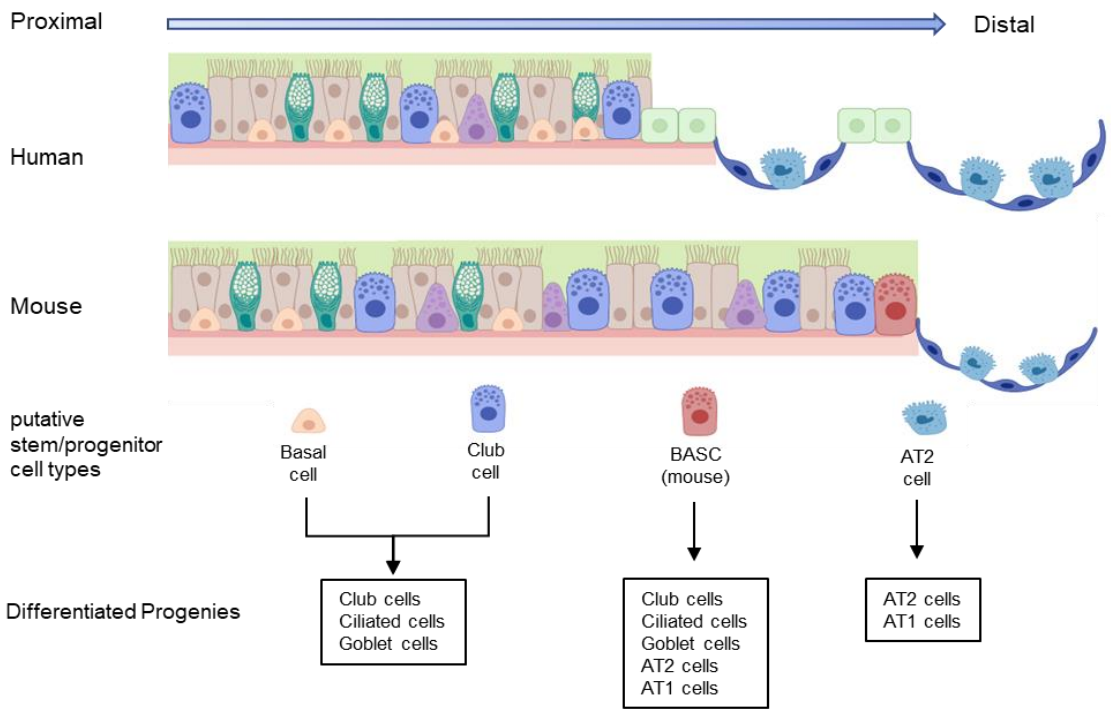

Fig 3. Illustration of potential stem/progenitor cell niches in the adult lungs of humans and mice. The illustration and text have been adapted from Li et al. 2015; Parekh et al. 2020.

1.4 Potential niches for epithelial stem cells in adult lung

Fibroblasts express components of the extracellular matrix, such as collagen and fibronectin, as well as growth factors, and they interact closely with epithelial cells in the regulation of proliferation and differentiation. Fibroblasts are dynamic cells that can differentiate into different, overlapping subtypes, including parabronchial fibroblasts, adventitial fibroblasts, myofibroblasts, and alveolar fibroblasts (Tsukui et al. 2020; Ushakumary, Riccetti, and Perl 2021b). Fibroblasts expressing platelet-derived growth factor alpha (PDGFRα) are often found in close association with AT2 cells, and are implicated as a niche for AT2 cells in maintaining AT2 cell stemness or controlling AT2 cell self-renewal and differentiation (Barkauskas et al. 2013; Zepp et al. 2017). Recent work has revealed cellular heterogeneity in the adult Pdgfra^{+} fibroblast population through scRNA-seq. One subpopulation of fibroblasts co-expression of *Axin2* and *Pdgfra*, named as mesenchymal alveolar niche cells, influences AT2 cell self-renewal and differentiation into AT1 cells through Fgf7, Il-6, and Bmp antagonists in mice (Zepp

et al. 2017). Another distinct population of $Lgr5^+$ cells located in alveolar compartments were also sufficient to promote alveolar differentiation of epithelial progenitors through Wnt activation (Lee et al. 2017).

The mesenchymal niche surrounding the airways has a critical role in both maintaining homeostasis and regenerating airway epithelium. The parabronchial airway smooth muscle (ASM) cells induce the expression of FGF10, which, in turn, promotes the proliferation of secretory cells (Volckaert et al. 2011). Lee et al. showed, for example, that using mouse and organoid studies, ASM cells expressing *Lgr6* promote the differentiation of airway progenitor cells via a Wnt-Fgf10 cooperation (Lee et al. 2017) .

1.5 In vitro models to understand the maintenance, regeneration, and disease of lung alveoli

The alveoli make up the distal gas exchange region of the lungs. Alveolar epithelial cells are mainly composed of AT1 and AT2 cells. AT1s are large, flattened, squamous cells that cover approximately 95% of the alveolar surface area, while AT2s are cuboidal cells that act as stem cells in the alveoli and are able to maintain the alveolar epithelium after injury (Vasilescu et al. 2012). Dysfunction of AT2s has been implicated in the pathogenesis of several lung diseases, such as chronic obstructive pulmonary disease (Christenson et al. 2022) and idiopathic pulmonary fibrosis (Raghu et al. 2011). As the pathogenesis of these diverse diseases is incompletely understood and drug screening for patients remain limited *in vivo*, suitable *in vitro* culture models are necessary for understanding alveolar biology and disease.

1.5.1 Alveolar organoids

Alveolar organoids differentiated from murine epithelial cells have been well characterized by several groups (Barkauskas et al. 2013; Shiraishi et al. 2019). Murine AT2 cells can be isolated using $EPCAM^+Sca1^-$ or $EPCAM^{med}$ surface markers or lineage tracing approaches by FACS. To support the formation of AT2 organoids, either co-culture with supporting cells such as PDGFRα+ lung fibroblasts or the addition of

small molecule inhibitors and growth factors is required. Depending on the exact protocol, 3D spheroids called alveolospheres form within 14 days with AT2 cells on the outside and AT1 cells inside the lumen (Barkauskas et al. 2013; Shiraishi et al. 2019). Three independent studies identified a transitional cell population in alveolospheres by scRNA-seq analysis (Kobayashi et al. 2020; Choi et al. 2020; Strunz et al. 2020), which shared similarly characterized genes such as high expression of *Krt8* and *Cldn4*, low expression of AT2s and AT1s markers, and activation of TGFβ, NF-κB in IPF lungs (Adams et al. 2020; Habermann et al. 2020).

In contrast to the mouse alveolospheres, further development is needed for human alveolar organoids. The first adult human alveolospheres were formed by co-culturing EPCAM-positive HT2-280-positive human AT2s and the fetal human lung fibroblast cell line MRC5. AT2 marker SFTPC and HT2-280 are expressed in these spheres, but there is no detectable AT1 marker expression (Barkauskas et al. 2013). In a more recent study, a subset of HT2-280^{+}TM4SF1^{+} AT2s co-cultured with MRC5 was found to exhibit a higher clonogenic potential than bulk human AT2s (Zacharias et al. 2018). Stroma-free human alveolospheres were also established for expansion and differentiation into AT1s using a chemically defined medium and serum (Ebisudani et al. 2021; H et al. 2020). A recent study showed that co-cultivation with primary lung mesenchymal cells induces transdifferentiation of human AT2 cells into Krt5^{+} basal cells. This suggests that human AT2 cells exhibit different plasticity than their murine counterparts, and that mesenchymal cells in the co-culture system strongly influence the AT2 cell phenotype (Kathiriya et al. 2022). An intermediate cluster expressing SFTPC^{low}/ABCA3^{low}/KRT17^{pos}/KRT5^{neg} was found in these transdifferentiated KRT5^{+} organoids, which were also present in IPF lungs (Adams et al. 2020; Habermann et al. 2020) . These results implicated a suitable organoid model might be a useful platform for studying pulmonary disease.

1.5.2 Air liquid interface (ALI) cultures

ALI culture models are also a valid tool for reproducing typical aspects of the respiratory tract *in vitro*. ALI cultures are characterized by the apical surface of the cells being exposed to air while the basolateral surface is nourished by contact with cell culture medium. This in vitro model allows the differentiation and maturation of lung epithelial cells in a controlled environment, mimicking physiological conditions much better than conventional 2D cultures, in which the epithelial cells mostly simply grow on plastic. ALI cultures permit *in vitro* modeling of cell-cell interaction, developmental processes, drug screening, and infections (Ong et al. 2016; Ootani et al. 2000).

ALI models depicting the different epithelia of the lungs can be established using cell lines, primary cells, and induced pluripotent stem cells (iPSCs). The advantages of cell lines include homogeneity and low phenotypic variation, making cultures more stable and easier to handle. However, it must be emphasized that due to the transformation process and homogeneity, there is a risk that they lack important properties that are normally found *in vivo*. Stem cell-derived models are attractive for research in developmental biology, regenerative medicine, and *in vitro* pharmacology. However, the complex protocols and costs required to obtain, maintain and differentiate stem cells are some of the drawbacks of these models. Primary cultures isolated directly from tissues, however, have the disadvantage of donor variability and the isolated cells, particularly pneumocytes, can often only be multiplied to a limited extent. Nevertheless, primary epithelial cells better represent the native microenvironment and are, in principle, the best candidates for mimicking *in vivo* conditions.

1.6 Idiopathic pulmonary fibrosis (IPF): Overview

Interstitial lung diseases (ILDs) are a group of diseases characterized mainly by fibrosis of the lung. It is a general term for different groups of diseases with diffuse parenchymal, alveolar inflammation and interstitial fibrosis as the basic pathological changes (Rosas et al. 2014). As one of the most common types of ILD, IPF is a rare, chronic, and fatal disease of unknown cause that develops gradually over several years and is typically

characterized by the formation of scar tissue in the lungs and progressive shortness of breath (Lederer and Martinez 2018; Martinez et al. 2017; Raghu et al. 2011).

The incidence of IPF appears to be higher in Europe and North America than in East Asia and South America. The prevalence of IPF gradually increases with age, which is more common in men and adults over the age of 65 years. The prognosis for IPF patients is poor, with survival rates even worse than for many cancers. Survival varies greatly from patient to patient, with a life expectancy of 3–5 years after diagnosis (Lederer and Martinez 2018; Martinez et al. 2017; Raghu et al. 2011).

Currently, only two medications, nintedanib and pirfenidone, have been shown to slow the rate of forced vital capacity decline and to have some efficacy in reducing severe respiratory events (Lederer and Martinez 2018; Martinez et al. 2017; Raghu et al. 2011). Therefore, the pathophysiological mechanisms and drug development need to be further explored.

1.6.1 Pathological features of IPF

IPF is diagnosed by identifying a pattern of usual interstitial pneumonia (UIP) based on radiological or histological criteria, with no evidence of an alternative cause. High-resolution CT (HRCT) of the chest in IPF is characterized by grid shadowing and honeycomb lung, often accompanied by distended bronchial dilatation. Honeycomb lungs are an important basis for determining the classification of UIP. Histopathological findings show that the UIP pattern is characterized by interstitial fibrosis with distinct areas of distorted fibrotic architecture, as well as the appearance of microscopic honeycombing. Fibroblastic foci are a major histopathological feature of UIP, appearing at the interface of fibrosis and normal lung tissue with massive fibroblast proliferation and aggregation of myofibroblasts.

1.6.2 Mechanisms/pathophysiology of IPF

The pathogenesis of IPF is linked to a variety of risk factors, including genetic risk (mutations of telomeres, *SFTPC* and *MUC5B* etc.) (Armanios et al. 2007; Mulugeta,

Nureki, and Beers 2015; Seibold et al. 2011), environmental exposures (smoking, chronic viral infections and certain comorbidities etc.) (Baumgartner et al. 1997; Taskar and Coultas 2006) and ageing, with accelerated 'lung ageing' being a driving force in the development of IPF (Moisés Selman, López-Otín, and Pardo 2016). It is suggested that repetitive microinjuries in the ageing alveolar epithelium play an important role in the development of IPF. These microinjuries lead to abnormal communication between epithelial cells and fibroblasts, induce myofibroblast activation and proliferation, accumulating large amounts of extracellular matrix (ECM) and remodeling the interstitial lung matrix, which destroys the normal alveolar architecture and disrupts gas exchange, ultimately leading to death (Fig. 4).

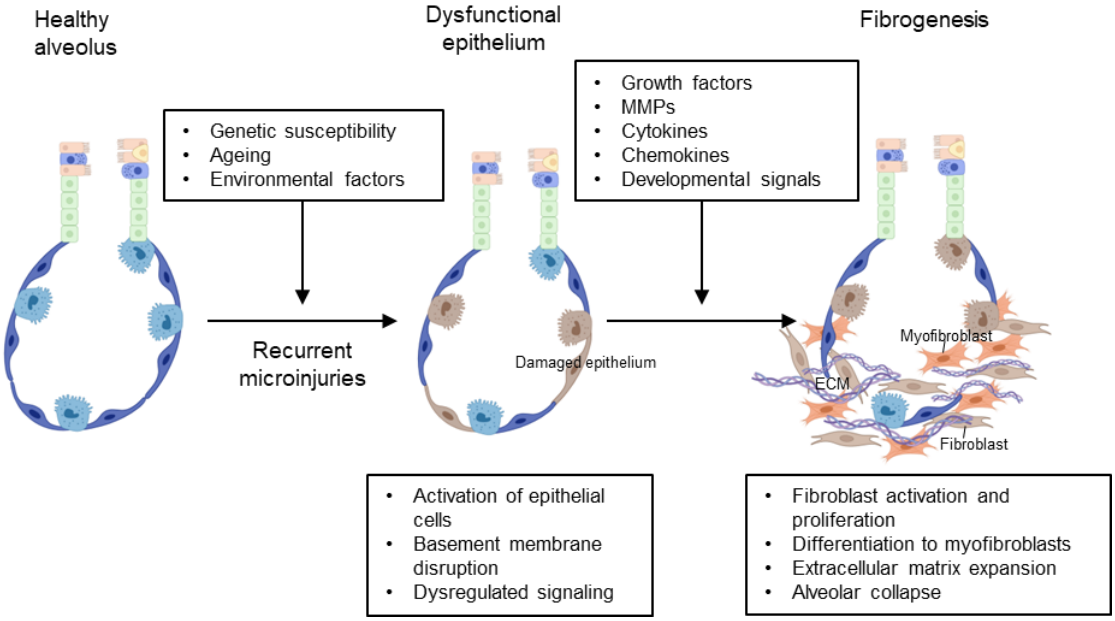

Fig 4. Proposed mechanism for the pathogenesis of IPF. The illustration and text have been adapted from Martinez et al. 2017; Richeldi, Collard, and Jones 2017.

1.6.2.1 The role of epithelial cells

The mechanisms of fibrogenesis in IPF are hardly understood. However, chronic dysregulation of AT2s, the stem cells of the lung that contribute to the renewal of AT1s in homeostasis or following lung injury, is thought to be central to dysregulated regeneration and repair in IPF. Abnormalities in AT2s and loss of AT1s are found in IPF tissue, and fibrotic lesions are usually located near apoptotic or proliferating alveolar

epithelial cells (M. Selman et al. 2001).

It is assumed that abnormal activation of alveolar epithelial cells leads to signal dysregulation and the secretion of large amounts of fibrogenic growth factors, cytokines and coagulants. These mediators include connective tissue growth factor (CTGF), platelet-derived growth factor (PDGF), angiotensinogen, osteopontin, TGFβ, TNF, some matrix metalloproteinases (e.g. MMP1, MMP7, MMP19, etc.), and chemokines (e.g. CXCL12, CCL2, etc.) (Horowitz and Thannickal 2006). Senescence of AT2 cells was also observed in the lungs of IPF patients. These senescent AT2 cells are described as secreting a large number of growth factors, cytokines, development-related molecules, and matrix-degrading enzymes (Moisés Selman, López-Otín, and Pardo 2016). These secretions strongly modify the microenvironment, recruit myofibroblasts, and induce the proliferation and differentiation of fibroblasts to myofibroblasts.

1.6.2.2 The role of myofibroblasts

Myofibroblasts, which are found in large numbers in the diseased lung, may be of various origins, including resident fibroblasts proliferation, circulating fibrocytes, interstitial pericytes, endothelial-mesenchymal transformation (EndMT) and epithelial-mesenchymal transformation (EMT) (Hung et al. 2013). Myofibroblasts that are activated resist apoptosis, accumulate ECM , and alter the composition and stiffness of the ECM, which further contributes to the positive feedback loop of myofibroblast activation (Parker et al. 2014). Experiments on the differentiation of lung fibroblasts *in vitro* showed that myofibroblasts are characterized by increased contraction, collagen production, activation of TGFβ and release of ECM proteins (MMP2, MMP3, MMP10, COL1A1, COL1A2, COL3A1, COL4A2, COL5A2 and TIMP2) (Lee et al. 2016). Abnormal extracellular matrix production is accompanied by abnormal lung remodeling, including alveolar stem cell depletion, basal cell dysfunction, bronchiolization, and honeycomb cyst formation of the distal airspaces (Richeldi, Collard, and Jones 2017).

1.7 Function and biological role of the Dickkopf family

The Dickkopf (Dkk) family encodes secreted proteins consisting of five major members in vertebrates, including DKK1, DKK2, DKK3, DKK4, and a divergent member DKKL1 (also called Soggy). The DKKs share two conserved cysteine-rich structural domains (CRDs), the N-terminal CRD, Dkk_N (also referred to as Cys1) and C-terminal CRD (also referred to as Cys2). Cys1 is unique to the Dkks, while the Cys2 is related to the colipase fold. DKK1-4 contain both Cys1 and Cys2 domains, separated by a variable linker region. DKKL1 has sequence similarity to Dkk3, but not to other Dkks. The sgy-domain is only found in DKKL1 and DKK3 (Niehrs 2006; Krupnik et al. 1999).

Members of the DKK family are modulators of the Wnt/β-catenin pathway. DKK1, DKK2, and DKK4 have been shown to be antagonists of the Wnt/β-catenin pathway, disrupting their binding to Wnt ligands by interacting with the Wnt coreceptor low-density lipoprotein receptor-related protein 5/6 and Kremen1/2. However, the role of DKK3 in Wnt signaling is not yet fully understood. Some publications suggest that DKK3 inhibits Wnt signaling, while others claim that DKK3 enhances Wnt signaling, depending on the cellular environment (Niehrs 2006).

1.8 DKK3 in fibrosis diseases

Recently, DKK3 has been implicated in the pathogenesis of fibrosis, particularly in renal fibrosis. Renal tubular epithelial cells (TECs) express DKK3 during postnatal development in mice and re-express it under pathological conditions. The overexpression of DKK3 in TCEs promotes tubulointerstitial fibrosis by supporting the Wnt/β-catenin signaling pathway and upregulating the expression of stress-induced inflammatory factors. Genetic and antibody-mediated abrogation of DKK3 *in vivo* resulted in decreased tubular atrophy, reduced tubulointerstitial accumulation, and prevented tubulointerstitial fibrosis in several murine kidney fibrosis models (Federico et al. 2016). Lipphardt et al showed DKK3, an agonist of the Wnt pathway, enhances differentiation of renal fibroblasts to myofibroblasts, induces

endothelial-mesenchymal transition, and impairs angiogenesis in renal microvascular endothelial cells (Lipphardt et al. 2019). In addition, DKK3 secreted by human amniotic mesenchymal stem cells attenuated liver fibrosis in mice by inhibiting the activation of hepatic stellate cells through suppression of the Wnt/β-catenin pathway (Liu et al. 2022). Overexpression of DKK3 greatly reduces AngII infusion-induced cardiac fibrosis by inhibiting the GSK-3β/β-catenin pathway (Zhai et al. 2018). However, the role and mechanism of DKK3 in pulmonary fibrosis is not yet clear.

2. METERIALS AND METHODS

2.1 Materials

2.1.1 Instruments

Instruments	Company
gentleMACS™ Dissociators	Miltenyi Biotec, Germany
Safe 2020 Class II Biological Safety Cabinets	Thermo scientific, USA
Heracell™ 240i CO2 Incubators	Thermo scientific, USA
CFX 96^{TM} Real-Time PCR Detection System	Bio-Rad, USA
C1000^{TM} thermal cycler	Bio-Rad, USA
NanoDrop™ 8000 Spectrophotometer	Thermo scientific, USA
Fresco™ 21 Microcentrifuge	Thermo Fisher, USA
ChemiDoc MP Imaging System	Bio-Rad, USA
The Millicell-ERS (Electrical Resistance System) MERS00001	Millicell, Germany
Cellspin® II	Tharmac, Germany
LSM 900 with Airyscan 2	Zeiss, Germany
BX 51 Fluorescent Microscope	Olympus, Japan
BMG microplate reader	Fluostar omega, Germany
2100 Bioanalyzer	Agilent, Germany
FlexiVent^{TM} system	SCIREQ, Canada

2.1.2 Experimental material

Experimental materials	Source	Catalog
gentleMACS™ C Tubes	Miltenyi Biotec	130-093-237
70 µm Falcon™ Cell Strainers	Corning	353350
40 µm Falcon™ Cell Strainers	Corning	352340
100 µm Falcon™ Cell Strainers	Corning	352360
LS columns	Miltenyi Biotec	130-042-401
Transwell Plates, sterile, 12 wp, pore size 0.4 µm; diamerter: 6.5 mm	Corning	CLS3470-48EA

2.1.4 Reagents

Reagents	Source	Catalog
Collagenase type I	Life technologies	17100-017
Dispase	Corning	354235
DNase1	Roche	10104159001
Sterile PBS	Sigma-Aldrich	D8537-500ML
Antibiotic-antimycotic	Gibco	15240062
ACK lysis buffer	Gibco	A1049201
Fetal Bovine Serum (FBS)	Gibco	10270106
EDTA	Roth	8043.2
Primocin	invivogen	Ant-pm-1
TrypLE™ Express Enzyme (1X)	Gibco	12605010
Penicillin-Streptomycin	Gibco	1514
Glutamax	Thermo Fisher Scientific	35050061
HEPES (1M)	Thermo Fisher Scientific	15630080
Bovine Serum Albumin (BSA)	Sigma-Aldrich	A9647-100G
Insulin-Transferrin-Sodium-Selemite Supplement	Roche	11074547001
MEM Non-essential Amino Acids (NEAA)	Sigma-Aldrich	M7145-100mL
laminin from Engelbreth-Holm-Swarm murine sarcoma basement membrane	Sigma-Aldrich	L2020-1mg
L-glutamine (200mM)	Life technologies	25030-081
Fibronectin, human, 1mg	Corning	354008
Dulbecco's Modified Eagle Medium (DMEM)	Gibco	41965039
DMEM/F-12	Gibco	11320033
Ethanol Absolute 99.8+%	Fisher Chemical	E/0650df/08
Mounting Medium with DAPI	abcam	ab104139
Triton X-100	Roche	SIG10789704001
$CaCl_2$ *$2H_2O$	Merck	1.02382.1000

NaCl	Roth	9265.2
KCL	Roth	6781.1
Na_2HPO_4 * 7 H_2O	Sigma Aldrich	S9390-100G
HEPES	Roth	9105.4
Glucose	Roth	6887.1
$MgSO_4$ *7 H_2O,	Roth	P027.2
Formaldehyde	Fisher Chemical	F/1501/PB17
Growth Factor Reduced (GFR) Matrigel	Corning	354230
Y-27632	Sigma-Aldrich	Y0503
SB431542	Abcam	Ab120163
CHIR99021	Tocris	4423
BIRB796	Tocris	5989
Heparin	Sigma-Aldrich	H3149
N-Acetyl-L-cysteine	Sigma-Aldrich	A9165
Human EGF	Gibco	PHG0313
B-27 Supplement (50X)	Thermo Fisher Scientific	17504044
Human FGF10	BioLegend	559304
Advanced DMEM/F12	Thermo Fisher Scientific	12634010
Agarose NEEO ultra-quality	Roth	2267.3
Recombinant Mouse IL-6 Protein	R&D system	406-ML
0.9% NaCL	BERLIN-CHEMIE AG	2337206
2% xylazine	Bayer	1320422
Ketamine	Bayer	3151811

2.1.5 Kits

Title	**Source**	**Catalog**
RNA isolation Kit	Macherey-Nagel	740955.250
RevertAid RT Reverse Transcription Kit	Thermo Scientific	1691
SensiMix™ SYBR® & Fluorescein (2X)	Bioline	QT615-05
Mouse IL-6 DuoSet ELISA	R&D Systems	DY406
Human Single-Cell Multiplexing Kit	BD Rhapsody	633781

Mouse Immune Single-Cell Multiplexing Kit	BD Rhapsody	633793
Whole Transcriptome Analysis (WTA) Amplification Kit	BD Rhapsody	633801
High Sensitivity DNA Kit	Agilent	5067-4626
Picro-Sirius red staining kit	ScyTek	SRS030

2.1.6 Antibody

Title	**Dilution**	**Source**	**Catalog**
Rat monoclonal Anti-CD326-PE (G8.8)	/	eBioscience	12-5791-82
Anti-PE microbeads	/	Miltenyi	130-048-801
Mouse monoclonal anti-HT2-280	1:50	Terrance	TB-27AHT2-280
Anti-mouse IgM microbeads	1:10	Miltenyi	130-047-302
Mouse monoclonal Anti-Hop (E-1)	1:100	Santa Cruz	sc-398703
Rabbit polyclonal anti-Clara Cell Secretory Protein	1:200	Merck	07-623
Rabbit polyclonal anti-Prosurfactant Protein C	1:100	Abcam	ab90716
Mouse monoclonal anti-SP-C (H-8)	1:100	Santa Cruz	sc-518029
Rabbit monoclonal anti-Aquaporin 5	1:100	Abcam	ab92320
Mouse monoclonal anti-Mucin 5B (A-3)	1:100	Santa Cruz	sc-393952
Rabbit polyclonal anti-UGRP1	1:200	Invitrogen	PA5-12-195
Mouse monoclonal anti-Fibroblasts (TE-7)	1:100	Merck	CBL271
Mouse monoclonal anti-collagen I (COL-1)	1:200	Invitrogen	MA1-26771
Mouse monoclonal anti-KI67(B56)	1:100	Abcam	ab279653
Mouse monoclonal anti-α-SMA (1A4)	1:100	R&D	MAB1420

Rabbit polyclonal anti-KI67	1:100	Abcam	ab15580
Rabbit polyclonal anti-DKK3	1:100	Invitrogen	PA5-102626
Goat anti-rabbit Alexa 488 secondary antibody	1:200	Invitrogen	A11034
Donkey anti-mouse Alexa 647 secondary antibody	1:200	Jackson IR	715-605-151
Goat anti-mouse Alexa 488 secondary antibody	1:200	Cell signalling	4408S
Goat anti-rabbit Cyanine5 secondary antibody	1:200	Invitrogen	A10523

2.2 Buffers and solutions

CMM-complete mouse medium:

DMEM/F12 supplemented with 1 mM L-glutamine, 10 mM HEPES, 0.25% BSA, 1% NEAA, 100 µg/mL primocin, 0.05% Insulin-transferrin-sodium-selenite

BSSB buffer

Add 1000 mL of dd H_2O with 8 g NaCl, 0.40 g KCL, 0.14 g Na_2HPO_4 * 7 H_2O, 2.38 g HEPES, 1 g Glucose, 0.29 g $MgSO_4$ *7 H_2O, 0.27 g $CaCl_2$ *2H_2O, adjust pH to 7.4 and sterile filtration, then add 10 mL penecillin/streptomycin

Washing buffer for MACS columns

100 mL of PBS with 0.5 g BSA, 54.5 mg EDTA and sterile filtration

Digestion solution

16.8 mg of collagenase type I (285 U/mg), 1 mL of Dispase (50 U/mL), 600 µL of DNase1 (165 U/mL stock) filled to 10 mL with PBS.

FACS buffer

1% FBS, 186 mg EDTA (1 mM) in 500 mL PBS

SFFF -serum-free feeder-free medium

Advanced DMEM/F12 supplemented with 10 µM SB431542, 3 µM CHIR99021, 1 µM BIRB796, 50 ng/mL Human EGF, 10 ng/mL Human FGF10, 5 µg/mL Heparin, 1x B-27 supplement, 1x antibiotic-antimycotic, 15 mM HEPES, 1x GlutaMAX, and 1.25 mM N-Acetyl-L-Cysteine

Blocking buffer

2% BSA in 1X PBS

Permeabilization solution

0.1% Triton X-100 detergent in 1X PBS

4% paraformaldehyde (PFA)

280 mL formaldehyde in 2220 mL 1X PBS

Preparation of the anaesthetization (shown here for 10 mice)

1650 µL 0.9% NaCl, 80 µL 2% xylazine, 270 µL Ketamine (stock:100 mg/mL)

Preparation of the kill-solution (shown here for 10 mice)

250 µL 0.9% NaCl, 256.5 µL 2% xylazine, 1312.5 µL Ketamine

2.3 Cell culture and outcome measurements

2.3.1 Human alveolar organoid culture

2.3.1.1 Human lung alveolar epithelial cell isolation and sorting

Alveolar epithelial cells were isolated from resected human lung tissue (parenchymal lung and distal airway specimens). The tissue was washed 3 times with cold sterile PBS containing 1% antibiotic-antimycotic. Pleura and airways were carefully removed as much as possible and the tissue was cut into small pieces. These small pieces of tissue were collected into a gentleMACS tube with 10 mL digestion solution.

Miltenyi gentleMACS dissociator was used to mince and incubate the tissue at 37°C for 35 mins with rotation to process it into a single-cell suspension. Cells were passed through 70 µm cell strainer into new 50 mL tube, and 10-20 mL of PBS was rinsed through the 70 µm cell strainer to maximize yield. Spin the cell suspension at 450 x g for 10 mins at 4℃ and decant the supernatant carefully. 10 mL of ACK lysis buffer was added to lyse red blood cells and incubated at room temperature (RT) for 10 mins, followed by 5 mins of centrifugation at 450 x g. Cells were washed twice with FACS buffer and passed through 40 µM filters. After a single-cell suspension was obtained, cells were incubated with the HT2-280 antibody in the dark for 1 hour at 4℃ and anti-mouse IgM microbeads in the dark for 30 mins at 4℃ and sorted by MACS LS columns. HT2-280$^+$ cells were verified by cytospin staining and PCR.

The protocols for human material were approved by the ethics committee of the Landesärztekammer des Saarlandes (34/18) and informed consent has been obtained from all patients.

2.3.1.2 Human lung fibroblasts isolation and culture

A ~1 cm^2 piece of lung tissue was cut into 6-10 individual small pieces. These tissue fragments were transferred into a 150 mm tissue culture dish containing 20 mL of DMEM with 10% FBS and 1%P/S, and placed in an incubator at 37°C with 5% CO2, with the medium being changed every 4 days. Tissue fragments were discarded after 14 days, when all viable fibroblasts exited from the tissue fragments. After the cells had reached 80-90% confluence, they were harvested and frozen in -80℃ for future use. Fibroblasts were verified by staining and PCR.

2.3.1.3 Human alveolosphere culture and passage

Alveolosphere culture was as described previously (H et al. 2020). Briefly, HT2-280$^+$ human AT2s (5x10^3) were resuspended in SFFF medium and mixed with an equal amount of GFR-Matrigel in 24-well plates, and allowed to solidify in a 50 µL droplet per well at 37°C for 20 mins, followed by submersion in 500 µL of

pre-warmed SFFF medium. Y-27632 (10 μM) was added for the first 3 days of culture to promote cell survival. The medium was changed every 3 days. Cells in 3D cultures were passaged at different days depending on size, with culture days varying from 21-35 days. For passaging, Matrigel was disrupted by incubation with dispase at 37°C for 45 mins, followed by single cell dissociation through the addition of TrypLE™ Express Enzyme for 5 mins at 37°C. The cells were centrifuged at 450 x g for 5 mins and resuspended in fresh GFR-Matrigel at a ratio of $5x10^3$ cells as before.

2.3.1.4 Alveolosphere assay

After expansion of alveolosphere, HT2-280^+ AT2s and human lung fibroblasts were co-cultured (5000 AT2s: 5000 human lung fibroblasts per well) in SFFF medium diluted 1:1 with GFR-Matrigel. The cell suspension–Matrigel mixture was seeded in 24-well plates as above. After 21 days of culture, the alveolospheres were assessed by mRNA, protein, staining and single cell RNA sequencing. In the bleomycin experiments, bleomycin (3 mg/mL) produced by clinical pharmacy in Homburg was added to cultures at a concentration of 30 ng/mL starting at day 14. The cultures were analyzed at day 21.

2.3.2 ALI culture for mouse lung epithelial cells

2.3.2.1 Transwell insert coating

Coating buffer was made by combining 10 mL of ddH2O with 100 μL of fibronectin and 100 μL of laminin. 200 μL of coating buffer was added to each insert and incubated for 24 hours at 37°C. The coating buffer was then discarded and the plates were stored in 4°C fridge. Notifications of killings for scientific purposes was submitted via the animal welfare officer of the Saaralnd University before the start of the experiments (§4. Abs. 3 des Tierschutzgesetzes).

2.3.2.2 Lung removal in mice

The lung of mouse was perfused with PBS to free the pulmonary vasculature from blood. 2 mL preheated (37°C) dispase solution was injected into the lung via intratracheal injection and incubated for 1-2 mins. The lung was excised and incubated in 2 mL of dispase at 37°C for 45 mins (in a 15 mL tube).

2.3.2.3 From tissue to cell suspension

The lungs and dispase were transferred in a 10cm culture dish (normally 3 lungs/dish) with 20 mL CMM and 1 mL DNase 1(both preheated to 37°C). Bronchi, connective tissue, etc. were removed, and the lung tissues were cut into small pieces and incubated at 37°C for 30-45 mins. The cell suspension was resuspended with a 10 mL serological pipette until it was resuspended without resistance, and then filtered through a 100 μm and a 40 μm cell strainer.

2.3.2.4 Lung epithelial cells and fibroblasts isolation

The cell suspension was centrifuged at 1350 rpm for 5 mins. The supernatant was transferred to a new 50 mL tube and centrifuged again. The cell pellets were pooled in 10 mL ACK lysis buffer to lyse red blood cells, and incubated at RT for 10 mins, followed by 5 mins of centrifugation at 1350 rpm. The pellet was then resuspended in 20 mL CMM medium supplemented with 1 mL DNase1, and transferred to two culture dishes (10 mL/culture dish) for 60-90 mins of incubation at 37°C to remove attached cells. The cell suspension was collected in a 50 mL tube. 10 mL BSSB buffer was used to rinse the culture dish and transferred into the 50 mL tube, followed by centrifugation at 1350 rpm for 5 mins. The cell pellet was resuspended with 1mL BSSB buffer and transferred to a 2 mL tube. 800 uL BSSB buffer was used to rinse the 50 mL tube again and transferred to the 2 mL tube. The 2 mL tube was incubated with anti-EPCAM antibody (10 μL/tube for 3 mice) for 30 mins at 4°C on a rotating apparatus. After centrifugation at 1350 rpm for 5 mins, the cell pellet was resuspended with 400 uL BSSB buffer. It was then incubated with 100 μL PE-microbeads each tube for 30 mins

at 4°C on a rotating apparatus. Labeled $EPCAM^+$ cells were enriched by using magnetic-activated cell sorting (MACS) LS Columns and separator. The $EPCAM^-$ cells, including mesenchymal cells, were cultured with CMM medium for 1~2 passages and stored for further use. $EPCAM^+$ cells and mesenchymal cells were verified by PCR.

2.3.2.5 ALI culture

$5x10^5$ $EPCAM^+$ cells were seeded in 200 µL CMM supplemented with 10% FCS/ insert, and 500 µL CMM including 10% FCS with/without $5x10^4$ mesenchymal cells was added to the basolateral compartment of each transwell. After 48 hours culture, the apical medium was removed and the medium of the basolateral compartment was refreshed. RNA, protein, single cells suspension and insert membrane were collected for further analysis. In IL-6 experiments, different concentrations of IL-6 (20 ng/mL, 2 ng/mL, 0.2 ng/mL) were added to the basal layer from day 1 and the medium was changed daily.

2.3.2.6 Transepithelial electrical resistance (TEER) measurement for ALI culture

Before using the Millicell-ERS instrument, two electrode probes should be sterilized with ethanol for no more than 5 mins and allowed to air dry. 200 µL of prewarmed CMM medium was added to the insert. The basolateral electrode should be touching the bottom of the well and the apical electrode should be kept well away from the transwell membrane. Then, press the test button to measure the TEER value; either the 2000 ohm or 20k ohm scale can be selected, depending on the anticipated resistances of the transwell. The formula for TEER calculation was as follows:

TEER= (the measured resistance – blank resistance) ohm * $0.33cm^2$ (for a 24-well transwell)

2.3.3 Preparation for histological section

Alveospheres were washed with PBS and fixed in 4% PFA for 1 hour at RT. After removing the 4% PFA, 200 µL of warmed 3% agarose was added to the spheres until

the gel became firm. The gel was taken out from the plate and kept in a cassette, which was incubated in 4% PFA overnight. The cassettes were processed for paraffin sectioning to obtain 4-micron thin sections. Alveolospheres sections were ready for staining after deparaffinization and antigen retrieval.

Cytospins and ALI transwell membranes were ready for staining after fixation with 4% PFA for 1 hour.

Human lung tissues from patients undergoing lung surgery were immediately fixed in 4% PFA and embedded in paraffin for staining.

2.3.4 Hematoxylin and eosin (H&E) staining

After deparaffinization and rehydration, sections were incubated with hematoxylin for 3 mins and washed in water for 5 mins. Sections were quickly immersed in acidic ethanol 8-12 times and washed twice in water. Incubation with eosin for 30 secs and dehydration (3 x 5′ 95% ethanol, 3 x 5′ 100% ethanol, 3 x 15′ Xylene). Permount (xylene-based) was used to mount slides and allowed to dry.

2.3.5 Immunofluorescence (IF) staining

Cytospins, membranes or alveolospheres were permeabilized by 0.1% Triton X-100 for 15 mins and blocked with 2% BSA in PBS for 1 hour at RT. They were then incubated with primary antibody at 4°C overnight. After 3 washes with PBS on the second day, secondary antibody diluted in blocking buffer was used to incubate the cells for 2 hours at RT in the dark. The membrane of insert was carefully cut off after 3 washes with PBS. Mounting medium with DAPI was mounted and left to cure overnight at RT in the dark. Cytospins and alveolospheres were visualized with an Olympus fluorescent microscope (BX 51, Japan), and membranes were visualized with a Zeiss confocal microscope (LSM900, Germany).

2.3.6 Reverse transcription and quantitative PCR for analysis of gene transcripts

2.3.6.1 RNA isolation

An RNA isolation kit was used to isolate RNA from cells and organoids. Briefly, for each isolation, 350 µL of buffer RA1 with 3.5 µL β-mercaptoethanol was used to lyse cell components while maintaining the integrity of RNA. The lysate was transferred to a NucleoSpin® Filter and centrifuged for 1 min at 11,000 x g to reduce viscosity. 350 µL of 70% ethanol was added to the homogenized lysate and vigorous mixed 5 times. The mixed lysate was loaded onto one NucleoSpin® RNA Column and centrifuged for 30 secs at 11,000 x g. After placing the column in a new collection tube (2 mL), 350 µL of MDB (Membrane Desalting Buffer) was added and centrifuged at 11,000 x g for 1 min to dry the membrane. 95 µL of DNase reaction mixture (10 µL reconstituted rDNase + 90 µL reaction buffer for rDNase) was directly added to the center of the silica membrane of the column and incubated at RT for 15 mins. 200 µL of buffer RAW2 was added into the column to inactivate the rDNase and centrifuged for 30 secs at 11,000 x g. The column was then placed into a new collection tube. 600 µL of buffer RA3 was added and centrifuged for 30 secs at 11,000 x g. After discarding the flowthrough, 250 µL of buffer RA3 was added to the column and centrifuged for 2 mins at 11,000 x g to dry the membrane completely. The column was transferred to a nuclease-free collection tube and eluted RNA in 40~60 µL of RNase-free H_2O by centrifuging at 11,000 x g for 1 min. The RNA was left on ice for further processing or stored at -80°C.

2.3.6.2 RNA quantification

A Nanodrop spectrophotometer was used to measure the concentration of RNA at 260/280 nm wavelength, and the OD260/OD280 ratio was used to assess the purity of RNA (a ratio of ~2.0 is generally accepted as “pure” for RNA).

2.3.6.3 cDNA synthesis by reverse transcription

RevertAid RT Reverse Transcription Kit was used to convert RNA to complementary DNA (cDNA). For each reaction, 80 ng of RNA from epithelial cells, 200 ng of RNA from mesenchymal cells, or 80 ng of RNA from human organoids was needed. The volume of RNA required was calculated based on the concentration of RNA determined from a Nanodrop spectrophotometer. Briefly, the volumes of RNA, primer and water were added in the indicated order as described in Table 1. After incubating the RNA samples at 65°C for 5 mins, the master mix was added in the indicated order to each tube during a 5-min incubation time at 4°C as described in Table 1. Under RT-PCR conditions (Table 2), the RNA samples were reverse transcribed to cDNA by a C1000^{TM} thermal cycler. The product was stored at -80°C for subsequent use.

Table 1 Reverse transcription reaction mixture composition:

Template RNA	Total RNA	80 ng epithelial cells
		80 ng organoids
		200 ng fibroblasts
Primer	100 uM Oligo(dT)$_{18}$ primer	1 µL
Water, nuclease-free		to 12 µL
Master Mix	5X Reaction Buffer	4 µL
	RiboLock RNase Inhibitor (20 U/µL)	1 µL
	10 mM dNTP Mix	2 µL
	RevertAid RT (200 U/µL)	1 µL
Total volume		20 µL

Table 2 Reverse transcription reaction conditions:

Tm	**Time**	**Number of cycles**
65 ˚C	5 min	1
4˚C	5 min	1
42˚C	60 min	1
70˚C	5 min	1
4˚C	Indefinite	1

2.3.6.4 Semi-quantitative real time polymerase chain reaction (qRT-PCR)

The sequences for the primers were obtained from Origene and primers were obtained from Metabion. Primers are listed in Table 3. SensiMix™ SYBR® & Fluorescein (2X) reagent was used for all RT-PCR reaction. They were mixed together to make a master mix, with the component and volume for each reaction listed in Table 4. Then, samples were placed in a CFX 96^{TM} Real-Time PCR Detection System under the following conditions (Table 5).

Table 3 Primer sequences:

Primer	Sequence
Mouse *Scgb1a1*	Forward: 5'-GGTTATGTGGCATCCCTGAAGC-3' Reverse: 5'-GCTTACACAGAGGACTTGTTAGG-3'
Mouse *Sftpc*	Forward: 5'-GTCCTCGTTGTCGTGGTGATTG-3' Reverse: 5'-AAGGTAGCGATGGTGTCTGCTC-3'
Mouse *Sftpb*	Forward: 5'- TGTCCTCCGATGTTCCACTGAG-3' Reverse: 5'- AGCCTGTTCACTGGTGTTCCAG-3'
Mouse *Aqp5*	Forward: 5'- TCCATGAACCCAGCCCGATCTT-3' Reverse: 5'- GAAGTAGAGGATTGCAGCCAGG-3'
Mouse *Hopx*	Forward: 5'- TCTCCATCCTTAGTCAGACGC-3' Reverse: 5'- GGGTGCTTGTTGACCTTGTT-3'
Mouse *Ccnd1*	Forward: 5'- GCAGAAGGAGATTGTGCCATCC-3' Reverse: 5'- AGGAAGCGGTCCAGGTAGTTCA-3'
Mouse *Cldn18*	Forward: 5'- TGGTAGCATGGATGACTCTGCC-3' Reverse: 5'- GCTGTGGACATCCAGAAGTTGG-3'
Mouse *Gapdh*	Forward: 5'- CATCACTGCCACCCAGAAGACTG-3' Reverse: 5'- ATGCCAGTGAGCTTCCCGTTCAG-3'
Human *SFTPC*	Forward: 5'- GCA AAG AGG TCC TGA TGG AG-3' Reverse: 5'- TGT TTC TGG CTC ATG TGG AG-3'
Human *SFTPB*	Forward: 5'- TGC CTG GAC CAC CTC ATC CTT G-3' Reverse: 5'- GTC CTC ACA CTC TTG GCA TAG G-3'
Human *ACTA2*	Forward: 5'- CTATGCCTCTGGACGCACAACT-3' Reverse: 5'- CAGATCCAGACGCATGATGGCA-3'

Human *CTHRC1*	Forward: 5'- CAGGACCTCTTCCCATTGAAGC-3' Reverse: 5'- GCAACATCCACTAATCCAGCACC-3'
Human *SCGB3A2*	Forward: 5'- GGCTAAGGAAGTGTGTAAATGAGC-3' Reverse: 5'- CCATCCACCTCCGCTCTTTATC-3'
Human *MUC5B*	Forward: 5'- CTGCTACGACAAGGACGGAAAC-3' Reverse: 5'- AAGGCTGTGAGCGCACTGGATG-3'
Human *DKK3*	Forward: 5'- GTGCATCATCGACGAGGACTGT-3' Reverse: 5'- TGGTCTCCACAGCACTCACTGT-3'
Human *GAPDH*	Forward: 5'- GTCTCCTCTGACTTCAACAGCG -3' Reverse: 5'- ACCACCCTGTTGCTGTAGCCAA -3'

Table 4 Polymerase chain reaction mixture composition:

PCR component		**Volume/reaction (µL)**
Master Mix	2x SensiMix™ SYBR® &Fluorescein	12.5
	100 µM Forward primer	0.1
	100 µM Reverse primer	0.1
	H_2O	7.3
cDNA		5
total		25

Table 5 RT-PCR cycle conditions:

Step	**Tm**	**Time**	**Number of cycles**
Initial denaturation	95 °C	10 min	1
denaturation	95 °C	15 sec	40
Annealing	60-65 °C	30 sec	40
Extension	72 °C	60 sec	40
Final extension	72 °C	1 min	1
Hold	4 °C	indefinite	1

2.3.7 ELISA

The concentration of IL-6 cytokine in the supernatant was quantified using a commercially available sandwich ELISA kit carried out according to the manufacturer's instructions and a BMG microplate reader.

2.3.8 Single-cell RNA sequencing

2.3.8.1 Single-cell dissociation

ALI cultures of three transwells per group were dissociated to obtain a single-cell solution after 2 days of airlift using TrypLE™ Express Enzyme. Organoids were digested by 200 uL dispase/well at 37°C for 45 mins, followed by single-cell dissociation through the addition of TrypLE™ Express Enzyme for 5 mins at 37°C. Cell suspensions were filtered through a 40 μm strainer and washed twice in PBS, counted, and critically assessed for single-cell separation and overall cell viability.

2.3.8.2 Cell captures and library preparation

Cell captures and library preparation were performed by Sarah Miethe from Marburg using the BD Rhapsody™ Single-Cell Analysis System according to manufacturer’s protocols. Briefly, cells were initially incubated with an individual barcode-labelled antibody (Human Single-Cell Multiplexing Kit or Mouse Immune Single-Cell Multiplexing Kit) for 20 mins at RT. Cells were washed twice with BD pharmingen stain buffer and viability-stained with 2 mM calcein AM and 0.3 mM Draq7 for 5 mins at 37°C. Cells were counted using a disposable hemocytometer and cell viability was determined. The BD Rhapsody cartridge was primed with 100% ethanol followed by 2 washes with cartridge wash buffer 1 and one wash with cartridge wash buffer 2. Approximately 30000 labelled cells were loaded and incubated for 15 mins at RT. Excess fluid was removed, the cartridge was loaded with cell capture beads and incubated for 3 mins at RT. Excess beads were washed off using sample buffer. Lysis buffer was applied and beads were extracted from the cartridge using the BD rhapsody express instrument and washed twice with cold bead wash buffer. The cDNA reaction

mix was prepared as indicated in the manufacturer's protocol and mixed with the beads. The mixture was incubated in a thermomixer at 37°C with 1200 rpm for 20 mins. The supernatant was removed and replaced by the exonuclease I mix prepared according to the manufacturer's protocol. The bead suspension was incubated in the thermomixer at 37°C with 1200 rpm for 30 mins, followed by 80°C without shaking for 20 mins. The suspension was then briefly placed on ice and the supernatant was removed. Finally, the beads were resuspended in bead resuspension buffer.

Single-cell mRNA and multiplex sample tag libraries were prepared using the WTA Amplification Kit according to the manufacturer's recommendations. Briefly, the bead resuspension buffer was removed, the beads were resuspended in elution buffer and incubated on a heat block at 95°C without shaking for 5 mins. The tube was briefly centrifuged and the supernatant was retained as sample tag product. The random primer mix was prepared as indicated in the manufacturer's protocol and mixed with the beads, then incubated using the following conditions: a heat block without shaking at 95°C for 5 mins, and at 1200 rpm in the thermomixer at 37°C for 5 mins followed by 25°C for 15 mins. The extension enzyme mix was prepared as indicated in the manufacturer's protocol and added to the beads, then incubated at 1200 rpm in the thermomixer at 25°C for 10 mins, 37°C for 15 mins, 45°C for 10 mins, and 55°C for 10 mins. The primer and enzyme mix were replaced by elution buffer and denatured on a heat block without shaking at 95°C for 5 mins. Afterwards, the beads were resuspended using a thermomixer at 1200 rpm for 10 secs. The supernatant was retained as the random primer extension product (RPE Product) and purified using AMPure XP magnetic beads. The purified product was further amplified by a second PCR of 12 cycles and then purified using AMPure XP beads, resulting in the RPE PCR product. The concentration of the RPE PCR product was determined using the Agilent 2100 Bioanalyzer with the High Sensitivity DNA Kit. The RPE PCR product was diluted with elution buffer to yield concentration of 2 nM of the 150 - 600 bp peak and then amplified by the final WTA index PCR for 8 cycles with subsequent dual-sided cleanup using AMPure XP beads afterwards.

The sample tag PCR1 reaction mix was prepared as indicated in the manufacturer's protocol and mixed with the sample tag product. The sample tag product was amplified in the thermal cycler for 11 cycles of the PCR program indicated in the protocol, followed by purification using AMPure XP beads. Sample tag PCR1 product was amplified with a second PCR of 10 cycles, followed by purification using AMPure XP beads. The resulting sample tag PCR2 product was amplified by the final sample tag index PCR for 7 cycles, followed by purification. Concentrations of WTA and sample tag index PCR products were determined using the Qubit Fluorometer and the Qubit dsDNA HS Kit and quality control was performed on the Agilent 2100 Bioanalyzer with the High Sensitivity DNA Kit.

Cells were captured and final libraries were sequenced on the Novaseq 6000 platform (Illimina, USA) with 50,000 reads per cell. Raw sequencing reads were processed with the BD Rhapsody™ WTA Analysis Pipeline on the Sevenbridges platform.

2.3.8.3 Processing of scRNA-seq data

Unique Molecular Identifier (UMI) counts were processed using the Seurat package (version 4.1.1) in R software (version 4.1.3). Low-quality cells were removed, i.e. those with less than 300 genes expressed or with mitochondrial reads greater than 20% of the total reads per cell. The filtered dataset was normalized and scaled using the Seurat NormalizeData and ScaleData functions, using the default parameters. Data were integrated using the RunHarmony command and cell clusters were identified using a Shared Nearest Neighbour (SNN) based algorithm. Unified Modal Approximation and Projection (UMAP) was used for cell cluster visualisation.

Single-cell pseudotime trajectories were generated using the Monocle3 package (Version 1.2.7) in R. The FindMarkers command in Seurat was used for Differentially Expressed Gene (DEG) analysis. GSVA and AUCell were used for signaling pathway analysis, with the gene set list of signaling pathways obtained from the MSigDB database.

Regulon analysis was performed by Kathrin Kattler from Saarbrücken using the python

implementation of SCENIC pySCENIC (version 0.12.0) based on CPM normalized counts. Adjacencies were calculated with pyscenic grn, and motifs were pruned with pyscenic ctx against mm10 databases (mm10__refseq-r80__10kb_up_and_down_tss.mc9nr.genes_vs_motifs.rankings.feather; mm10__refseqr80__500bp_up_and_100bp_down_tss.mc9nr.genes_vs_motifs.rankings.feather). The activity scores of the regulons were then obtained using pyscenic AUCell and visualized using scanpy (version 1.9.1).

2.3.9 Animal experiments

2.3.9.1 Mice

DKK3 knockout (*DKK3*$^{-/-}$) mice were kindly provided by Prof. Timoteus Speer (University Hospital Frankfurt, Germany). Littermates were used as WT control. Animal experiments were performed in accordance with all relevant national regulations and were authorized by the local research ethical committee. All animal experiments were approved by the Landesamt fur Soziales, Gesundheit und Verbraucherschutz of the State of Saarland in agreement with the national guidelines for animal treatment.

2.3.9.2 Bleomycin-dependent model

In the bleomycin-dependent model, 8- to 10-weekold male mice were treated with a single intratracheal administration of bleomycin induced by intubation (maximum 50 µL). It is known that the effect of bleomycin depends on the respective batch, so a range of 0.35 to 0.65 mg/kg body weight in NaCl was used. Control animals received NaCl (0.9%). The bleomycin and NaCl were administered under anesthesia (10 µL/g of anaesthetization cocktail per mouse). The animals woke up from the anesthesia after about 1-2 hours. Body weight of the mice was observed over 21 days. 21 days after administration of bleomycin the lungs were analyzed histologically and by means of lung function.

2.3.9.3 Lung function measurements

Lung function measurements were obtained using FlexiVent^{TM} system equipped with SCIREQ flexiWare software. After calibrating the cylinder pressure, airway opening pressure and dynamic tube, the mouse was anaesthetized by injecting the suggested volume (10 µL/g per mouse) of the solution. After waiting 7-10 mins until the mouse was completely reflex-free, the trachea was exposed and a steel cannula was inserted into the upper trachea as a bypass. The mouse was then computer-assisted ventilated via the bypass. A pump was used to deliver oscillating air streams into the respiratory system of the mouse and the resulting pressure and volume changes were recorded. The exact maneuvers of the lung function measurement are listed in Table 6. After the measurement, the animal was euthanized for further sampling.

Table 6 Ventilation maneuvers of the lung function measurement and their measurement parameters:

Maneuver	**Model**	**Parameter**
Single-Frequency forced oscillation waveform	Single compartment model	Compliance Elastance Resistance of resp. systems
Multi-Frequency forced oscillation waveform	Constant Phase Model	Tissue damping
Pressure-Volume-Loop (P-V-Loop)	P-V Loop Salazar Knowles Equation	Total lung capacity Quasi-static compliance

2.3.9.4 Preparation of mouse lungs and embedding

The lung was carefully dissected from the mouse. 4% PFA was introduced into the lungs at a constant pressure of 30 cmH_2O for at least 15 mins. After that, the lungs were tied with a string under the pressure of the column and transferred to 50 mL reaction tubes and overlaid with 40 mL of 4% PFA. After 24 hours, the PFA was replaced and fixation continued for another 24 hours. The prepared lungs were washed out several times with PBS and dissected free of attached tissue and organs such as the heart,

thymus and esophagus. The whole lungs were pre-embedded in PBS buffered 1% agarose solution at 60°C overnight. After the lungs had cooled in the agarose the next day, they were pre-cut into 5-millimetre-thick blocks cranial to caudal and transferred to embedding dishes. The sections were overlaid with 1% agarose solution. The hardened blocks were stored in 4% PFA at room temperature until paraffin embedding. 4 µm thick sections were cut and stored in the dark and protected from dust at RT until further staining.

2.3.9.5 Fibrosis score

Bleomycin-induced lung fibrosis was assessed using the Ashcroft score as previously described (Ashcroft, Simpson, and Timbrell 1988). Lung tissue was scored from 0 to 8, with increasing extent of fibrosis in lung histological samples. Sections of mouse lungs were stained with H&E and scanned using an Olympus fluorescent microscope. The pictures from each mouse lung were graded by a technician who was blinded to the results.

2.3.9.6 Picro-Sirius Red staining

Collagen content was assessed by Picro-Sirius Red staining of lung sections, and the area of collagen was viewed using standard light microscopy according to the manual. Briefly, lung sections were deparaffinized and hydrated with distilled water. |Picro-Sirius Red Solution was added to the tissue section and incubated for 60 mins. The slide was then quickly rinsed in two changes of Acetic Acid Solution (0.5%). It was then rinsed using absolute alcohol and dehydrated in 2 changes of absolute alcohol, cleared, and mounted in synthetic resin.

2.3.10 Data analysis and statistics

GraphPad Software (version 8.0), San Diego, CA, was used for statistical analysis. Student's *t*-test was used to compare two experimental groups, and two-way ANOVA or one-way ANOVA were used for comparisons among more than two experimental

groups, as indicated in the figure legends. The results were considered statistically significant for $P < 0.05$.

2.3.11 Study approval

Human lung tissue was obtained from patients undergoing lung surgery at the Clinic of Saarland University and SHG Clinic Voelklingen/Saar. Ethical approval was obtained for the work described. Informed consent was obtained from patients. Mouse Organ harvesting was approved by the Landesamt für Soziales, Gesundheit und Verbraucherschutz of the State of Saarland in accordance with the national guidelines for animal treatment.

3. RESULTS

3.1 Establishment of human adult stem cell-derived lung alveolar organoid model

Fibroblasts are closely associated with physiological or pathological processes such as wound healing and IPF (Waters et al. 2018). It is believed that excessive proliferation and activation of fibroblasts in the lung parenchyma significantly contributes to the development and progression of IPF (Richeldi, Collard, and Jones 2017). Defective activation of fibroblasts probably also plays a role in other chronig lung diesases such as COPD. Organoid models have great potential to provide disease-relevant insights into the interaction between fibroblasts and pneumocytes (Kim et al. 2021). It was the aim to develop and characterize organoid models in which the effect of fibroblasts on pneumocytes can be examined.

3.1.1 Co-culturing with fibroblasts alters the morphology of the alveolar organoids

To study the interaction of fibroblasts with human lung pneumocytes, primary pneumocytes were differentiated into organoids in the presence of primary fibroblasts. Freshly excised human lung tissue was divided into two parts for the isolation of fibroblasts and pneumocytes. AT2 cells were isolated using the MACS system with a primary HT2-280 antibody and differentiated into organoids in Matrigel. Organoids were dissociated, pneumcytes were sorted again by MACS and cultued in Matrigel in the absence or presence of fibroblasts (Fig. 5A). Fibroblasts were verified by H&E staining and fluorescence microscopy. The primary fibroblast stained positively for collagen I and anti-fibroblast (TE-7) antibodies. The human bronchial epithelial cell line 16HBE-14o served as a negative control and MRC5 (a human fetal lung fibroblast cell line) as a positive control (Fig. 5B). Cytospins showed that immediately after pasaging, 89.6% of the cells were double positive for SFTPC and HT2-280 (Fig. 5C).

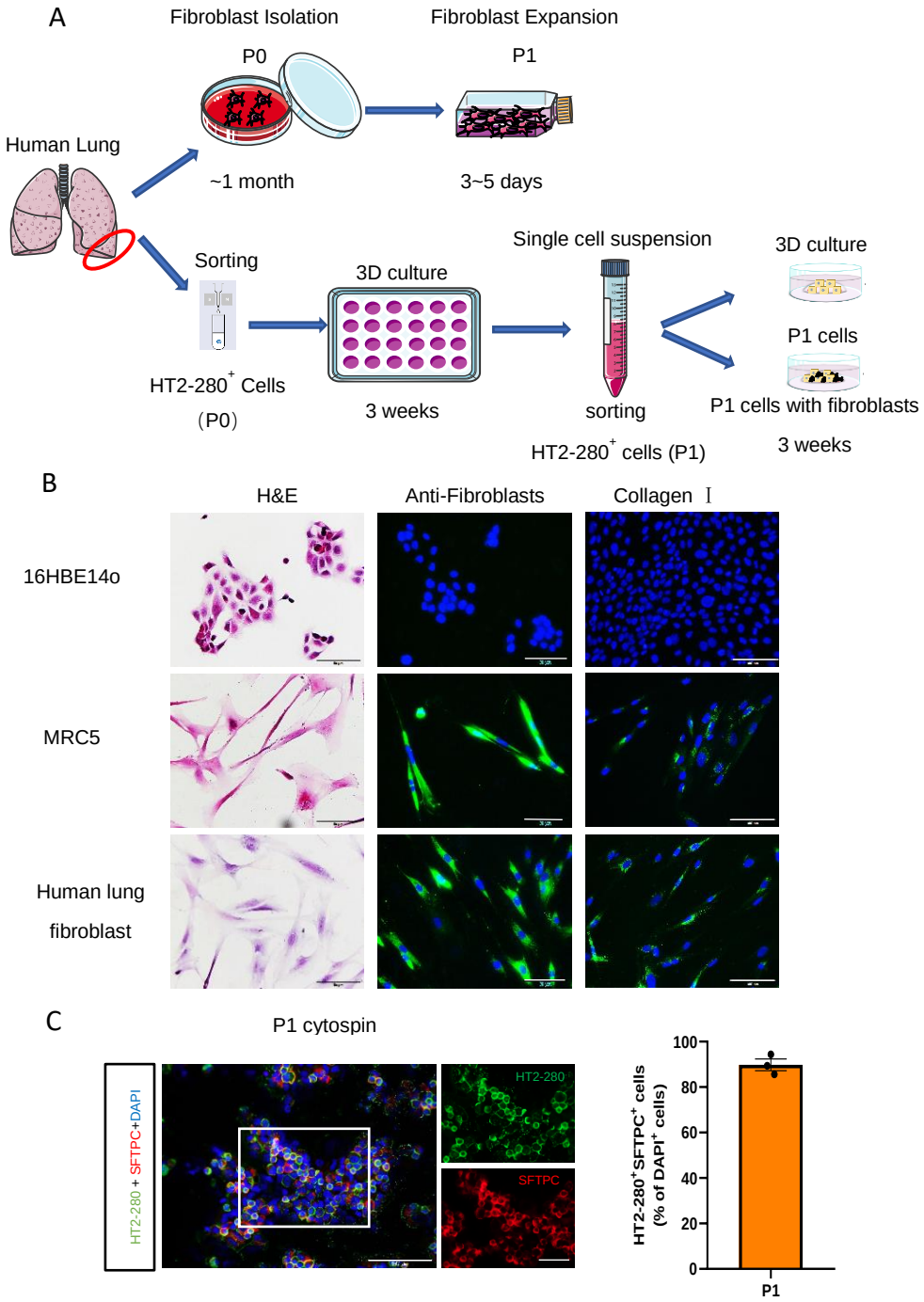

Fig 5. Establishment of the pneumocyte-fibroblast co-culture organoid model. **(A)** Scheme of the experimental procedures. **(B)** Fibroblasts were verified by H&E and IF staining. Scale bar = 50 µm. **(C)** Cytospins derived directly after passaging (P1) were stained for SFTPC and HT2-280 by immunofluorescence (Left panel: Scale bar = 100 µm; Right panel: scale bar = 50 µm). The fraction of cells double positive for SFTPC and HT2-280 was quantified (n=3 independent experiments, data are shown as mean ± SEM).

The morphology of alveolar spheroids was modified when co-cultured with fibroblasts (Fig. 6A). Approximately 96% of organoids in the absence of fibroblasts were grape-like, whereas organoids in the presence of fibroblasts had significantly increased luminal cystic and decreased grape-like architecture (Fig. 6B). H&E staining also showed that organoids without fibroblasts consisted mainly of cuboidal cells, while those with fibroblasts consisted of flattened cells (Fig. 6C). The co-culture with fibroblasts led to a larger diameter (Fig. 6D) of the organoids and a slightly increased colony formation efficiency (CFE) (Fig. 6E).

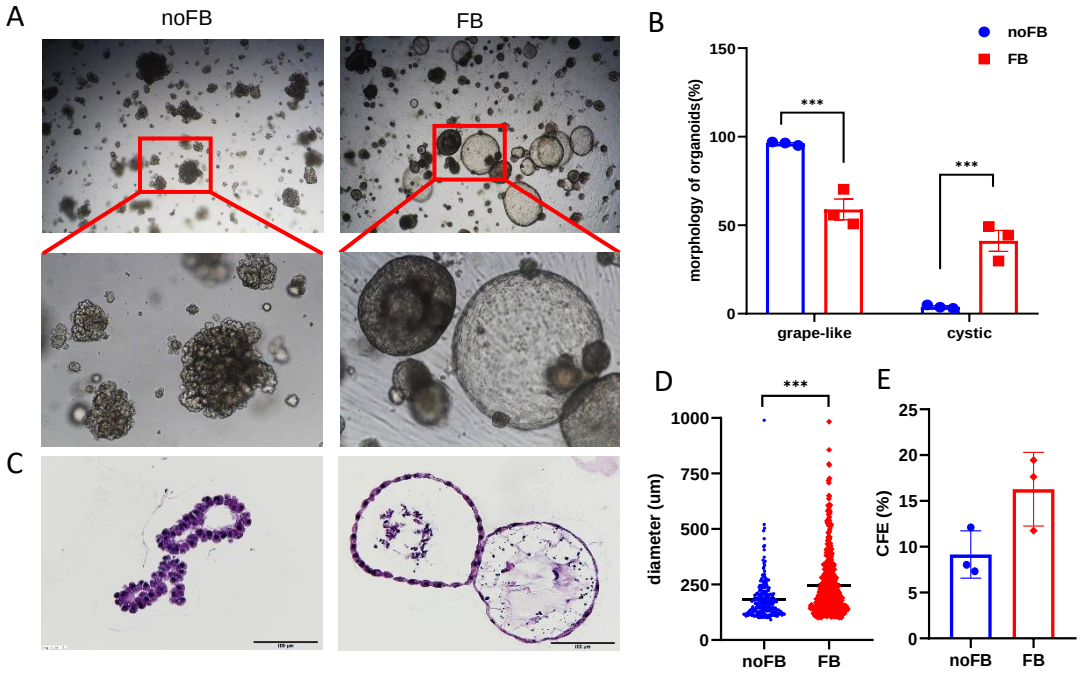

Fig 6. Morphological appearance of alveolar organoids in the absence or presence of fibroblasts. **(A)** Live-cell imaging (phase contrast) of the organoid cultures (noFB: without fibroblasts, FB: with fibroblasts) was performed at low magnification (×2.5, up) and high magnification (×10, down). **(B)** Quantification of the shape of the alveolar spheroids (n=3 independent experiments). **(C)** Morphology staining by H&E. Scale bar = 100 μm. Quantification of **(D)** diameter (600 organoids from 3 independent experiments**)** and **(E)** CFE of alveolar spheroids (n=3 independent experiments). Data were shown as mean ± SEM and compared by unpaired t-test. ***$p < 0.001$.

3.1.2 scRNA-seq reveals a secretory phenotype in co-cultures

In order to characterize the cellular composition of alveolar organoids, the model was analyzed using scRNA-seq (BD Rhapsody™ Single-Cell Analysis System). For this purpose, organoids from pneumocytes from one donor were co-cultivated with fibroblasts from three different donors. scRNA-seq was performed on two technical control replicates and the three fibroblast co-cultures (Fig. 7A). One fibroblast cluster and four epithelial clusters were identified in the UMAP (Uniform Manifold Approximation and Projection): $SFTPC^{high}$ cells, proliferating cells with high expression of *MKI67* and *TOP2A*, $SFTPC^{low}$ cells characterized by high expression inflammatory mediators and mucin *MUC5B*, $SFTPC^{-}$/$SCGB3A2^{+}$ cells, and collagen expressing fibroblasts (Fig. 7B to D). The four epithelial clusters all expressed typical AT2 markers (e.g. *NAPSA*, *SLC34A2*, and *NKX2*), but did not express markers for the airway epithelium (e.g. *S100A2*, *KRT5*) (Fig. 7D). Fibroblasts strongly influenced the formation of the various clusters. The $SFTPC^{low}$ population resulted almost exclusively from cells co-cultured with fibroblasts, while the $SFTPC^{high}$ cluster consisted of non-co-cultured cells (Fig. 7E). Fibroblasts only appeared in co-cultures (Fig. 7A to E). The fibroblasts were annotated according previously published human lung cell atlas reference (Kathiriya et al. 2022). In addition to expressing typical fibroblast markers (e.g. *PDGFRA*, *VIM*), fibroblasts from three different donors all showed low expression of alveolar fibroblasts markers, but high expression of IPF-like fibroblast genes (e.g. *CTHRC1*, *ACTA2*) (Fig. 7F).

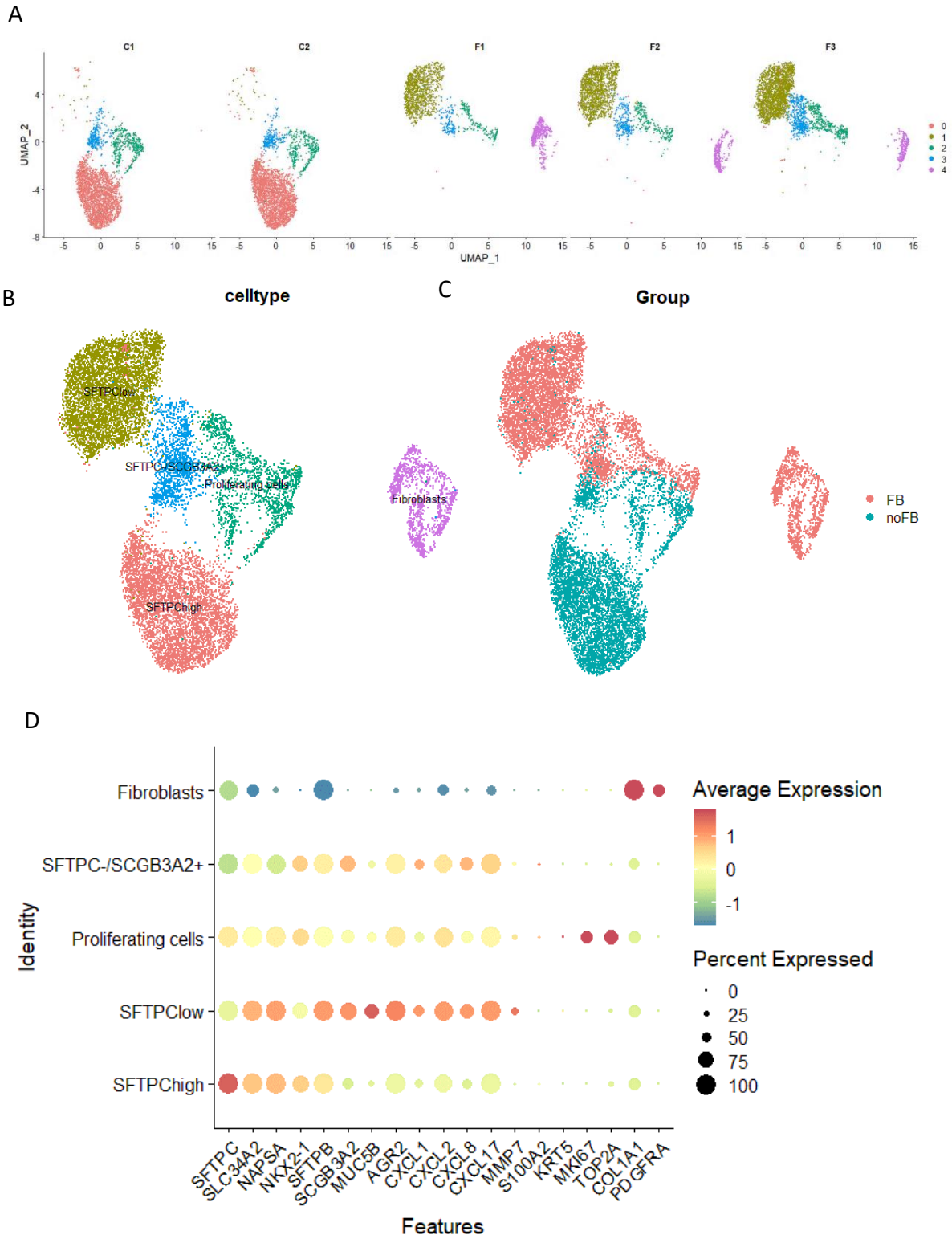
A
C1
C2
F1
F2
F3
UMAP_2
UMAP_1
0
1
2
3
4
B
celltype
SFTPClow
SFTPC-/SCGB3A2+
Proliferating cells
SFTPChigh
Fibroblasts
C
Group
FB
noFB
D
Fibroblasts
SFTPC-/SCGB3A2+
Proliferating cells
SFTPClow
SFTPChigh
Identity
Average Expression
1
0
-1
Percent Expressed
0
25
50
75
100
SFTPC
SLC34A2
NAPSA
NKX2-1
SFTPB
SCGB3A2
MUC5B
AGR2
CXCL1
CXCL2
CXCL8
CXCL17
MMP7
S100A2
KRT5
MKI67
TOP2A
COL1A1
PDGFRA
Features

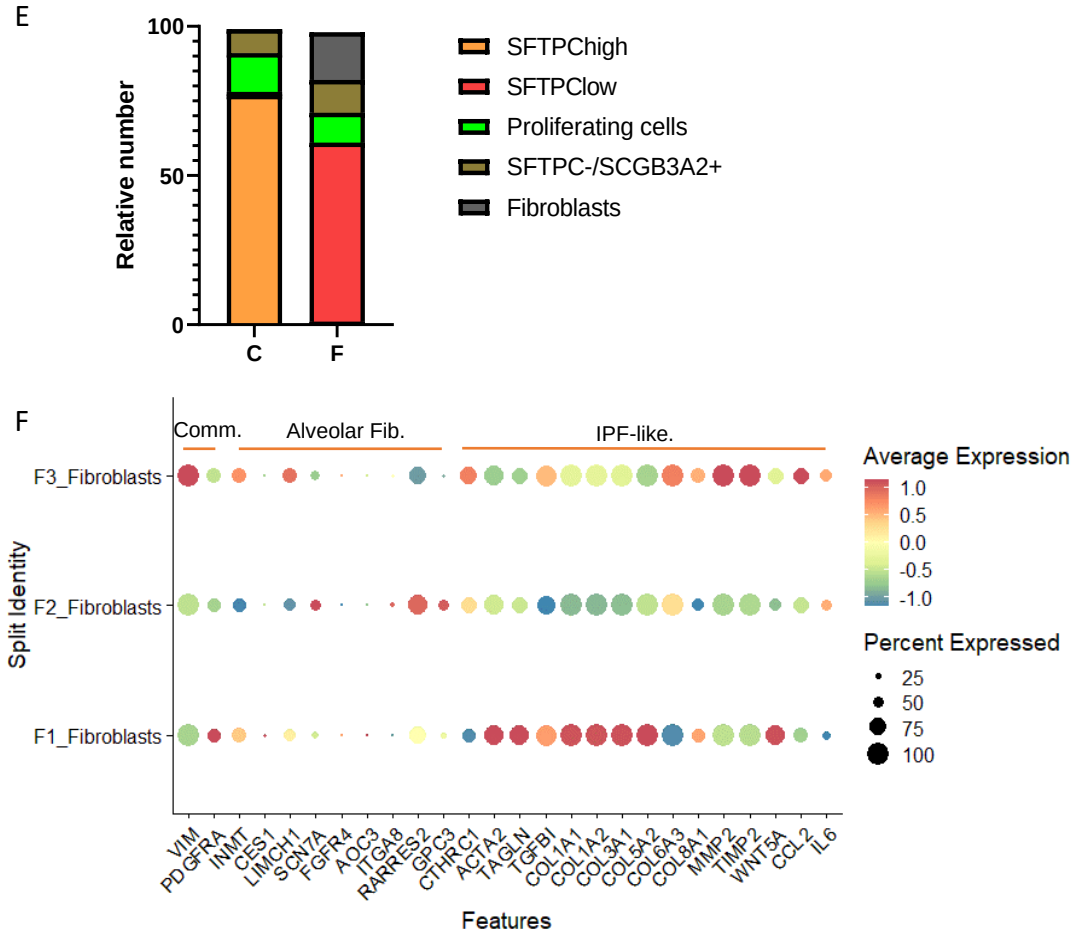

Fig 7. scRNA-seq analysis of the co-culture model. **(A)** UMAP visualization of five groups (C1 and C2: control groups. F1, F2 and F3: co-cultures with fibroblasts from 3 different donors). **(B)** UMAP visualization of all cells colored by the different clusters. **(C)** UMAP visualization of all cells colored by groups (red: FB. blue: noFB). **(D)** Intensity dot plot showing expression of epithelial cell type markers. **(E)** Proportion of different cell types in organoids in the absence (label: C) or presence (label: F) of fibroblasts. **(F)** Intensity dot plot showing expression of fibroblast cell type markers (comm.: common fibroblasts markers; Alveolar Fib.: Alveolar fibroblasts markers; IPF-like.: IPF-like fibroblasts markers).

Feature and violin plots further show the reduced expression of *SFTPC* and increased expression of *MUC5B* in cocultures (Fig. 8A and B). This finding was further verified by semi-quantitative RT-PCR in additional experiments. The expression of *SFTPC* was strongly reduced and the expression of *MUC5B* was strongly increased by the presence of fibroblasts (Fig. 8C).

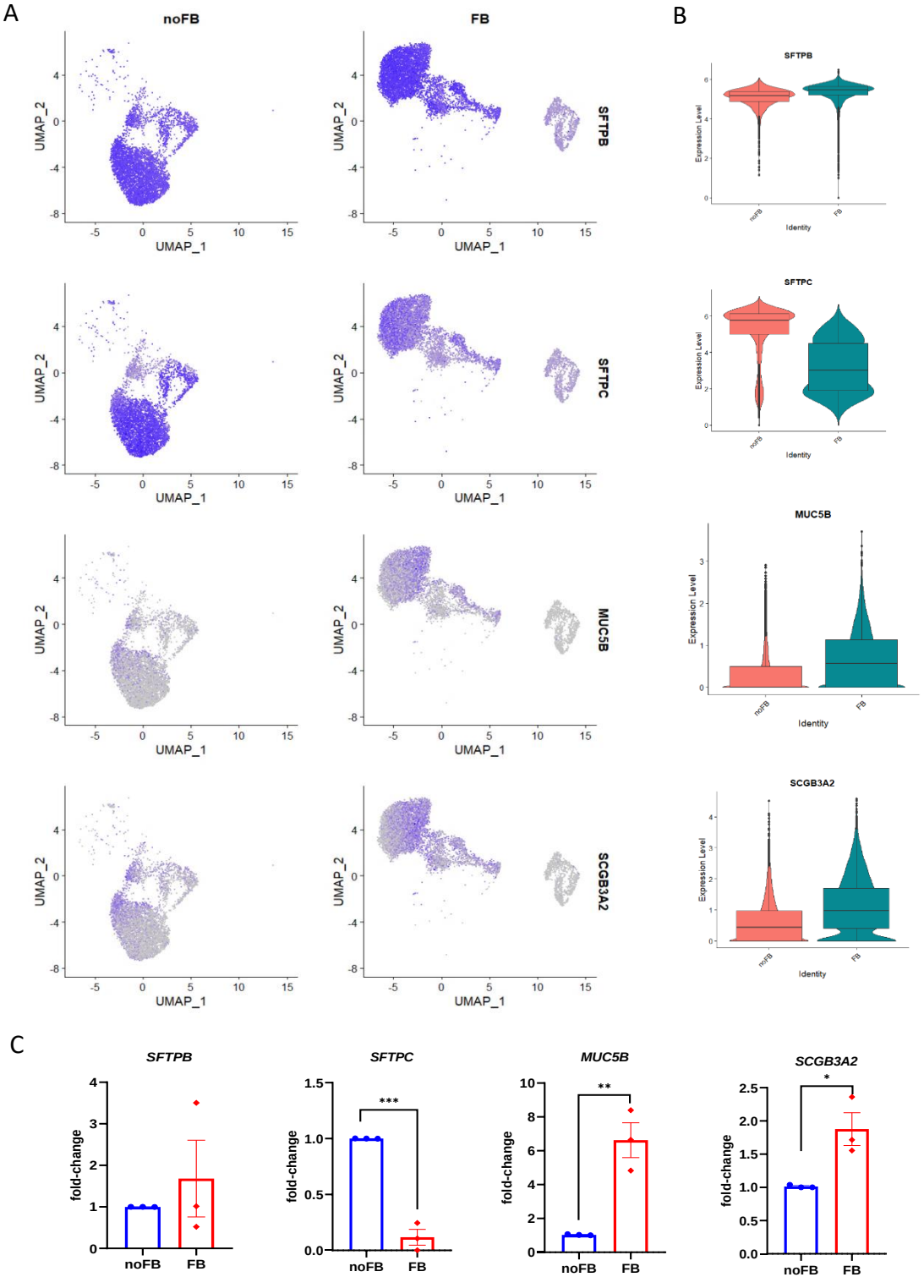

Fig 8. Fibroblasts enhance the expression of MUC5B in organoids. **(A)** Feature plots showing the expression of differentially expressed cell markers from organoids without (label: noFB)/with fibroblasts (label: FB). **(B)** Violin plots of selected cell markers. **(C)** The expression of selected cell markers was confirmed by semi-quantitative RT-PCR after 21 days culture (n=3 independent experiments with fibroblasts from 3 different donors in each experiment). Data were shown as mean ± SEM and compared by unpaired t test. *$p < 0.05$, **$p < 0.01$, ***$p < 0.001$.

3.1.3 Fibroblasts promote the formation and release of the MUC5B protein from organoids

Immunofluorescence staining showed that the co-culture with fibroblasts from all three donors led to a strongly reduced expression of SFTPC and an increased expression and release of MUC5B (Fig. 9A and B). 92% of organoids were positive for SFTPC in the fibroblast-free group, while only 7% of organoids were positive for SFTPC in the co-culture group. The proportion of $MUC5B^+$ organoids dramatically increased in organoids cultured with fibroblasts (Fig. 9C and D). The organoids were completely negative for airway markers SCGB1A1 and KRT5 (Fig. 9E).

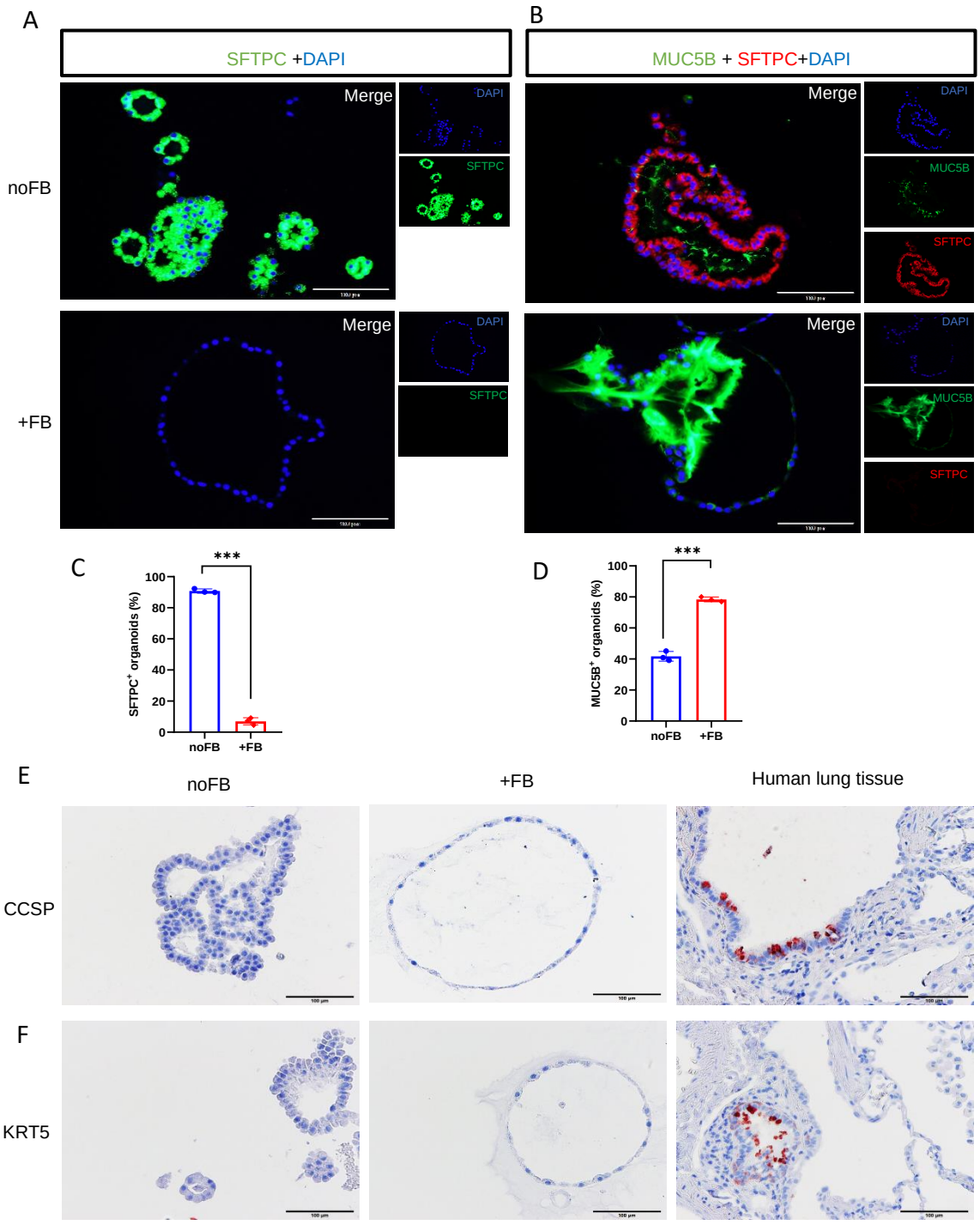

Fig 9. Fibroblasts induce the expression and release of MUC5B protein. Immunofluorescence was performed for **(A)** SFTPC alone or **(B)** the combination of SFTPC and MUC5B. Scale bar = 100 μm. The fraction of **(C)** $SFTPC^+$ organoids and **(D)** $MUC5B^+$ organoids was quantified (n=3 independent experiments). Data were shown as mean ± SEM and compared by unpaired *t* test. ***$p < 0.001$. **(E)** Immunohistochemistry was performed for CCSP and KRT5 in organoids and human

lung tissue. Scale bar = 100 μm. noFB: organoids without fibroblasts; +FB: organoids with fibroblasts.

3.1.4 Bleomycin treatment exacerbates MUC5B expression in human AT2 organoids co-cultured with fibroblasts

Bleomycin exhibits anticancer effects through DNA double-strand breaks, but its side effect is to cause pulmonary fibrosis. Therefore, it is used as an experimental inducer of pulmonary in mouse models (Moeller et al. 2008). To study whether bleomycin treatment of organoids could also create a model of pulmonary fibrosis, bleomycin was added to cultures at a concentration of 30 ng/mL starting at day 14. Cultures were analyzed at day 21. Semi-quantitative RT-PCR results showed that bleomycin did not affect expression of *SFTPC* or *MUC5B* in organoids without fibroblasts, whereas bleomycin further enhanced the expression of *MUC5B* in organoids co-cultured with fibroblasts compared to the untreated group (Fig. 10A and B). The myofibroblasts maker *ACTA2* and fibrosis marker *CTHRC1* were increased in bleomycin treated organoids with fibroblasts (Fig. 10C and D). The expression of *DKK3*, which is derived by tubular epithelial cells and mediates kidney fibrosis (Federico et al. 2016), was also increased in bleomycin treated organoids in the presence of fibroblasts (Fig. 10E).

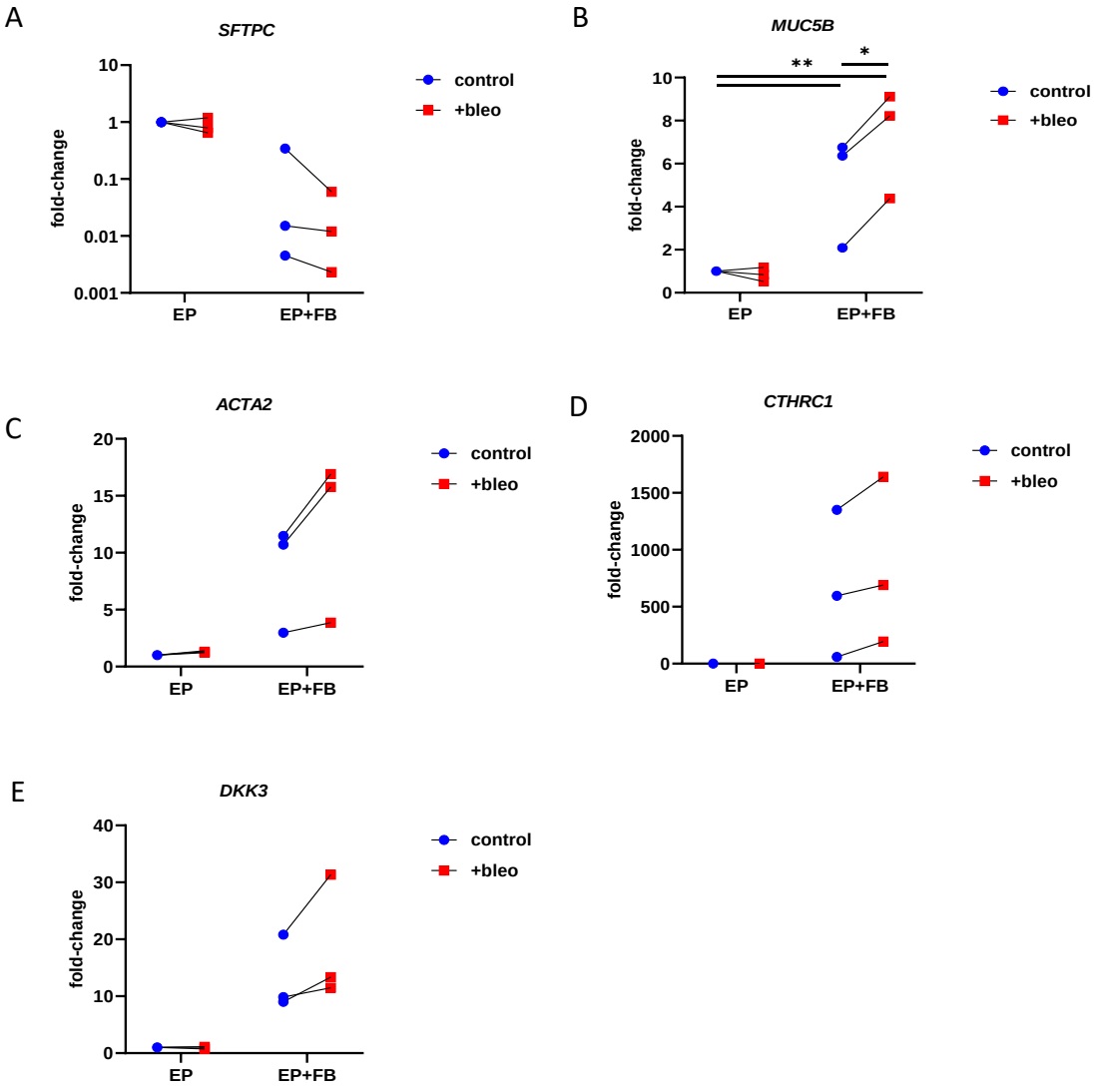

Fig 10. Treatment with bleomycin enhance MUC5B expression in organoids. The expression of **(A)** *SFTPC*, **(B)** *MUC5B*, **(C)** *ACTA2*, **(D)** *CTHRC1* and **(E)** *DKK3* was confirmed by semi-quantitative RT-PCR after bleomycin treatment (Control: untreatment, +bleo: Bleomycin treatment, EP: organoids without fibroblasts, EP+FB: organoids with fibroblasts, n=3 independent experiments). Data are shown as mean ± SEM and were compared by two-way ANOVA. $^{**}p < 0.01$, and $^{*}p < 0.05$

3.2 Establishment and characterization of an ALI- fibroblast coculture model

In ALI models, epithelial cells form an epithelial barrier on a filter membrane. Studies have shown that mouse lung cells express pneumocyte markers (e.g. *Sftpc*, *Hopx*) in such models (Wolf et al. 2016; 2017). However, the question is what is the composition of the lung epithelial cells in these models, how they differentiate and how fibroblasts regulate differentiation.

3.2.1 Fibroblasts enhance epithelial barrier formation in the ALI model

To analyze the interaction of murine fibroblasts and pneumocytes, pneumocytes were co-cultivated with primary fibroblasts in the ALI model. For this purpose, mouse lung tissue was freed from bronchial tissue and dissociated into cell suspensions. Lung epithelial cells were isolated using the MACS system by selecting for $EpCAM^+$ cells and $EpCAM^-$ cells. The $EPCAM^+$ cells were seeded directly onto the transwell, while the $EPCAM^-$ cells were cultured in conventional 2D cultures before being introduced into the ALI system. The $EpCAM^+$ cells were cultured in Transwell inserts with or without fibroblasts in the lower compartment. The apical chamber medium was aspirated after 2 days. Single cell sequencing was performed by the BD Rhapsody™ Single-Cell Analysis System 2 days after airlift (Fig. 11A). TEER was used to monitor the barrier formation of the epithelium. The results showed that co-culture with fibroblasts resulted in a significantly increased TEER as early as 48 hours after seeding (Fig. 11B). These results indicate that fibroblasts regulate the differentiation of pneumocytes and enhance the formation of an epithelial barrier.

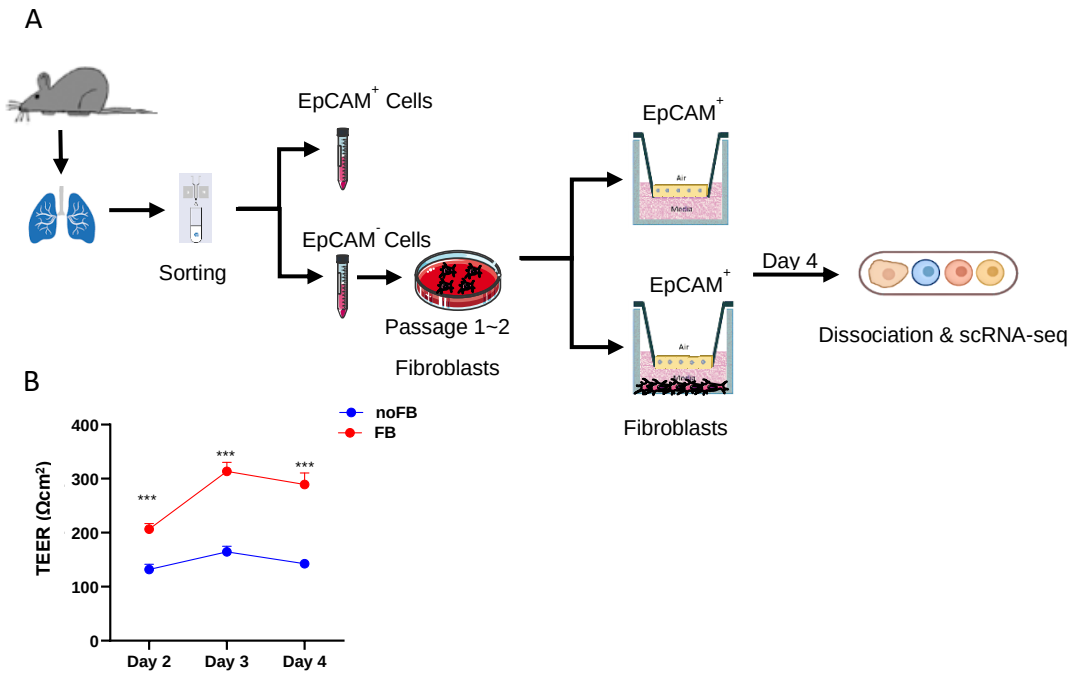

Fig 11. Fibroblasts support the formation of the epithelial barrier. **(A)** Schematic representation of the experimental setup. Mouse EpCAM$^+$ cells were isolated and cultured in ALIs for four days with and without fibroblasts. **(B)** TEER was measured every 24 hours (noFB: without fibroblasts, FB: with fibroblasts, n=5 independent experiments). Data were compared by two-way ANOVA. ***$p < 0.001$.

3.2.2 scRNA-seq reveals distinct populations of lung epithelial cells in the ALI model

scRNA-seq analyzes were performed 4 days after cell seeding. Cells grown at the filter membrane were differentiated by representative markers such as *Epcam* and *Cdh1* (Epithelial cells), *Pecam1* (Endothelial cells), *Ptprc* (Immune cells), *Cd3e* (T cells), *Cd19* (B cells), *Myh11* (Myoepithelial cells), *cd86* and *Itgae* (Dendritic cells), *Nkg7* and *Gzmb* (NK cells), *Wt1* (Mesothelial cells), and *Col1a1* (mesenchymal cells) (Fig. 12A and B). The co-culture with fibroblasts in the lower compartment had no major impact on the cell composition of the filter membrane. About 80.2% epithelial cells, 9.0% immune cells and 10.9% mesenchymal cells were identified in cultures without fibroblasts. About 85.1% epithelial cells, 6.1% immune cells and 8.8% mesenchymal cells were identified in cultures with fibroblasts (Fig. 12C and D).

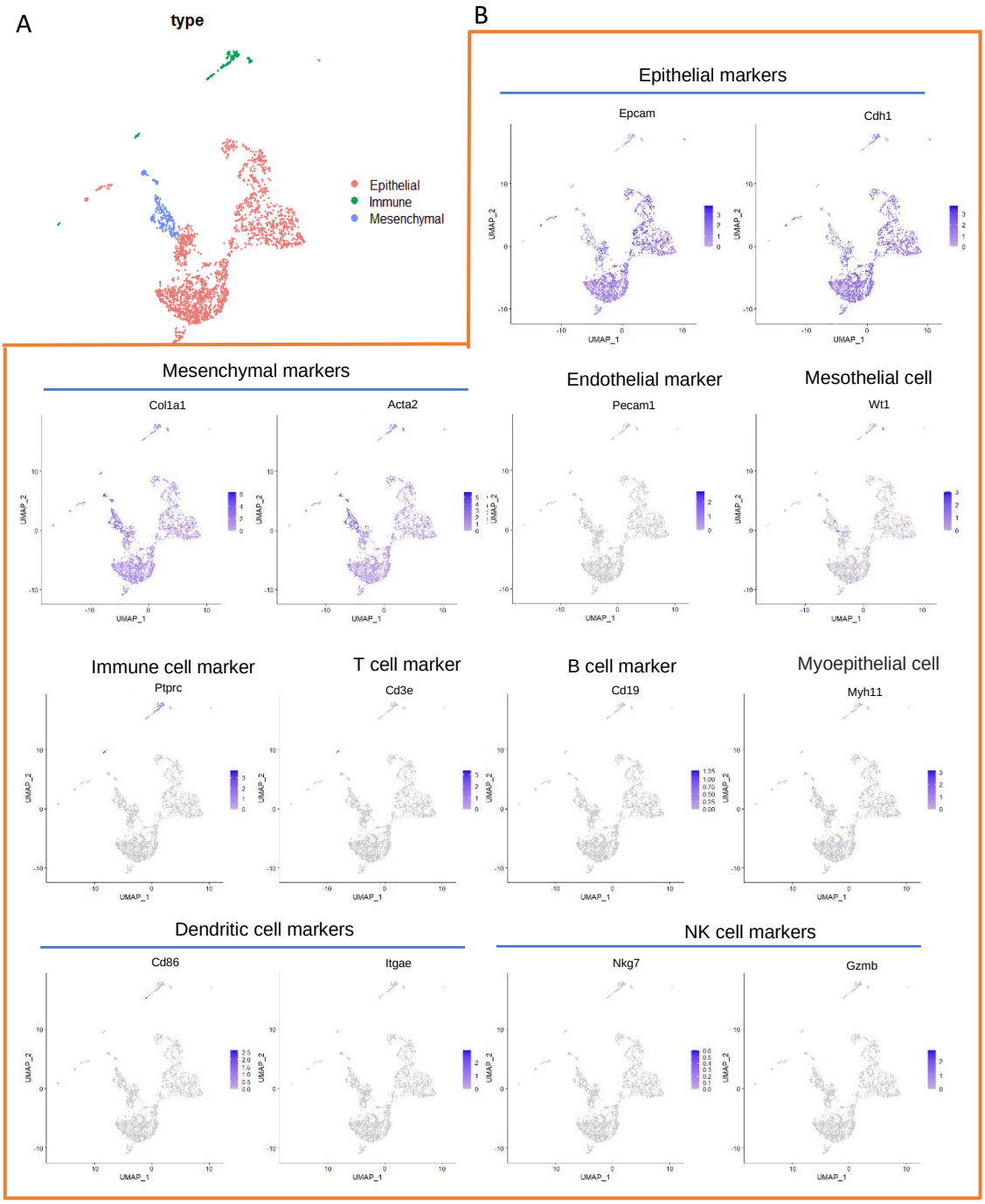
A
type
Epithelial
Immune
Mesenchymal
B
Epithelial markers
Epcam
Cdh1
Mesenchymal markers
Col1a1
Acta2
Endothelial marker
Pecam1
Mesothelial cell
Wt1
Immune cell marker
Ptprc
T cell marker
Cd3e
B cell marker
Cd19
Myoepithelial cell
Myh11
Dendritic cell markers
Cd86
Itgae
NK cell markers
Nkg7
Gzmb
UMAP_1
UMAP_2

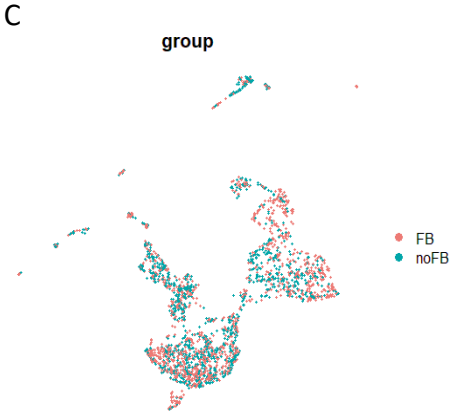
C
group
FB
noFB

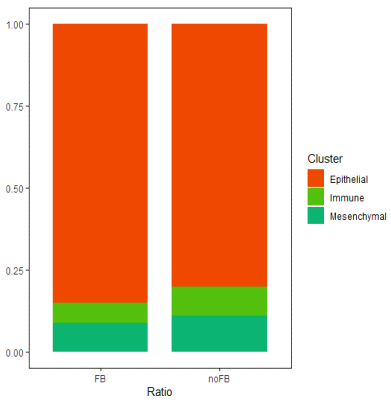
D
1.00
0.75
0.50
0.25
0.00
FB
noFB
Ratio
Cluster
Epithelial
Immune
Mesenchymal

Fig 12. scRNA-seq analysis of murine lung cells cultured in ALI. **(A)** UMAP visualization of major cell types. (**B**) UMAP plots of representative markers for the different cell types. **(C)** UMAP visualization of two group (noFB: without fibroblasts, FB: with fibroblasts). **(D)** Proportion of major cell types in the presence or absence of fibroblasts.

To further characterize the lung epithelial cells, the cells were divided into 8 clusters, which mainly consisted of pneumocytes and airway epithelial cells (Fig. 13A). The pneumocytes consisted of AT2-like cells with high expression of AT2 markers (e.g. *Sftpc*, *Lyz2*, *Lamp3*), immature AT1 (*Hopx*^{high}/*Sftpc*^{medium}) and AT1-like cells which had increased expression of AT1 markers (*Hopx*, *Aqp5*, *Krt7*). The pneumocytes thus formed a continuum from AT2 cells via immature AT1 cells to AT1 cells. A transitional cluster was also identified, which expressed both epithelial and mesenchymal cell markers (e.g. *Col1a1*, *Acta2*) at low levels. In the airway clusters, a large number of *Scgb1a1*-expressing club cells were identified, including intermediate club cells that co-expressed *Scgb1a1* and pneumocyte markers (eg, *Cldn18*, *Hopx*). Small numbers of *Krt5* and *Trp63*-expressing basal cells and *Mki67*-expressing proliferating cells were also found in this model (Fig. 13B and C). These data indicate that this regeneration model resembles the epithelia of the distal airways and lung parenchyma.

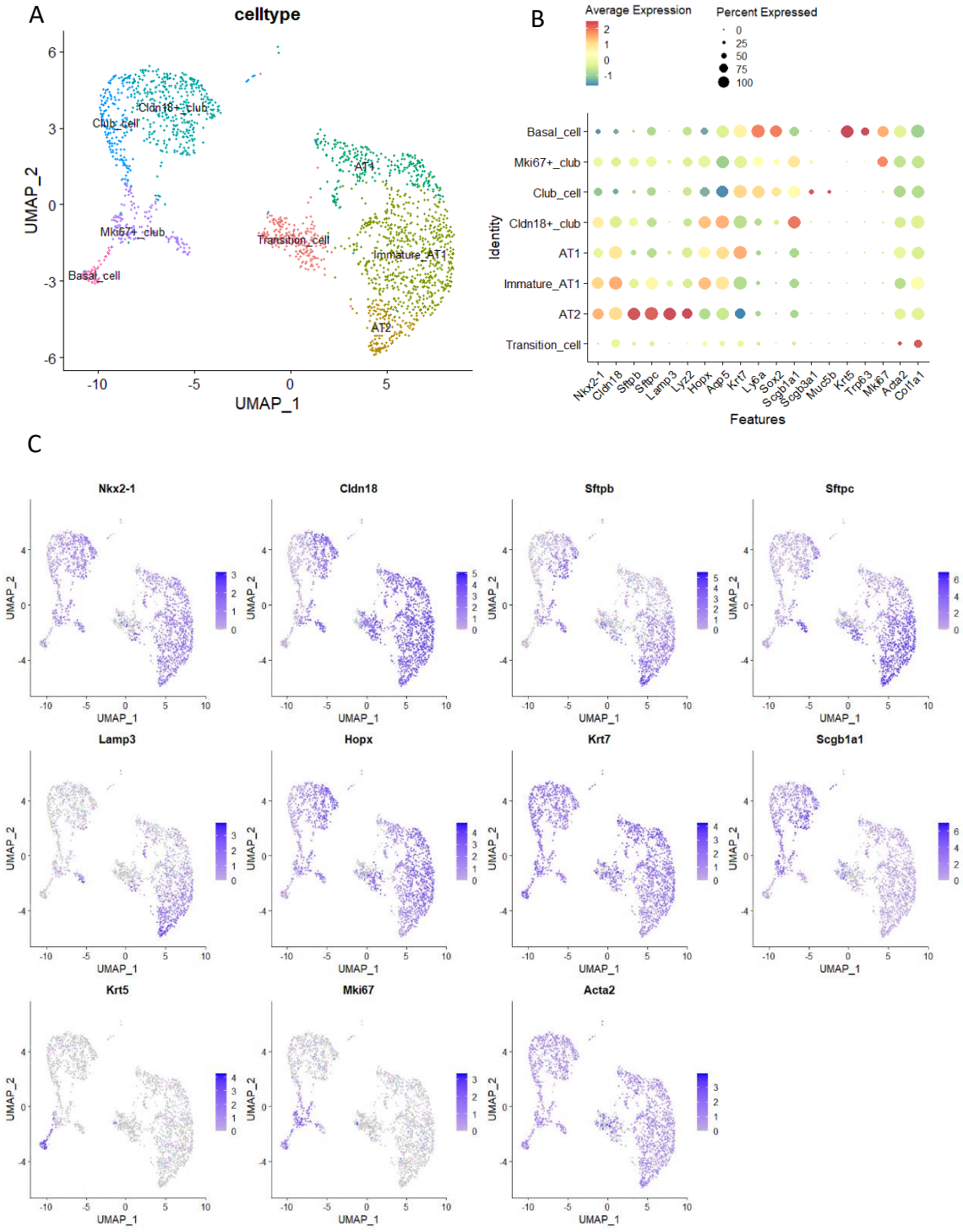

Fig 13. scRNA-seq analysis reveals distinct lung epithelial cell populations. **(A)** Major epithelial cell types identified are shown on a UMAP plot. **(B)** Gene expression of key markers for each epithelial cell types. **(C)** UMAP plots of representative markers for the different epithelial cell types.

3.2.3 Fibroblasts enhance expression of AT2 markers in AT2 cells and club cells

To further understand the role of fibroblasts on lung epithelial cells, differentially expressed gene (DEG) analysis was performed on epithelial cells co-cultured with and without fibroblasts. Results revealed the top five up-regulated genes in the co-culture group: *Sftpb* (avg_log2FC: 2.29, *P*=2.05e-55), *Scgb1a1* (avg_log2FC: 2.06, *P*=3.35e-10), *Cxcl15* (avg_log2FC: 1.91, *P*=2.95e-44), *Cbr2* (avg_log2FC: 1.86, *P*=3.96e-61), and *Cyp2f2* (avg_log2FC: 1.85, *P*=2.12e-21). *Sftpb*, *Cbr2* and *Cxcl15* are typical AT2 markers, while *Cyp2f2* and *Scgb1a1* mark club cells (Fig. 14A and B). Violin plots showed that co-culture with fibroblasts led to an increased expression of AT2 markers in both AT2 and club cells, whereas the expression of the club cell markers *Scgb1a1* and *Cyp2f2* was only enhanced in club cells. The expression of the cell cycle progress and proliferation marker *Ccnd1* was only increased in club cells (Fig. 14C). Additional experiments were performed for semi-quantitative RT-PCR analysis. Semi-quantitative RT-PCR analysis confirmed that co-culture with fibroblasts resulted in a significantly increased expression of pneumocyte and club cell markers (e.g. *Sftpc*, *Sftpb*, *Hopx*, *Aqp5* and *Scgb1a1*) as wells as tight junction factors (e.g. *Cldn18*) and *Ccdn1* (Fig. 14D). These results demonstrate that fibroblasts drive club cell proliferation and increase the expression of AT2 markers in AT2 cells and club cells.

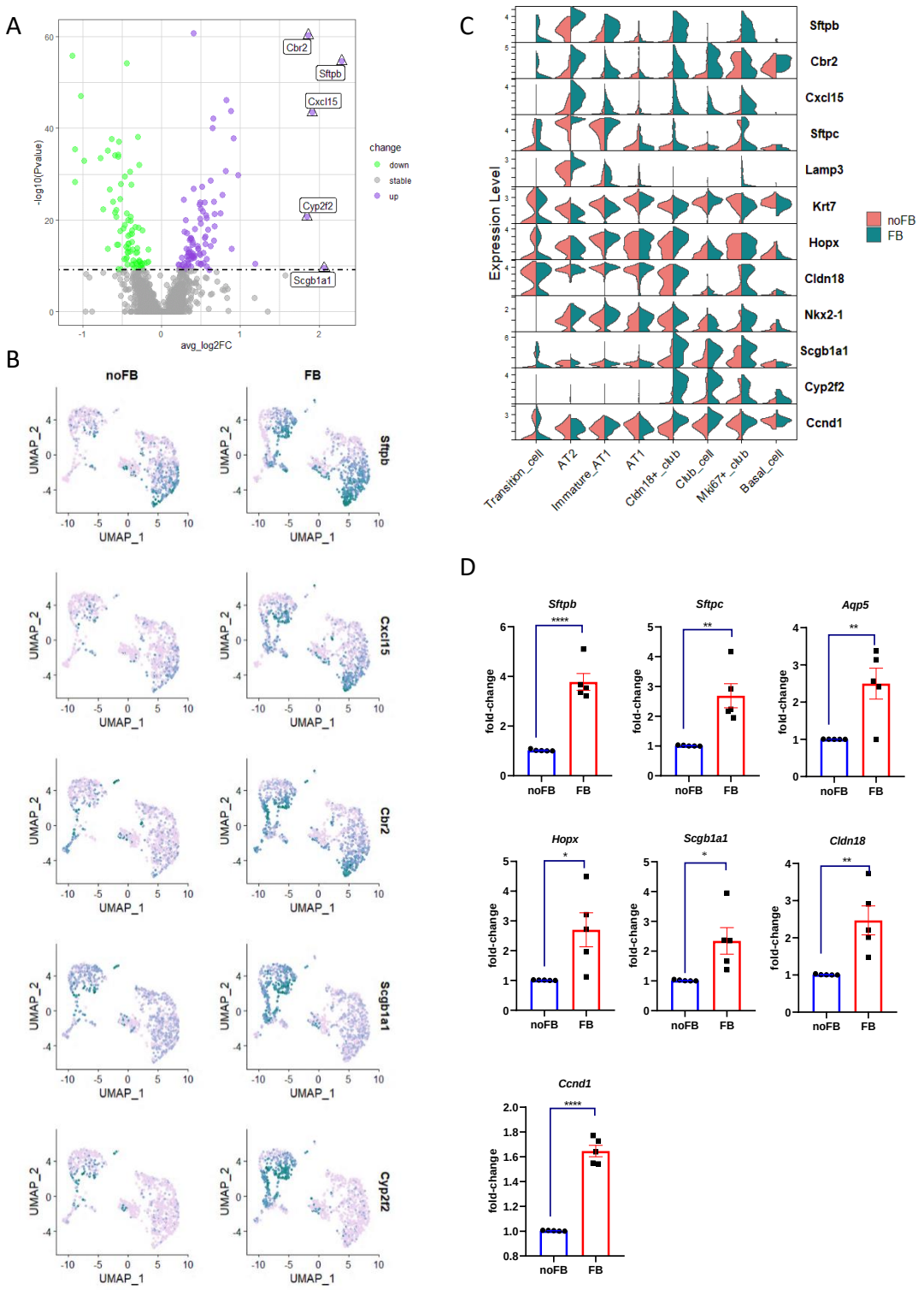

Fig 14. Co-culture with fibroblasts increases the expression of AT-2 markers in epithelial cells. **(A)** Volcano plot showing differentially expressed genes in epithelial cells co-cultured without fibroblasts. **(B)** Feature plots showing the expression levels of selected cell markers. **(C)** Violin plots showing the expression levels of differentially expressed genes in each cell type. **(D)** Expression levels of selected cell markers

(normalized to *Gapdh*) were analyzed by semi-quantitative RT-PCR 4 days after seeding (n=5 independent experiments). Data were compared by unpaired *t* test and are shown as mean ± SEM. *$p < 0.05$, **$p < 0.01$, ***$p < 0.001$, ****$p < 0.0001$.

Trajectory analysis of AT2 and club cells showed that mature AT2 cells (*Hopx*^{low}/*Sftpc*^{high}) differentiated into AT1 cells (*Hopx*^{high}/*Sftpc*^{low}) via immature AT1 cells (*Hopx*^{high}/*Sftpc*^{medium}). Typical club cells (*Scgb1a1*^{high}/*Cldn18*^{low}/*Hopx*^{low}) differentiated into *Cldn18*$^{+}$ club cells (*Scgb1a1*^{high}/*Cldn18*^{high}/*Hopx*^{high}) (Fig. 15A). To compare the cellular composition of pneumocytes and club cells immediately after isolation and after 4 days of ALI culture, cytospins were stained for SFTPC, CCSP and HOPX. Immunofluorescence staining showed that AT2 cells (45 %) and club cells (30 %) were the predominant cells in the isolated EpCAM^{+} cells. The proportions of AT2 cells and club cells were almost unchanged after 4 days in ALI cultures (Fig. 15B and C). However, there was a significant increase in SFTPC^{+} cells and CCSP^{+} cells co-expressing HOPX. The proportion of CCSP^{+}/HOPX^{+} club cells further increased when co-cultured with fibroblasts (Fig. 15C). The scRNA-seq results also showed an increase in the number of *Cldn18*$^{+}$ club cells in the co-culture group (Fig. 15D and E, Table 7).

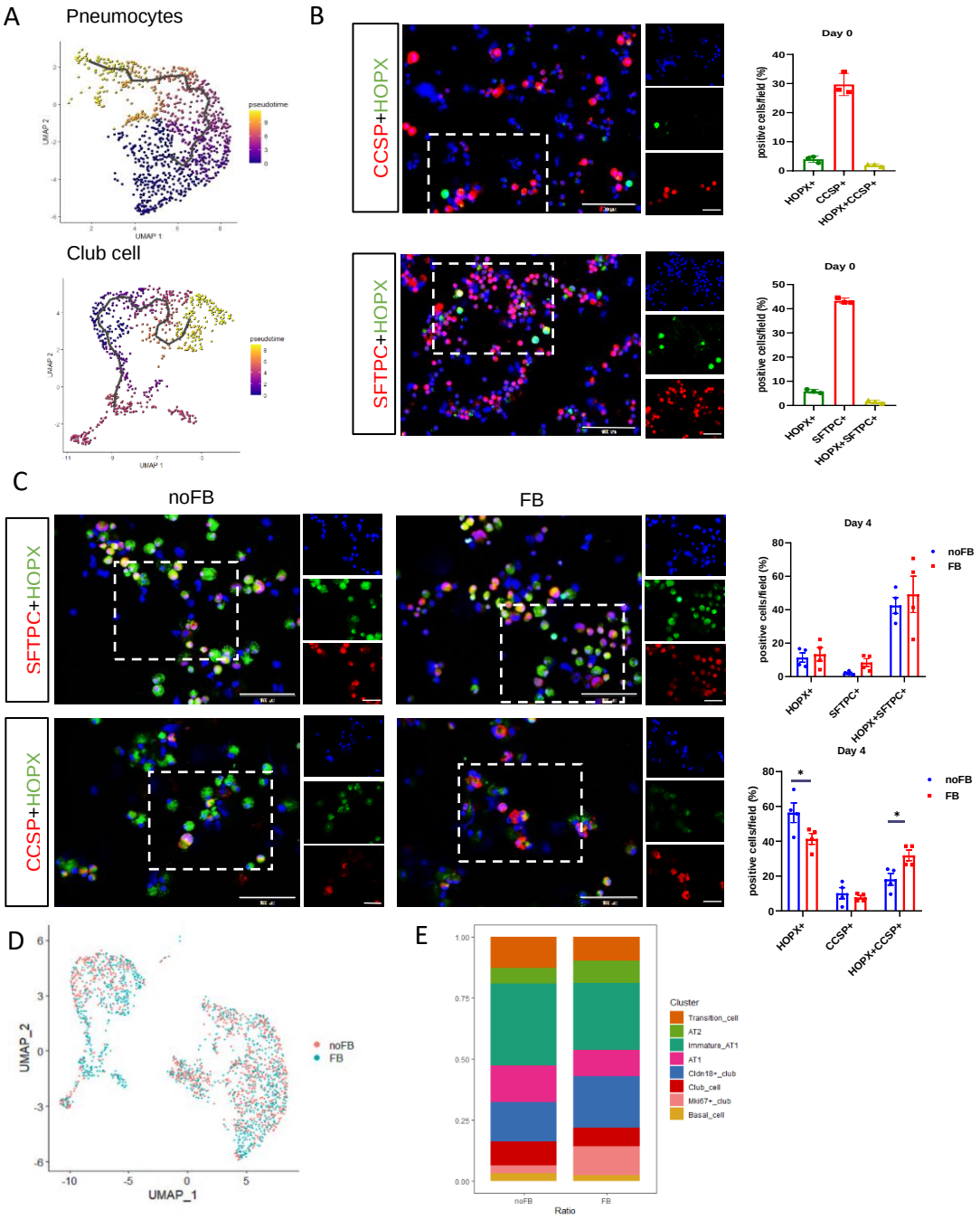

Fig 15. Fibroblasts promote AT-2 cell differentiation. **(A)** Pseudotime trajectory of epithelial cell types was determined by monocle3. Cytospins were prepared **(B)** before and **(C)** after four days of ALI culture and stained for SFTPC$^+$, HOPX$^+$, and CCSP$^+$ by immunofluorescence. Left panel: Scale bar = 100 µm; Right panel: scale bar = 50 µm. The proportion of cells that were positive for different markers was quantified. Data from a representative experiment was analyzed using Two-way ANOVA. *$p < 0.05$. **(D)** UMAP plot of epithelial cells colored by FB and noFB group. **(E)** Proportion of different epithelial cell types in the presence or absence of fibroblasts.

Table 7 Cell numbers and percentages of total cells for different epithelial cell types:

	cell number		**% of total**	
Celltype	**noFB**	**FB**	**noFB**	**FB**
Transition_cell	119	104	12.67	9.85
AT2	61	96	6.50	9.09
Immature AT1	315	289	33.55	27.37
AT1	140	115	14.91	10.89
Cldn18^{+} club	152	222	16.19	21.02
Club_cell	92	82	9.80	7.77
Mki67^{+} club	30	124	3.19	11.74
Basal cell	30	24	3.19	2.27
total	**939**	**1056**	**100**	**100**

The results show that in this ALI model, the isolated AT2 cells differentiate towards AT1 cells. There was only a slight difference in the ratio of club cells to pneumocytes immediately after isolation and after four days in culture, indicating a general potential of club cells and pneumocytes in the regeneration of the lung epithelium. Fibroblast promote the differentiation of club cells into AT2-like cells and the expression of AT2 markers in pneumocytes.

3.2.4 Co-culture with fibroblasts leads to increased activity of regulons that regulate AT2 cell differentiation

To analyze regulatory transcription networks, a regulon analysis was performed using SCENIC. The co-culture with fibroblasts led to the activation of numerous regulons in the different cell types (Fig. 16A). Regulon Irx1 was highly activated in pneumocytes in a fibroblast-independent manner. IRX1 was found to regulate AT2 cell differentiation (Yu et al. 2017) (Fig. 16B and C). The activity of Etv5, an essential regulon for AT2 identity and maintenance (Zhang et al. 2017), was increased in AT2 cells co-cultured with fibroblasts (Fig.16D and E). Co-culture with fibroblasts also increased the activity

of the Six1 regulon in club cells. Six1 plays an important role in the coordination of lung epithelial development (El-Hashash et al. 2011) (Fig. 16F and G).

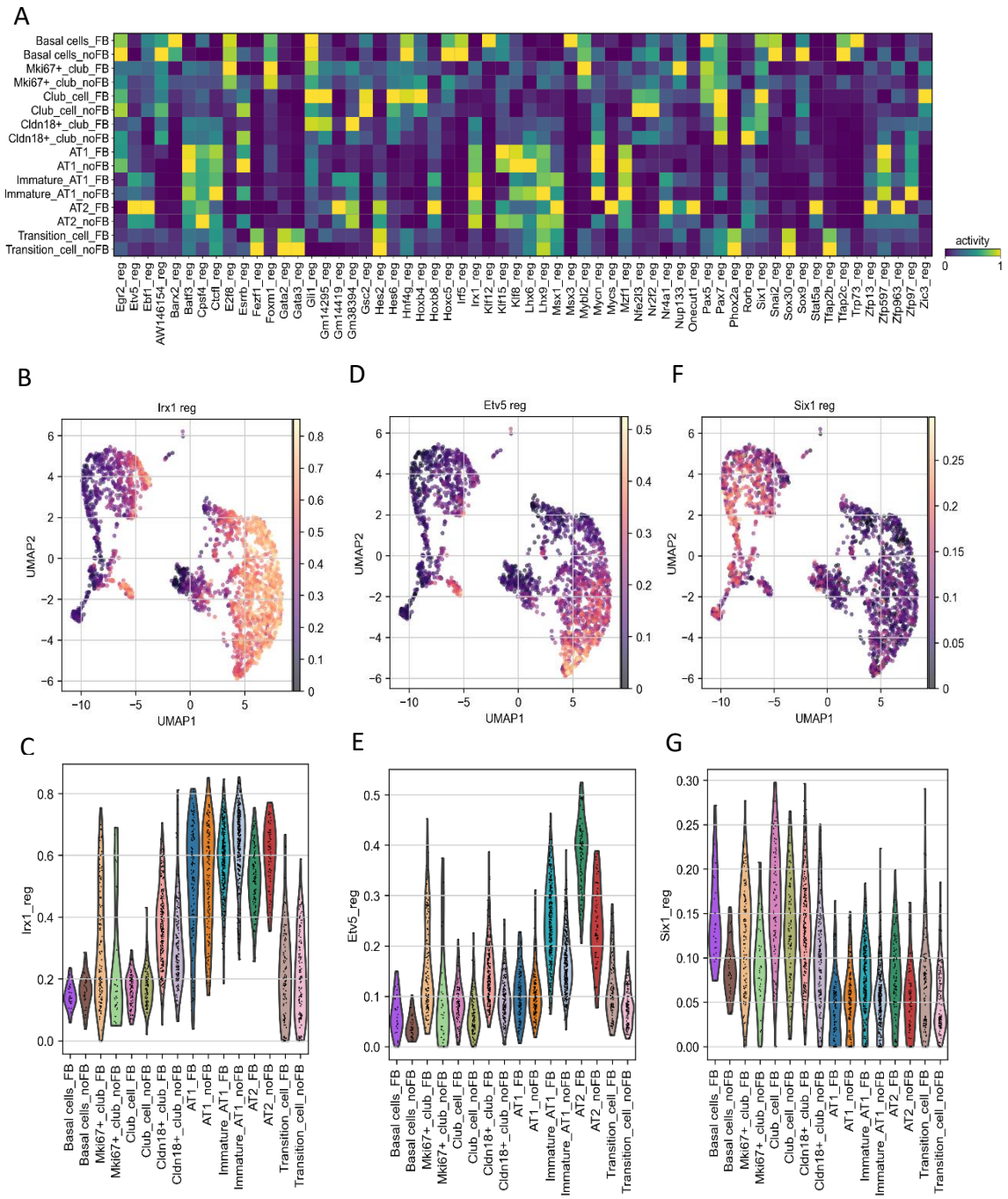

Fig 16. Regulon analysis in epithelial cells. **(A)** Heatmap of the activities of regulons in the different clusters. Regulon activity of (**B/C**) Irx1, (**D/E**) Etv5, and (**F/G**) Six1 shown in UMAPs and violin plots (analysis performed by Kathrin Kattler from Saarbrücken).

3.2.5 scRNA-seq of the fibroblast compartment in mouse ALI model

To study the influence of epithelial cells on the fibroblast transcriptome profiles, scRNA-seq was used to analyze fibroblasts from the lower compartment co-cultured with or without epithelial cells (Fig. 17A). ~90% of the cells in the lower compartment expressed fibroblast markers (e.g. *Col1a1*) (Fig. 17B and C).

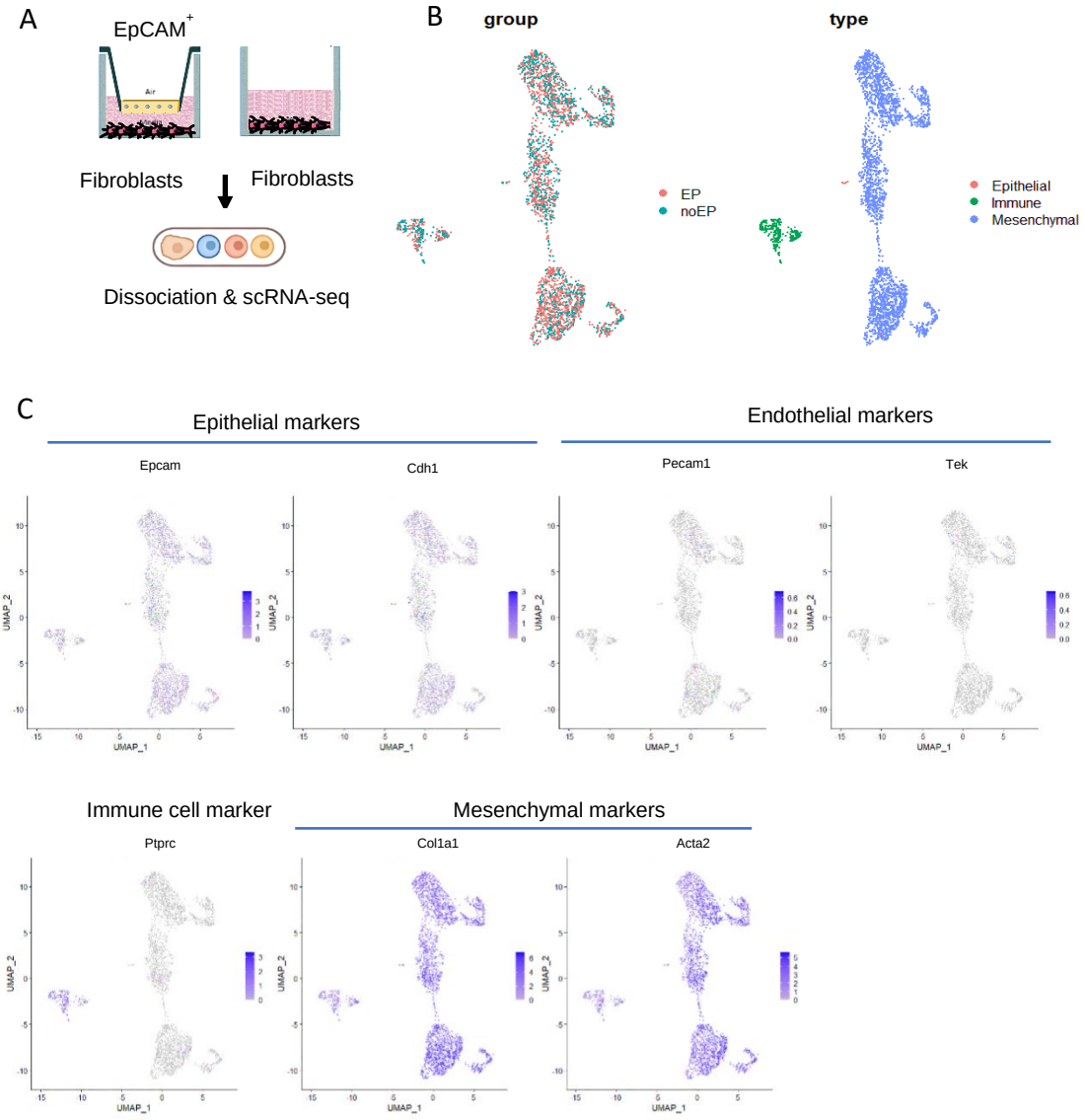

Fig 17. scRNA-seq analysis of the fibroblast compartment. Fibroblasts were cultured at the bottom of the ALI-cultures for four days in the presence or absence of ($EPCAM^+$) epithelial cells. **(A)** Schematic of the experimental setup. **(B)** UMAP clustering of the fibroblasts cultured with (EP) and without (noEP) epithelial cells (group) and major cell types (type). **(C)** UMAP visualization of cell type-specific markers.

The fibroblasts were further sub-clustered. Five sub-clusters were identified, four of which showed strong expression of *Pdgfra*. *Pdgfra*$^{+}$ fibroblasts were found to be important in alveolar proliferation and differentiation (Barkauskas et al. 2013). Two *Pdgfra* clusters specifically expressed *spint2*, named Pdgfra^{+}spint2^{+} and Pdgfra^{+}spint2^{+}Mki67^{+}. Two clusters specifically expressed *serpinf1*, named Pdgfra^{+}serpinf1^{+} and Pdgfra^{+}serpinf1^{+}Mki67^{+}. No cluster expressed *Lgr6*, *Lgr5*, *Axin2*, or *Wnt2*. The Mki67^{+} clusters probably represent the proliferating pool of fibroblast (Fig.18A to C).

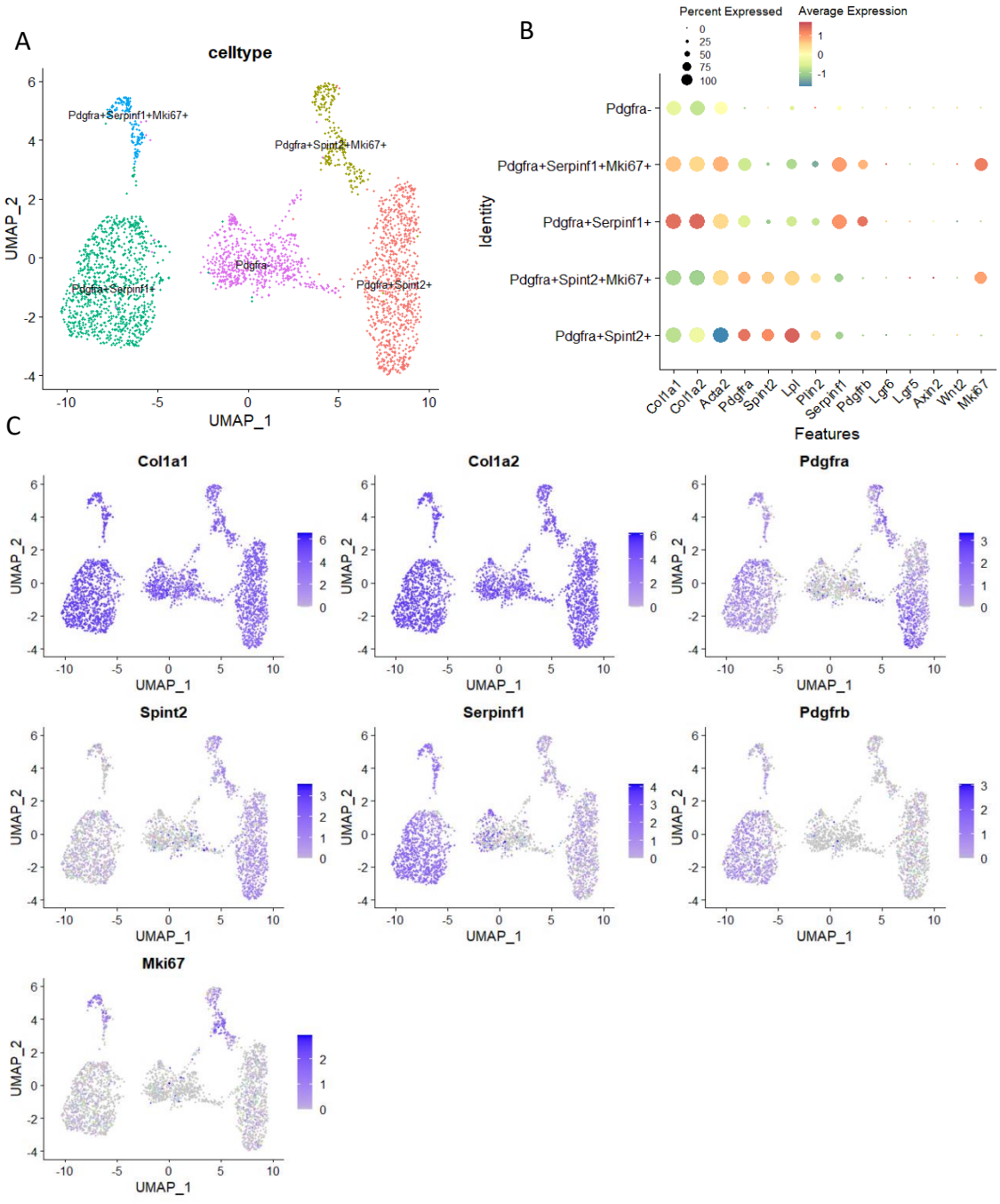

Fig 18. scRNA-seq analysis of the fibroblasts. **(A)** UMAP with major subtypes of fibroblasts. **(B)** Dot plot showing the expression of fibroblasts markers. **(C)** Feature plots for representative markers.

The ratio of different fibroblast clusters was compared between fibroblasts cultured with or without epithelial cells (Fig. 19A). Cultivation in the presence of fibroblasts had little effect on the ratio of the different clusters to each other. Co-culture with epithelial cells increased the proportion of $Pdgfra^{+}Serinf1^{+}$ clusters by approximately 10% (Table 8, Fig. 19B). Co-culture with epithelial cells also increased the expression of *Fgf7*, *Fgf10* and *Ereg* in the $Pdgfra^{+}Serinf1^{+}$ clusters (Fig. 19C and D). These growth factors are associated with alveolar regeneration (Shiraishi et al. 2019).

Table 8 Cell numbers and percentages of total cells for different fibroblast subtypes:

	cell number		**% of total**	
Celltype	**noEP**	**EP**	**noEP**	**EP**
$Pdgfra^{+}Spint2^{+}$	461	381	28.47	32.70
$Pdgfra^{+}Spint2^{+}Mki67^{+}$	116	110	7.16	9.44
$Pdgfra^{+}Serpinf1^{+}$	634	338	39.16	29.01
$Pdgfra^{+}Serpinf1^{+}Mki67^{+}$	77	59	4.76	5.06
$Pdgfra^{-}$	331	277	20.44	23.78
total	**1619**	**1165**	**100**	**100**

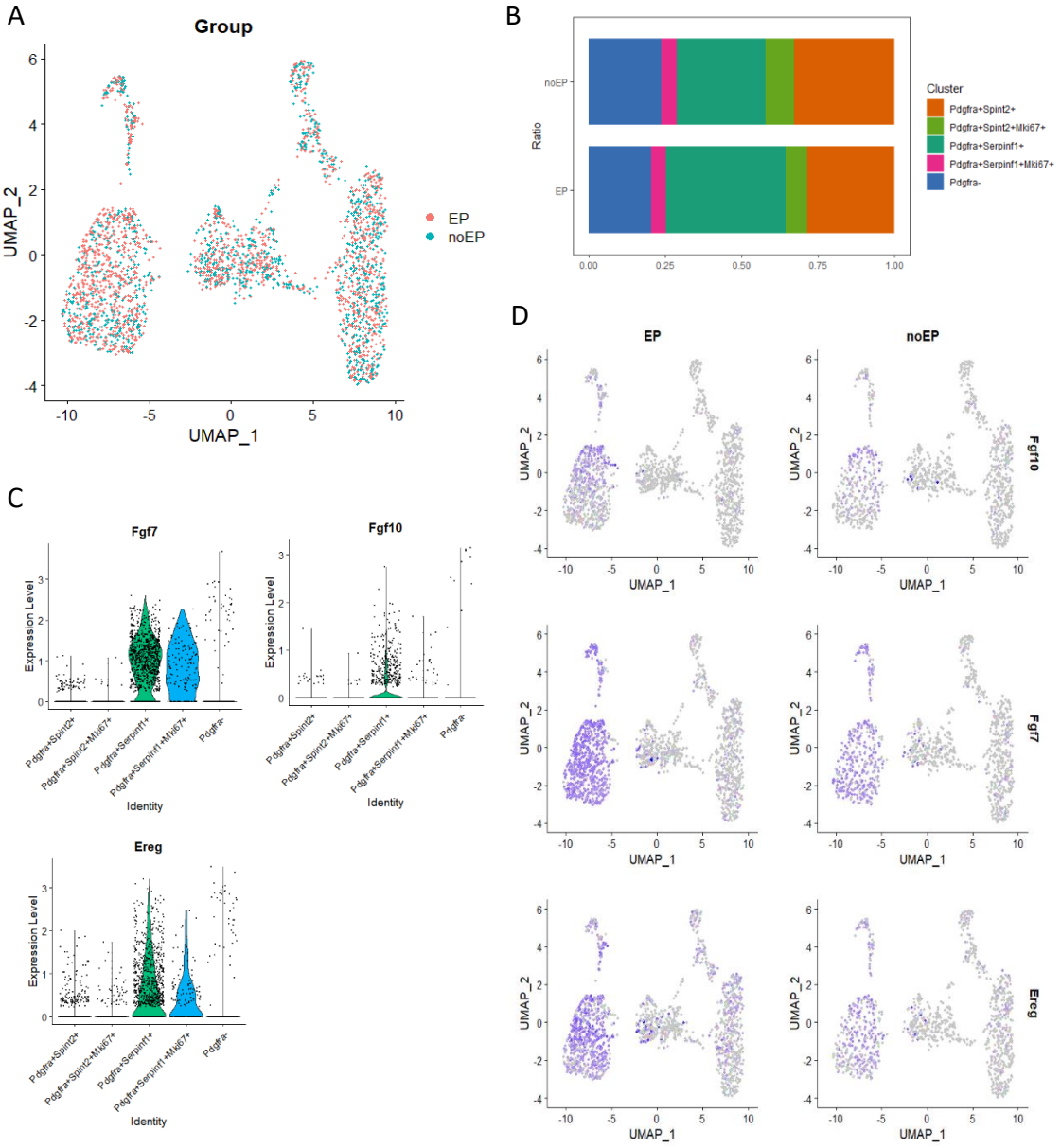

Fig 19. The presence of epithelial cells induce the expression of growth factors in the Pdgfra^{+}Serinf1^{+} clusters. **(A)** UMAP plot for fibroblasts cultured in the absence (noEP, blue) or presence of epithelial cells (EP, red). **(B)** The relative proportion of each fibroblasts subtype in noEP versus EP group. **(C)** Violin plots and **(D)** feature plots showing the expression levels of growth factors.

3.2.6 Co-culture with epithelium leads to the activation of the Cebpb regulon and expression of IL-6

GSVA and AUCell scores were used for pathway analysis. The co-culture with epithelial cells induced a dramatic activation of IL-6/STAT3 and TNFA/NFKB pathway, especially in Pdgfra^{+}Serinf1^{+} fibroblasts (Fig. 20A and B). The Cebpb regulon was also primarily activated in Pdgfra^{+}Serinf1^{+} fibroblasts when co-cultured with epithelial cells (Fig. 20C to E).

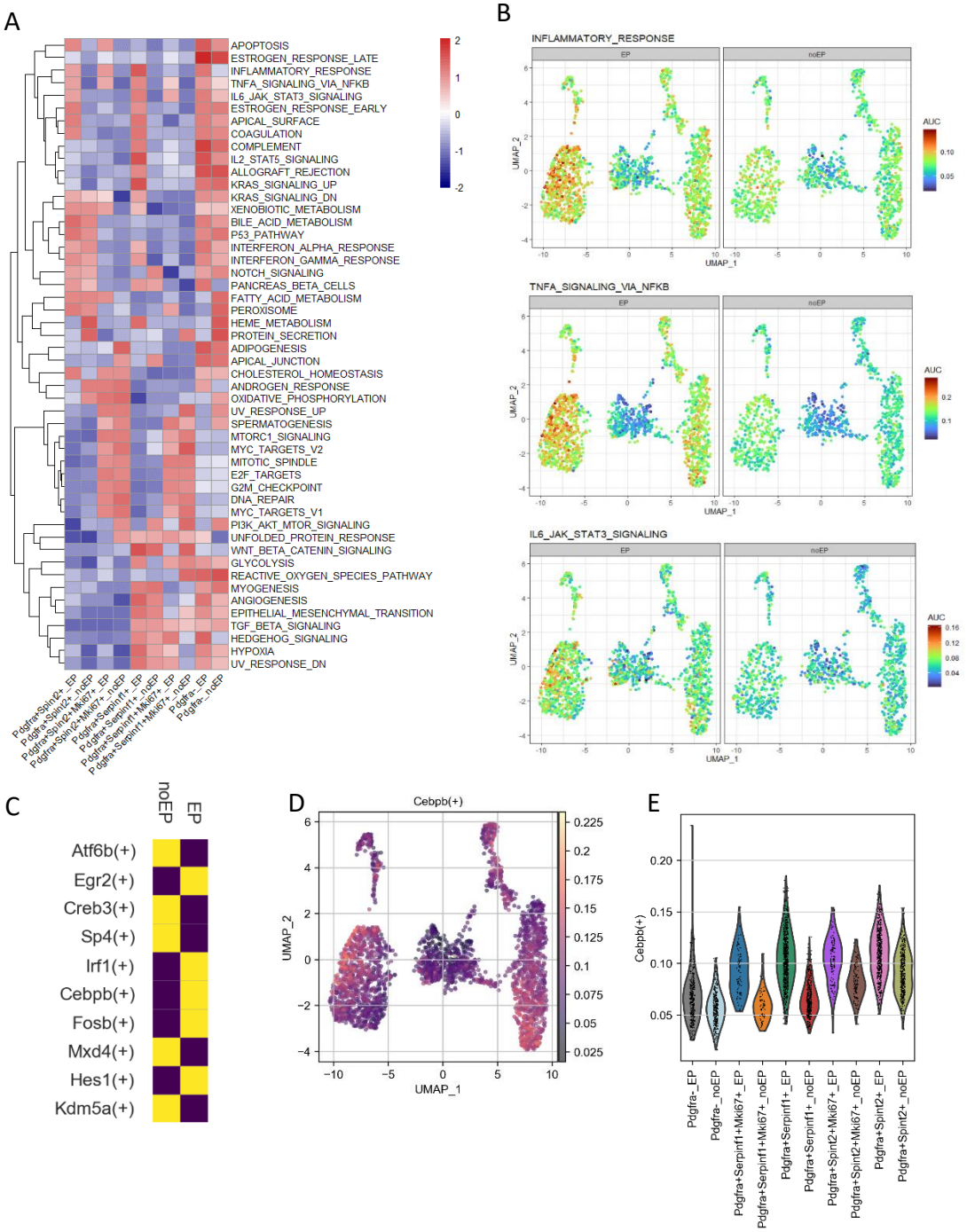

Fig 20. Epithelial cells activate IL-6/STAT3 and TNFA/NFKB pathways in fibroblasts. Differences in pathway activities were scored per cell type by **(A)** GSVA and individual cells by **(B)** AUCell. **(C)** Heatmap of the binarized regulon activity scores with a difference between the noEP versus EP group (Purple = no activity, yellow = high activity). The regulon activity of Cebpb was shown by **(D)** UMAP and **(E)** Violin plots.

DEG analysis of the fibroblasts showed that the top five up-regulated genes in co-culture group were *Cxcl1* (avg_log2FC: 1.80, *P*=4.45e-68), *Mt2* (avg_log2FC: 1.39, *P*=3.11e-54), *Nr4a1* (avg_log2FC: 1.39, *P*=3.86e-145), *Il6* (avg_log2FC: 1.39, *P*=3.01e-72), and *Nfkbia* (avg_log2FC: 1.30, *P*=1.17e-128) (Fig. 21A). *Il6* was mainly expressed in the Pdgfra^{+}Serinf1^{+} clusters, while other inflammatory genes were expressed in all clusters (Fig. 21B). The concentration of IL-6 was significantly increased in the supernatant of cocultures (Fig. 21C).

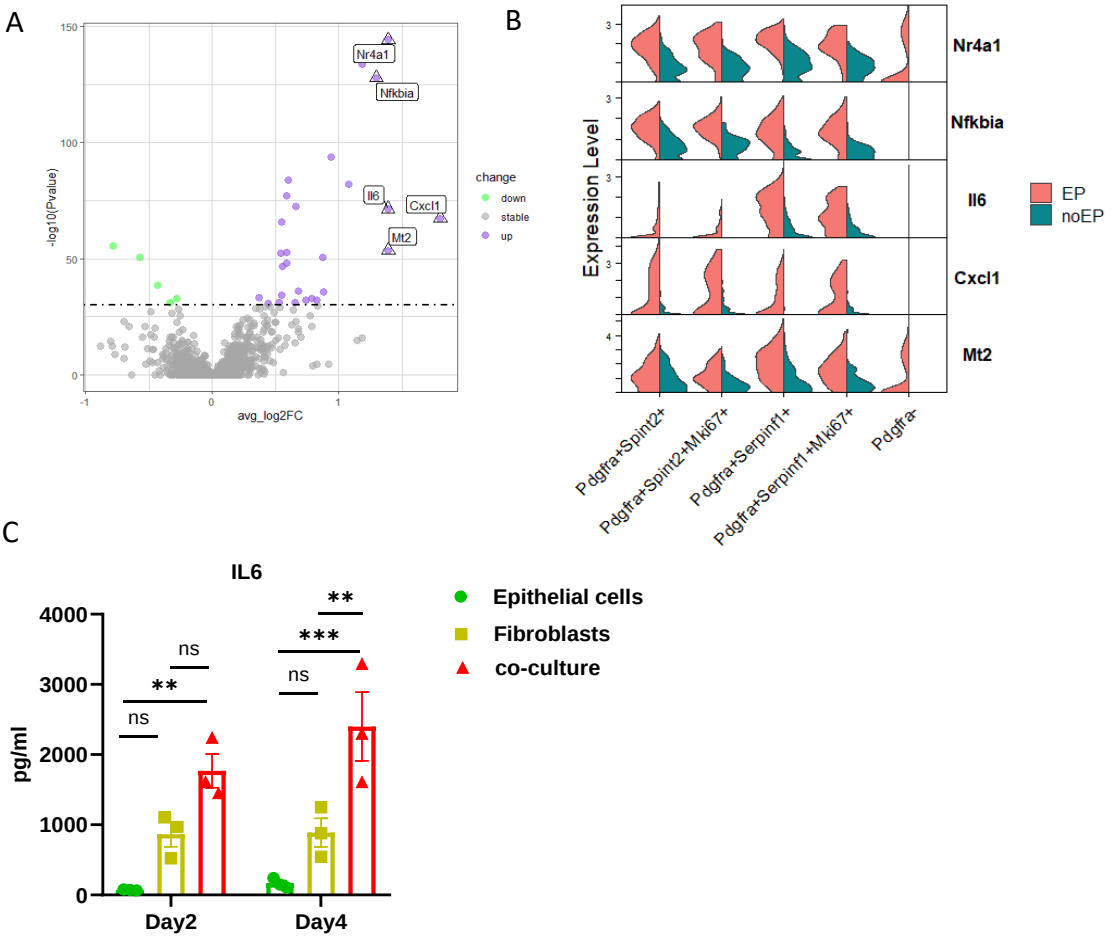

Fig 21. Co-culture with epithelium increases IL-6 expression and release in fibroblasts. **(A)** Volcano plots with differentially expressed genes after co-culture with epithelial cells. **(B)** Violin plots of the five most differentially expressed genes. **(C)** The concentrations of IL-6 in supernatants of the different cultures (n=3 independent experiments). Data are shown as mean ± SEM and were compared by two-way ANOVA. $^{**}p < 0.01$, and $^{***}p < 0.001$

3.2.7 IL-6 enhances the expression of AT2 and club cell markers in epithelial cells

To study the role of IL-6 in the regeneration of the lung epithelium, ALI cultures were treated with three different concentrations of IL-6 in the absence of fibroblasts. Results showed an increase in the transepithelial resistance at early time points (Fig. 22A and B) and a significantly increased expression of *Sftpc*, *Sftpb* and *Scgb1a1* after 4 days of IL-6 treatment at low concentration, but no effect on *Hopx* and *Ccnd1* (Fig. 22C and D). IF staining of cytospins showed that the proportion of $CCSP^+/HOPX^+$ club cells increased after IL-6 treatment (Fig. 22E). There was no difference in $Ki67^+$ cells between the IL-6 treated and untreated groups, while $Ki67^+$ cells were significantly increased in the group co-cultured with fibroblasts (Fig. 22F). These data demonstrate that IL-6 increases the proportion of $CCSP^+/HOPX^+$ club cells and the expression of AT2 and club cell marker genes.

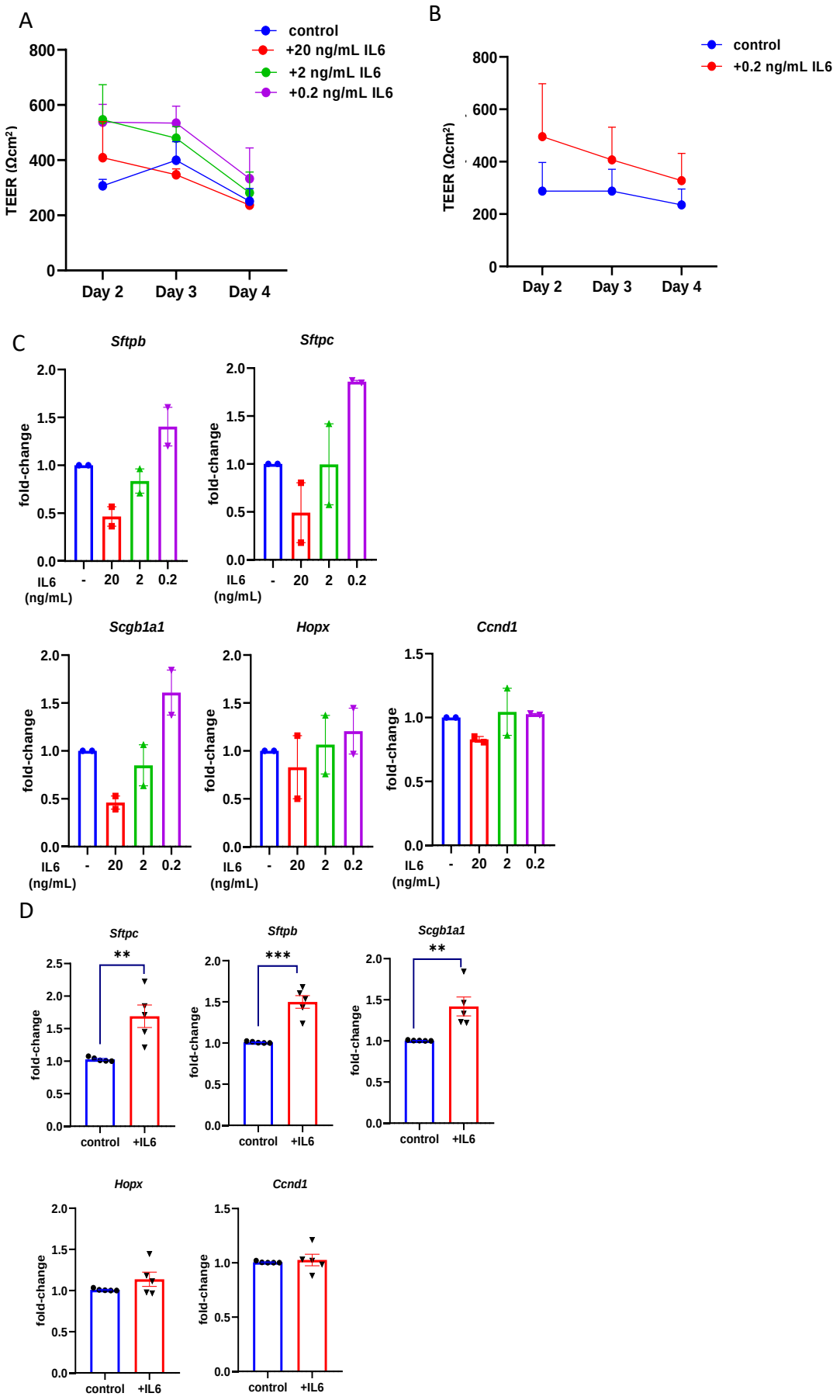
A
control
+20 ng/mL IL6
+2 ng/mL IL6
+0.2 ng/mL IL6
TEER (Ωcm²)
800
600
400
200
0
Day 2
Day 3
Day 4
B
control
+0.2 ng/mL IL6
TEER (Ωcm²)
800
600
400
200
0
Day 2
Day 3
Day 4
C
Sftpb
Sftpc
Scgb1a1
Hopx
Ccnd1
fold-change
IL6 (ng/mL)
-
20
2
0.2
D
Sftpc
Sftpb
Scgb1a1
Hopx
Ccnd1
**
***
control
+IL6
fold-change

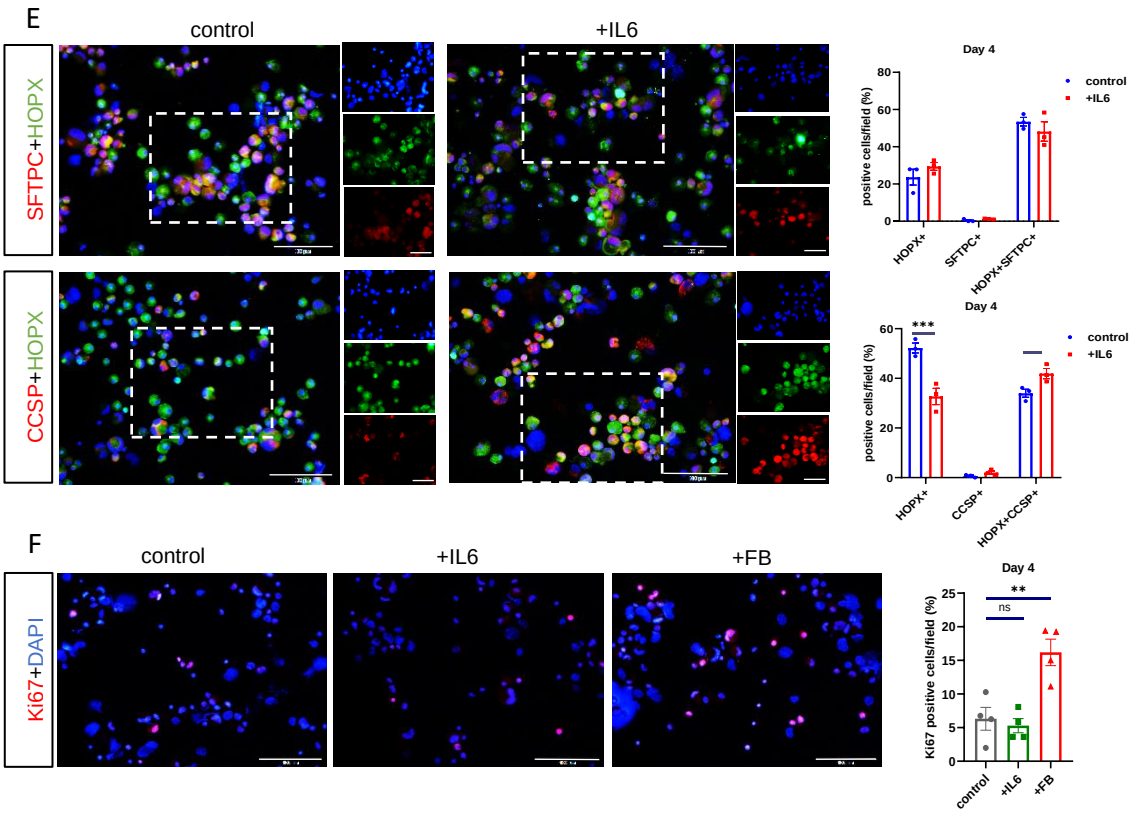

Fig 22. IL-6 increases the expression of AT2 and club cell markers in epithelial cells. Epithelial cells were treated with bioactive IL-6. **(A and B)** TEER was measured every 24 hours after airlift (n=2 independent experiments for dose-response experiments, n=5 independent experiments with low concentration of IL-6). **(C and D)** The expression of selected cell markers was analyzed by semi-quantitative RT-PCR after 4 days of culture with IL-6 (normalized to *Gapdh*, n=2 independent experiments for dose-response experiments, n=5 independent experiments with low concentration of IL-6). Cytospins were stained for SFTPC, HOPX, CCSP **(E)** and KI67 **(F)** and analyzed by IF after four days of culture. Left panel: Scale bar = 100 µm; Right panel: scale bar = 50 µm. The fraction of cells positive for the different markers was quantified. Data of a representative experiment. Data are shown as mean ± SEM and were compared by unpaired t test, two-way ANOVA and one-way ANOVA. *$p < 0.05$, **$p < 0.01$, and ***$p < 0.001$.

3.3 Function of DKK3 in lung regeneration

Previous studies found that DKK3 is highly expressed in tubular epithelial cells of the kidney and promotes fibrosis (Federico et al. 2016). DKK3 was also found to be upregulated in our human alveolar organoids model after bleomycin treatment. Publicly available single-cell data indicate that both airway epithelial and (alveolar) fibroblastic cells express DKK3 in the lungs (https://hlca.ds.czbiohub.org/). Subsequently, the function of DKK3 in the regeneration of the lungs was examined in the ALI model and in mouse experiments.

3.3.1 scRNA-seq analysis of wildtype and *Dkk3*$^{-/-}$ EpCAM^{+} cells in ALI-cultured model

The ALI model was used to study the role of DKK3 in lung epithelial regeneration. Lung epithelial cells were isolated from wildtype (WT) and *Dkk3* knockout (*Dkk3*$^{-/-}$) mice and cultured in transwell inserts. Single-cell suspensions were harvested at day 4 (2 days post-airlift) for scRNA sequencing (Fig. 23A). Cells from *Dkk3*-deficient cultures clustered like the WT cultures (Fig. 23B). There were no obvious differences in the expression of the various marker genes between WT and *Dkk3*-deficient cultures (Fig. 23C). *Dkk3* was mainly expressed in basal cells (Fig. 23D).

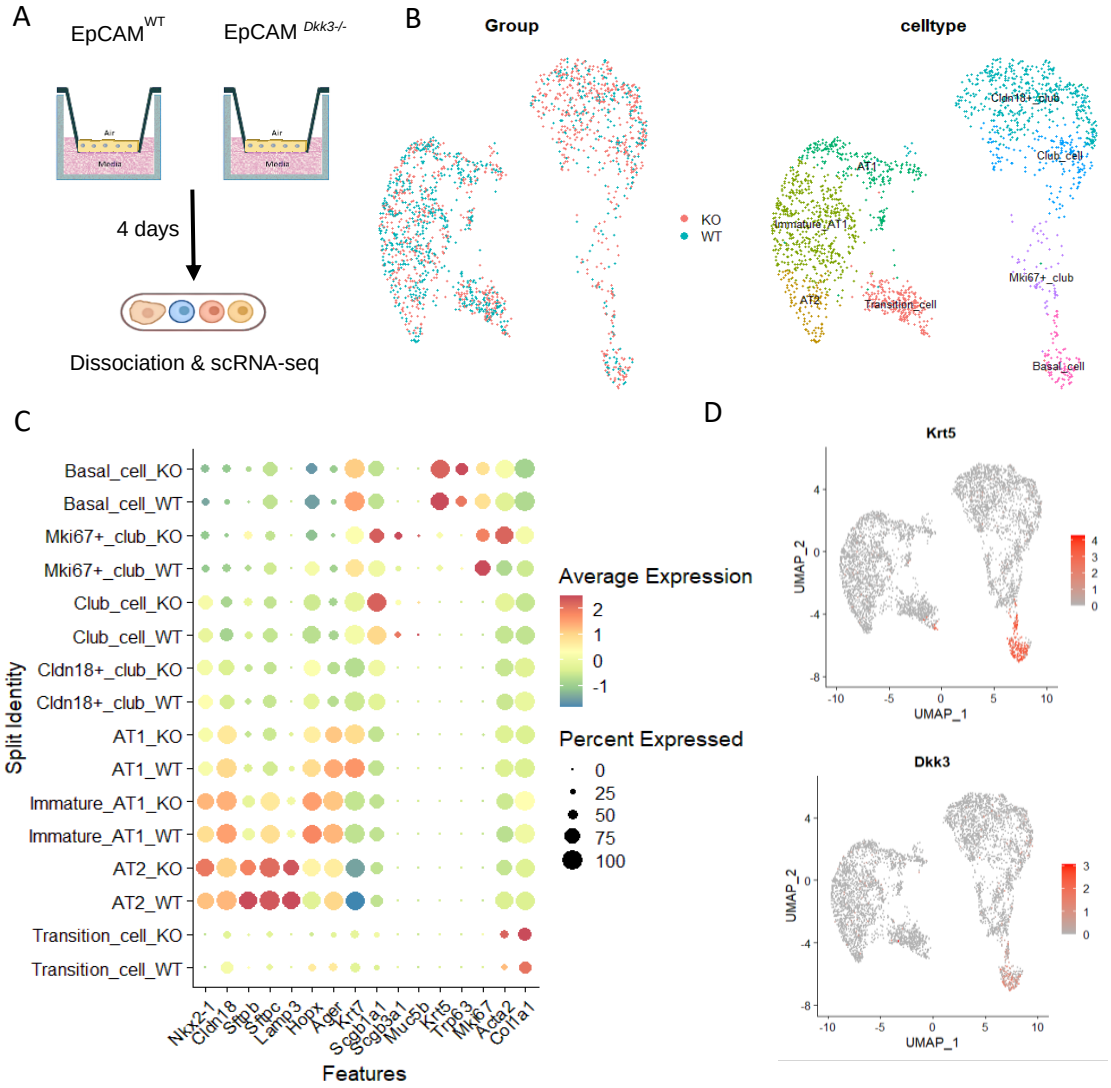

Fig 23. scRNA-seq analysis of ALI cultures derived from WT- and *Dkk3*$^{-/-}$-mice. **(A)** Scheme of the experimental setup. **(B)** UMAP clustering of the epithelial cells coloured by wildtype (label: WT)- and *Dkk3*$^{-/-}$ (label: KO)-mice (group) and major cell types (celltype). **(C)** Dot plot showing the expression of epithelial markers. **(D)** Feature plot for *Dkk3*.

A significantly reduced TEER developed in *Dkk3*$^{-/-}$-cultures (Fig. 24A). In addition, qRT-PCR also showed a reduced expression of pneumocyte markers in *Dkk3*$^{-/-}$ cultures (e.g. *Sftpc*, *Hopx* and *Aqp5*) (Fig. 24B). However, the single-cell data showed no altered expression of pneumocyte markers between WT and *Dkk3*$^{-/-}$ cultures within the different cell populations (Fig. 24C). Rather, there were differences in the ratio of the individual cell populations between WT and *Dkk3*$^{-/-}$-cultures. In WT cultures, the proportion of pneumocyte populations (AT2, AT1 and AT1 immature cells) was higher than in *Dkk3*$^{-/-}$-cultures, while a higher proportion of airway epithelial cells, including Cldn18^{+} club cells, club cells and Mki67^{+} club cells was increased in knockout cultures (Fig. 24D). Semi-quantitative RT-PCR results showed a decrease in *Sftpc* expression in wild-type epithelial cells after 4 days of ALI culture, accompanied by an increase in the expression of type 1 markers (e.g. *Hopx*, *Aqp5*), whereas there was no increase in the expression of type 1 markers in knockout epithelial cells (Fig. 24E). These indicated DKK3 might have a role in regulating the differentiation of AT2 cells to AT1 cells.

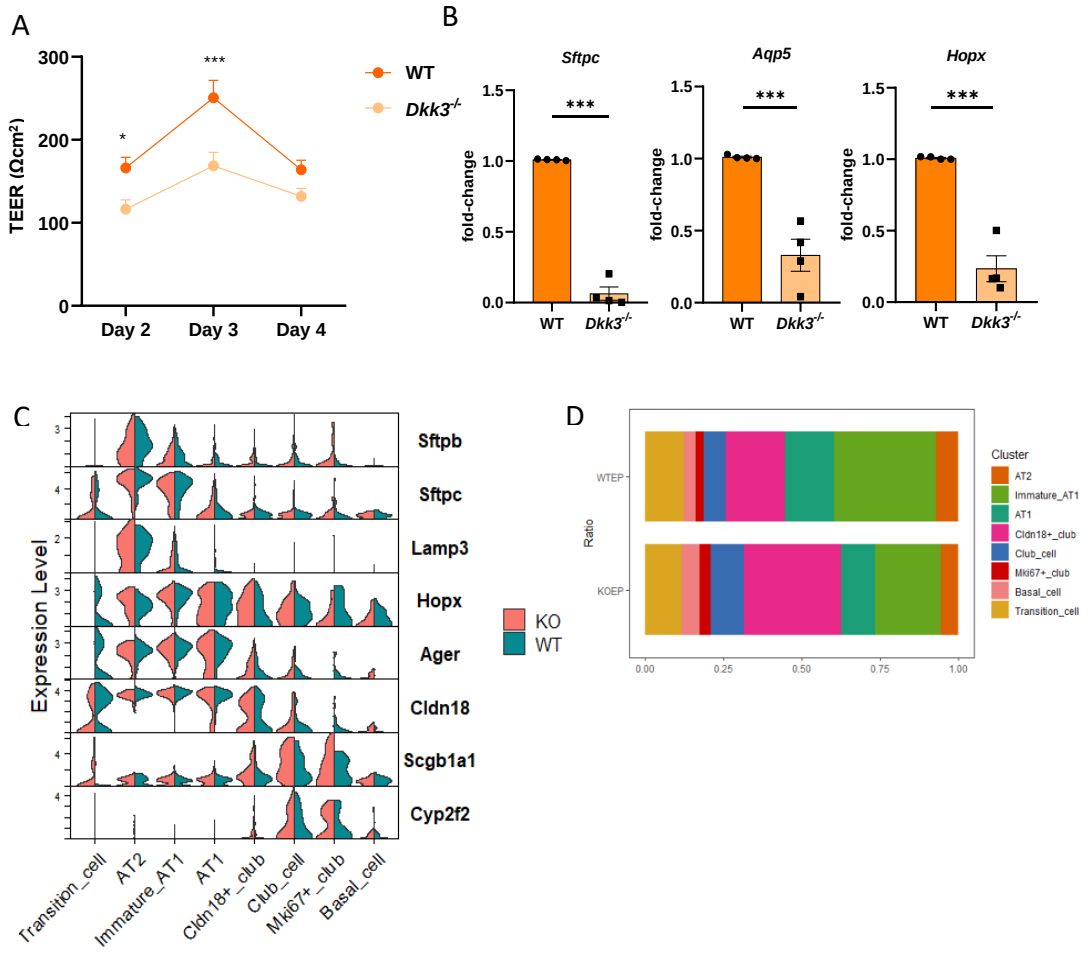

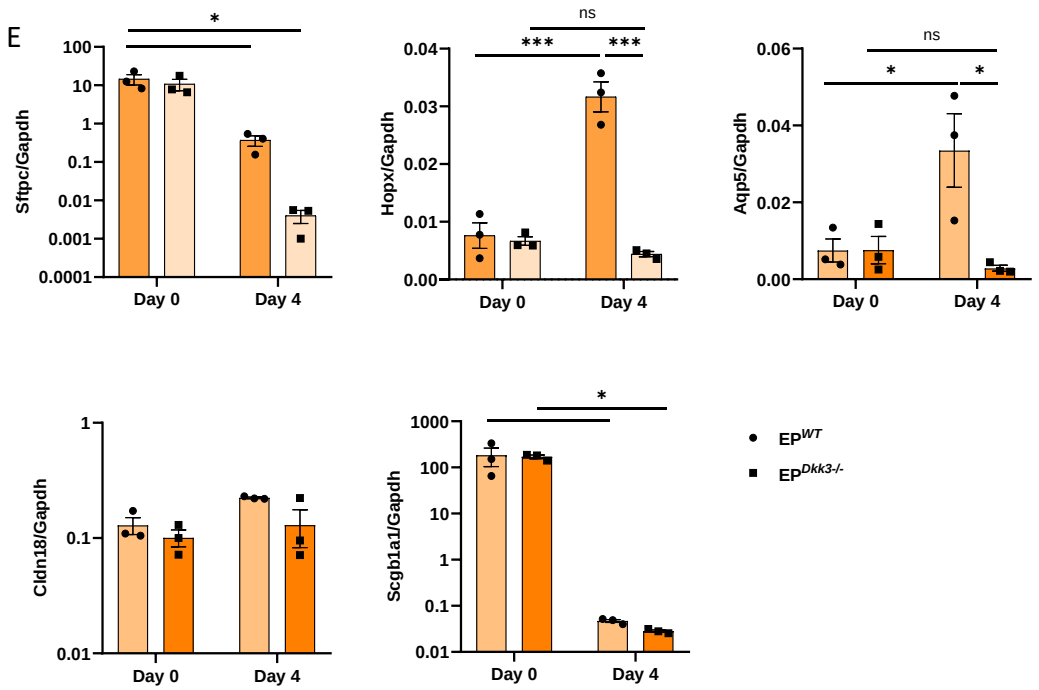

Fig 24. *Dkk3*$^{-/-}$-pneumocytes form a decreased epithelial barrier. **(A)** The TEER of WT and *Dkk3*$^{-/-}$-epithelial cells were measured at day of airlift and every 24 hours after airlift (n=4 independent experiments). **(B)** The expression of selected cell markers was analyzed by semi-quantitative RT-PCR at day 4 (normalized to *Gapdh*, n=4 independent experiments). **(C)** Violin plots showing the expression levels of marker genes in each cell type. **(D)** Proportion of different cell populations. **(E)** The expression of selected cell markers was analyzed by semi-quantitative RT-PCR at day 0 and 4 (normalized to *Gapdh*, n=3 independent experiments). Data were shown as mean ± SEM and compared by two-way ANOVA and unpaired t test. *$p < 0.05$, ***$p < 0.001$, ns=no significantly difference.

3.3.2 scRNA-seq analysis of wildtype and *Dkk3*$^{-/-}$ fibroblasts in 2D culture

Next, fibroblasts isolated from wildtype and *Dkk3*$^{-/-}$-mice were cultured in 24-wells plate and single cell suspensions were harvested at day 4 for scRNA sequencing (Fig. 25A). Cells from *Dkk3*-deficient cultures clustered like the WT cultures (Fig. 25B). *Dkk3* was expressed in all *Pdgfra*$^{+}$ fibroblasts, particularly in the Pdgfra^{+}Serpinf1^{+} cluster (Fig. 25C and D). DEG analysis showed that there were not strong differences even in the top five up-regulated genes between wildtype and

Dkk3$^{-/-}$ fibroblasts. Only *Saa3* and *Mmp3* was slightly higher in wildtype mice (Fig. 25E). There was also no significant difference in the proportion of cell types between the different isolations (Fig. 25F). These results indicated there were no significant difference in gene expression and cell type composition between wild-type and knockout fibroblasts grown on plastic.

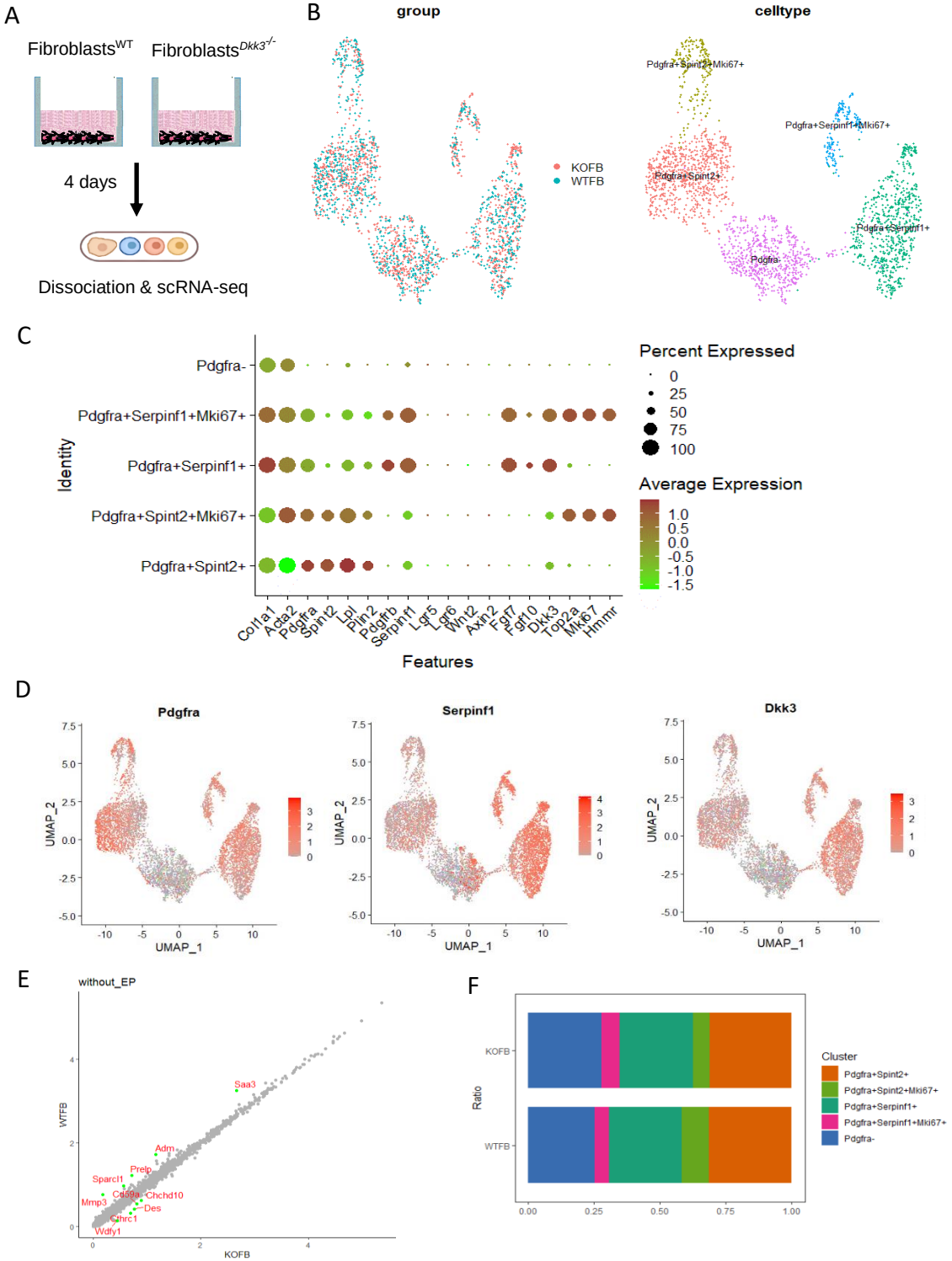

Fig 25. Single cell analysis of WT- and *Dkk3*$^{-/-}$-fibroblasts. **(A)** Scheme of the experimental setup. **(B)** UMAP plot of fibroblasts colored by WT (label: WTFB)- and *Dkk3*$^{-/-}$ (label: KOFB) -fibroblasts and cell types. **(C)** Gene expression of key markers for fibroblast phenotypes. **(D)** *Dkk3* expression on feature plots. **(E)** Volcano plot showing differential genes of WT- and *Dkk3*$^{-/-}$-fibroblasts. **(F)** Proportion of different cell types.

3.3.3 High expression of DKK3 in human pulmonary fibrosis lung tissue

To further understand the role of DKK3 in lung disease, tissues obtained from an IPF-patient and a donor without chronic lung disease were examined by immunofluorescence. In IPF tissue, the alveolar structure was significantly altered (Fig. 26A) and collagen I and III fibers were significantly increased, as shown by Picro-Sirius Red staining (Fig. 26B). Immunofluorescence staining showed increased numbers of DKK3^{+} cells (Fig. 26C) and DKK3 co-stained with α-SMA (a marker for myofibroblasts) in fibrotic lung tissue (Fig. 26D).

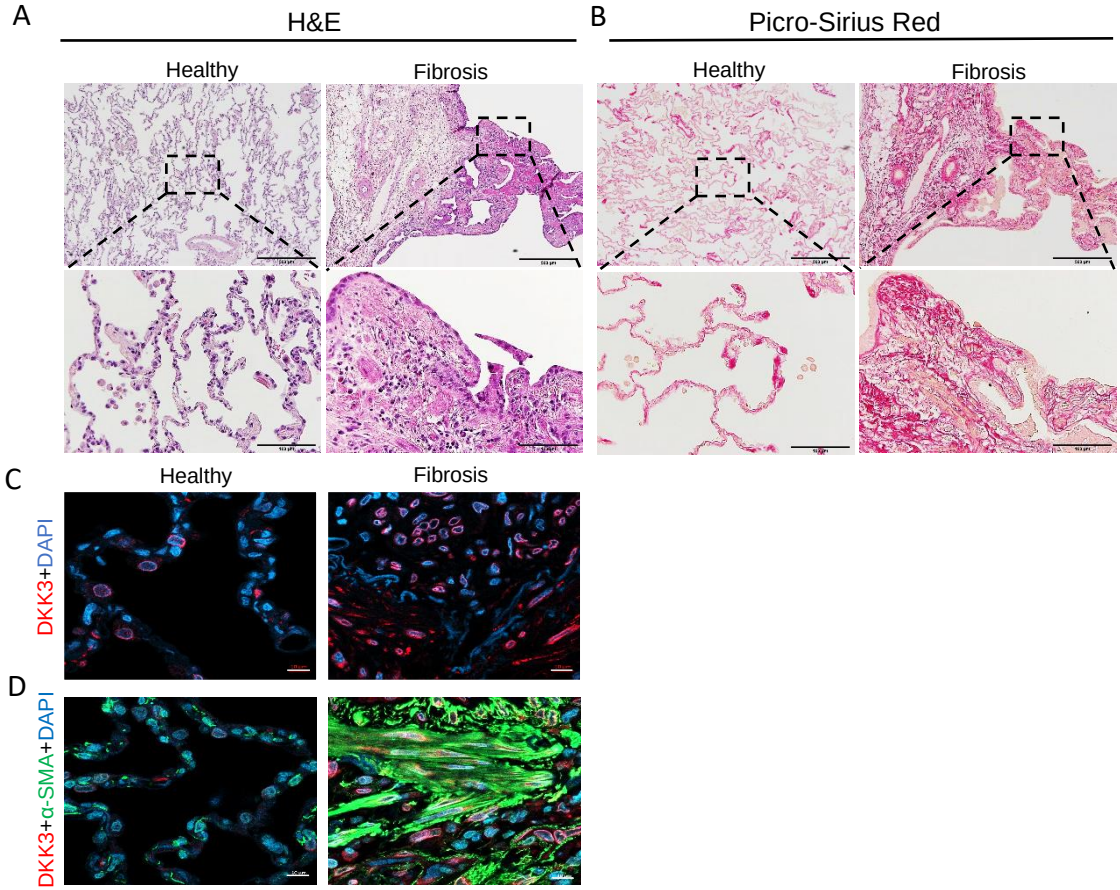

Fig 26. DKK3 is highly expressed in fibrotic human lung tissue. **(A)** H&E and **(B)** Picro-Sirius Red staining of healthy and fibrotic human lung tissue (Upper panel: Scale bar = 500 µm; Lower panel: scale bar = 100 µm). IF staining for **(C)** DKK3 alone or **(D)** the combination of DKK3 and α-SMA in healthy and fibrotic human lung tissue. scale bar = 10 µm

3.3.4 DKK3 is upregulated in the lungs of bleomycin-instilled mice

Next, a mouse model of bleomycin-induced pulmonary fibrosis was used to examine the function of DKK3 during the fibrogenic phase *in vivo*. Bleomycin or NaCl as control was given intratracheally to mice once. Mice were analyzed 21 days after bleomycin administration (Fig. 27A). Similar to human IPF, the number of $DKK3^+$ cells in lung tissue were significantly increased (Fig. 27B and C) and DKK3 co-stained with α-SMA 21 days after bleomycin treatment compared to NaCl control (Fig. 27D).

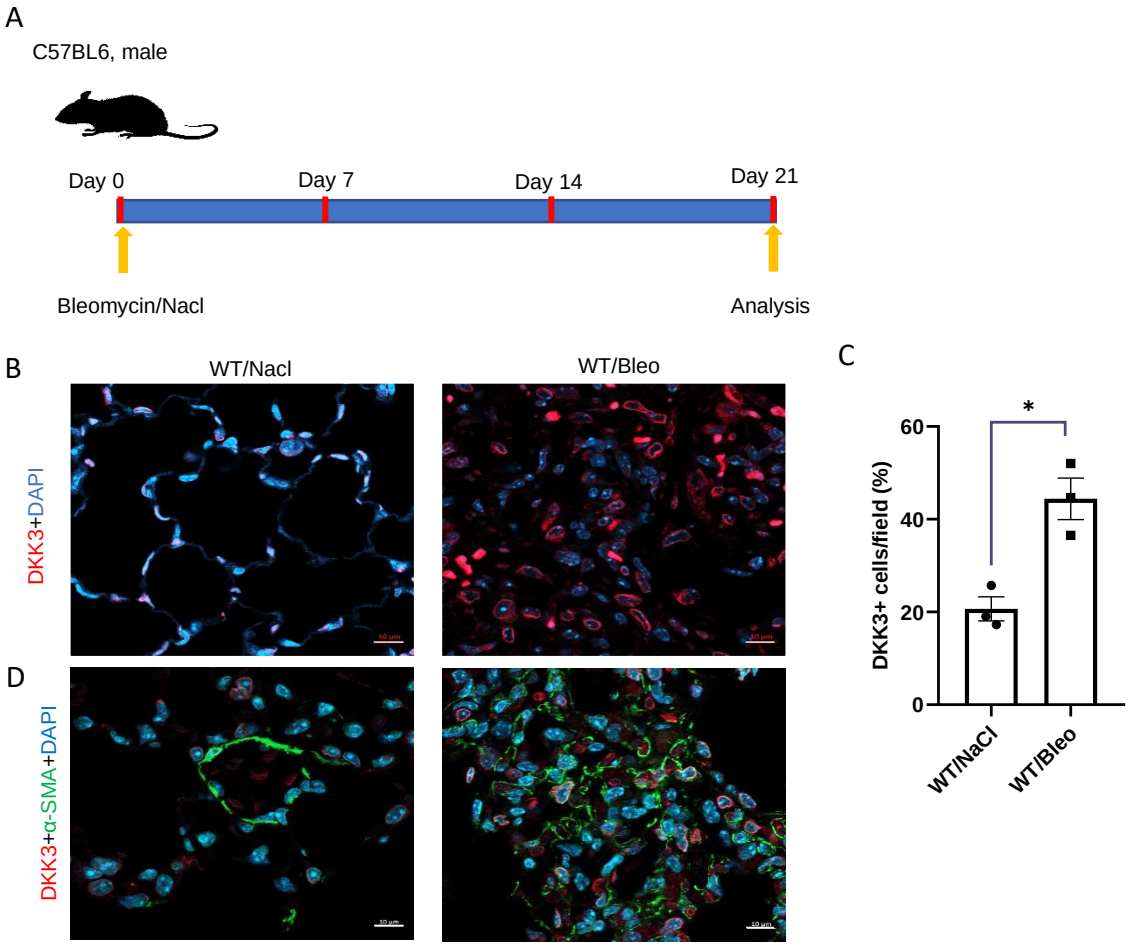

Fig 27. DKK3 is expressed in fibrotic mouse lungs. **(A)** Scheme of the experimental setup. IF staining for **(B)** DKK3 alone or **(D)** the combination of DKK3 and α-SMA in lung tissue. scale bar = 10 μm **(C)** Positive cells were counted in three random fields for each mouse lung (n=3). Data are shown as mean ± SEM and were compared by unpaired *t* test. **p* < 0.05

3.3.5 Bleomycin-induced pulmonary fibrosis is strongly reduced in *Dkk3*$^{-/-}$ mice

To further study the role of DKK3 in the process of fibrosis *in vivo*, *Dkk3*$^{-/-}$ and WT mice were injected intratracheally with bleomycin or NaCl and analyzed after 21 days. Administration of bleomycin led to a decrease in body weight in WT animals. Deficiency for *Dkk3*, however, protected against body weight loss (Fig. 28A). The bleomycin-induced pulmonary fibrosis in WT mice was also reflected in the invasive lung function, with a significantly increased tissue elasticity and dynamic resistance, while $FEF_{50\%FVC}$ was significantly reduced (Fig. 28B). Tissue damage shown by H&E staining, and Picro-Sirius Red staining was obvious in WT mice and the fibrotic score was significantly increased (Fig. 28C to E). Lung damage was greatly reduced in *Dkk3*$^{-/-}$ mice, which was significant both in the lung function and in the histology.

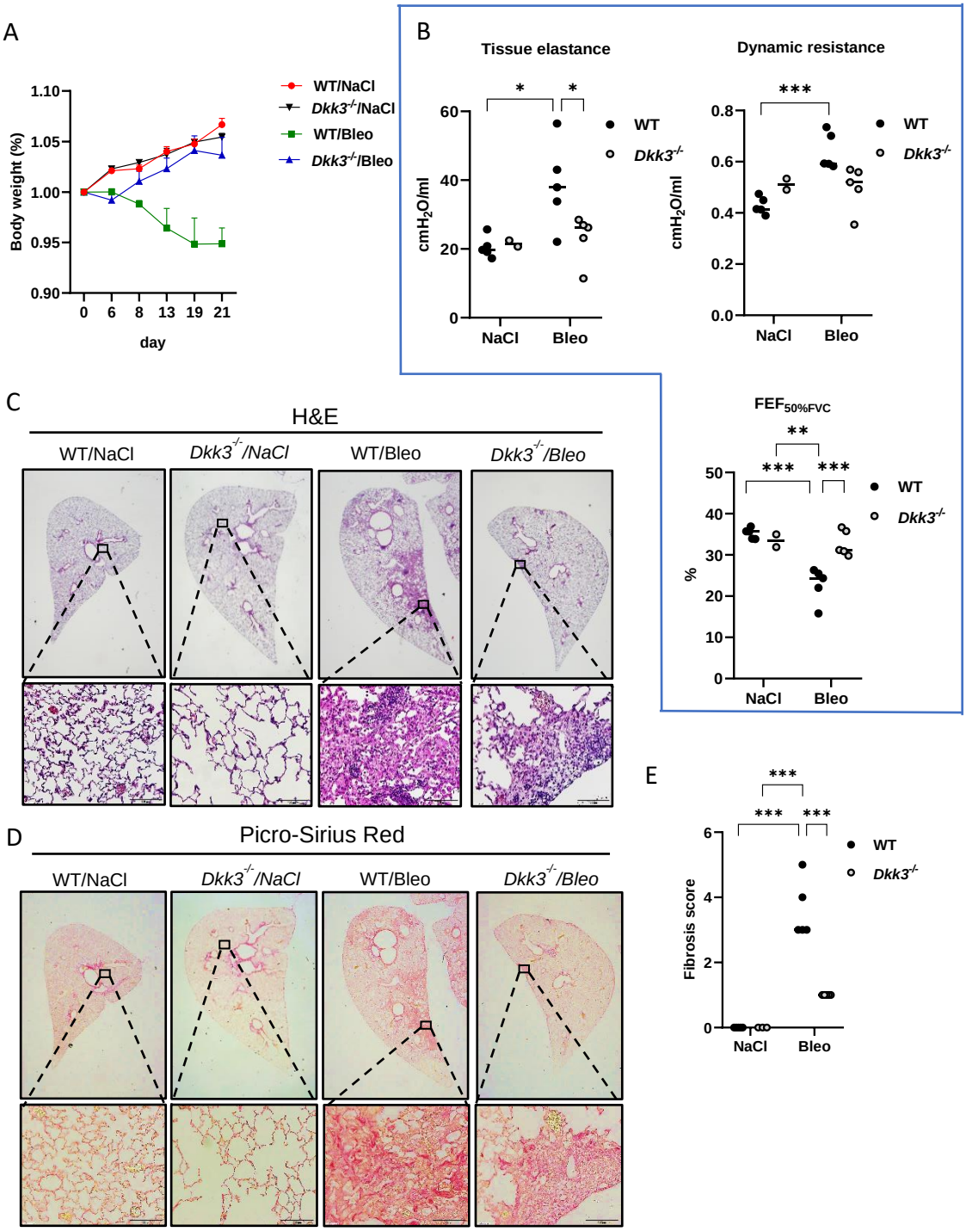

Fig 28. Belomyci-induced lung fibrosis is greatly reduced in *Dkk3*$^{-/-}$ mice. **(A)** Body weight of WT and *Dkk3*$^{-/-}$ mice challenged with bleomycin or NaCl. **(B)** Lung function measurements at day 21 after instillation (WT bleomycin, *Dkk3*$^{-/-}$ bleomycin, WT NaCl = 5 mice per group, *Dkk3*$^{-/-}$ NaCl = 2 mice). Representative H&E **(C)** and Picro-Sirius Red **(D)** staining of whole lung (upper panel) and higher magnification (lower panel). Scale bar = 100 µm. **(E)** Fibrotic score (WT bleomycin,

Dkk3$^{-/-}$ bleomycin, WT NaCl = 5 mice per group, *Dkk3*$^{-/-}$ NaCl = 3 mice). Data are shown as mean ± SEM and were compared by two-way ANOVA. *$p < 0.05$, **$p < 0.01$, and ***$p < 0.001$.

3.3.6 The loss of AT2 cells and the increase in myofibroblasts are greatly reduced in *Dkk3*$^{-/-}$ mice

Changes in the alveolar epithelium play a central role in IPF. It is believed that epithelial-fibroblast communication is disrupted in IPF and promotes excessive proliferation of myofibroblasts (Horowitz and Thannickal 2006). Therefore, IF staining was used to discriminate the expression of SFTPC and α-SMA in healthy and damaged lung tissue from WT and *Dkk3*$^{-/-}$ mice. The proportion of SFTPC^{+} cells was significantly reduced in bleomycin-treated WT mice compared to WT controls. *Dkk3*$^{-/-}$ mice were protected from the bleomycin-induced of loss of SFTPC^{+} cells. Notably, the knockout mice had slightly fewer SFTPC^{+} cells than wild-type mice, although there was no significant difference. KI67^{+}SFTPC^{+} cells were significantly increased in bleomycin-infused WT mice compared to the other three groups (Fig. 29A to D). Numbers of α-SMA^{+} cells and KI67^{+}α-SMA^{+} were significantly increased in fibrotic WT mice compared to *Dkk3*$^{-/-}$ mice and NaCl controls (Fig. 29E to H).

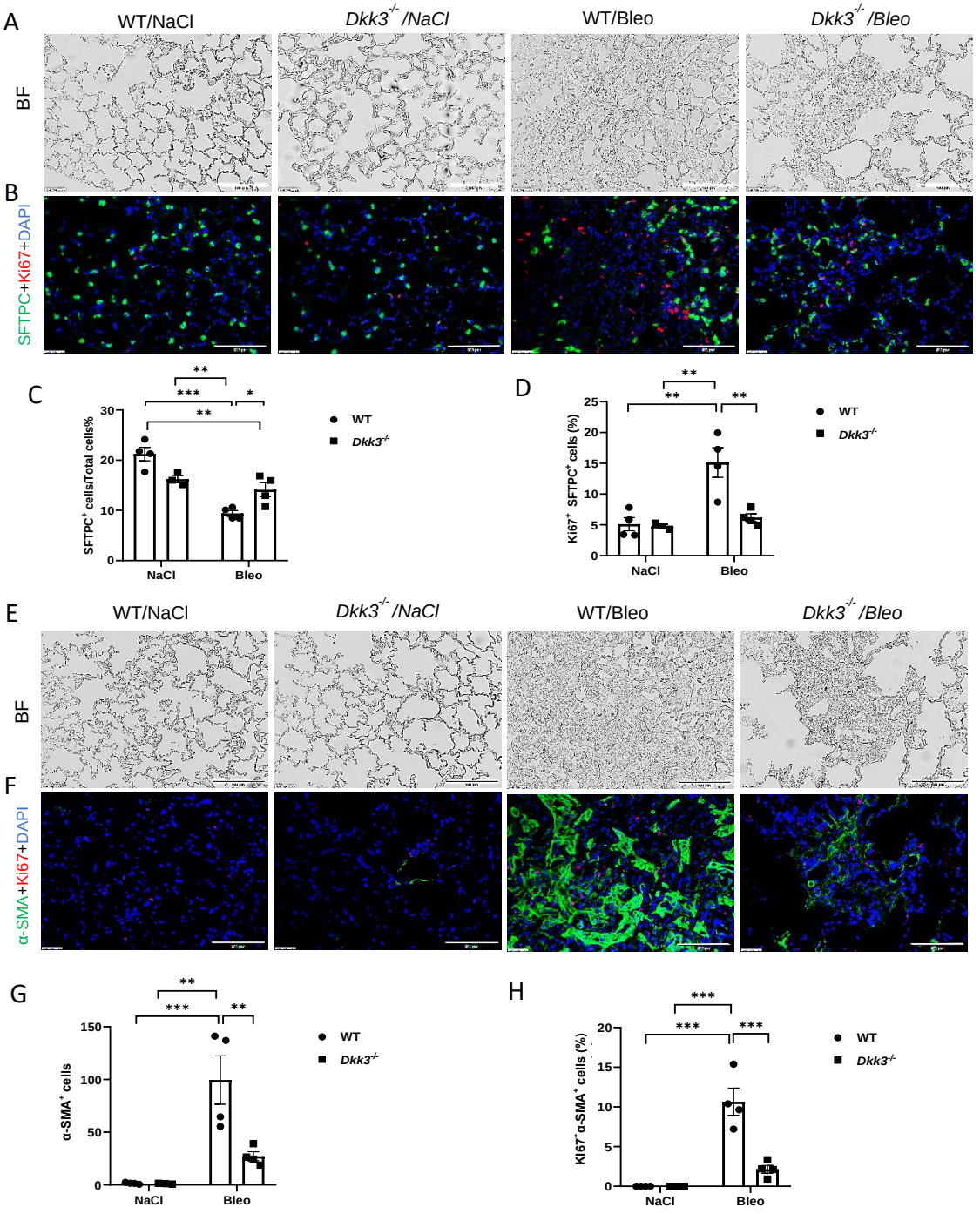

Fig 29. The deficiency of Dkk3 protects mice from the loss of AT2 cells and the proliferation of myofibroblasts. Representative BF **(A and E)** and IF staining for SFTPC and KI67 **(B)** , α-SMA and KI67 **(F)** in lung tissue. Scale bar = 100 μm. The fraction of cells positive for SFTPC and KI67 **(C** and **D)** and numbers of α-SMA and KI67 **(G** and **H)** was quantified (WT bleomycin, *Dkk3*$^{-/-}$ bleomycin, WT NaCl = 4 mice per group, *Dkk3*$^{-/-}$ NaCl = 3 mice). Data were shown as mean ± SEM and compared by two-way ANOVA. **p* < 0.05, ***p* < 0.01, and ****p* < 0.001. BF=bright field

4. DISCUSSION

AT2 cells and fibroblasts play important roles in lung development and disease progression, such as COPD and IPF (Olajuyin, Zhang, and Ji 2019; Ushakumary, Riccetti, and Perl 2021a). In this study, two in vitro models were established to study interaction between AT2 cells and fibroblasts in lung regeneration and disease by scRNA-seq. The main findings of this study were that hyperactivated fibroblasts promote the transdifferentiation of human AT2 cells into MUC5B-secreting cells in adult AT2 cells-derived organoids. In the ALI model, fibroblasts increase the epithelial barrier and drive club cells towards AT2 cells differentiation.

4.1 Type 2 cells differentiate into secretory cystic organoids when co-cultured with patient-derived fibroblasts

Recent data show that human AT2s, but not mouse AT2s, can transdifferentiate into $KRT5^+$ basal cell in organoid culture and xenotransplant models (Hoffmann et al. 2022; Kathiriya et al. 2022). In regenerating human lungs, AT2s differentiate into AT1s as well as terminal and respiratory bronchiole secretory cells (TRB-SCs) via a transitional state. These transitional cells likely can differentiate into TRB-SCs in fibrotic lesions in IPF. This indicates that human AT2s may have multiple plasticity in addition to differentiation into AT1s with potential harmful outcomes in IPF (Kadur et al. 2022). Numerous studies have identified a role for $MUC5B^+$ secretory cells in the pathobiology of IPF (Ballester, Milara, and Cortijo 2019; Hancock et al. 2018). MUC5B is abundantly expressed in honeycomb cysts, which are one of the characteristic structures of pulmonary fibrosis in humans and mice. Hancock et al. showed that, in IPF patients, MUC5B is co-expressed with SFTPC in epithelial cells lining the honeycomb cyst and in AT2 cells, suggesting that epithelial cells in the lung parenchyma express MUC5B in IPF (Hancock et al. 2018). Forced expression of MUC5B under the control of the Sftpc-promotor worsened the outcome in the bleomycin-induced mouse model. Functional promoter variants of MUC5B are a dominant risk factor for the development of IPF (Evans et al. 2016; Seibold et al. 2011).

Our AT2 organoid model revealed a dramatic loss of SFTPC accompanied by the progressive appearance of MUC5B (a secretory cell marker) in human AT2 organoids co-cultured with patient-derived fibroblasts. These cells were largely negative for respiratory epithelial markers such as KRT5 and SGB1A1, suggesting that these cells remain pneumocytes with some plasticity. Single-cell analysis of these *SFTPC^{low}MUC5B^{high}* cells revealed upregulation of IPF biomarkers such as *MMP7* and CXC chemokines (e.g. *CXCL1*, *CXCL2*, *CXCL8*, *CXCL17*) which potentially mediate the expansion and activation of fibroblasts. This suggests that human AT2s are able to transdifferentiate into MUC5B^{+} secretory cells and secrete pro-fibrotic factors in response to overactivation by fibroblast.

A recent study found that normal human adult lung mesenchymal cells undergo a dramatic phenotypic change from alveolar fibroblasts to IPF-like mesenchymal cells when conventionally cultured *in vitro* (Kathiriya et al. 2022). In our organoid model, single-cell analysis revealed that the cultured fibroblasts from three different patient origins were low in expression of alveolar fibroblasts markers, but strongly expressed markers of myofibroblasts and the IPF proteome extracellular matrix (e.g. *COL1A1, COL1A2, COL3A1, COL5A2, COL6A3, COL8A1, MMP2* and *TIPM2*), albeit at different levels of expression. However, all of these pathologic fibroblasts promoted metaplastic trans-differentiation of human AT2s into MUC5B^{+} secretory AT2 cells. Pro-fibrotic factors (e.g. *IL6, CCL2*) were also highly expressed in co-cultured fibroblasts. Previous studies have reported that IL-6 levels are increased in serum of patients with IPF and that blocking IL-6 transduction signaling attenuates pulmonary fibrosis (Le et al. 2014; Lee et al. 2021). IL-6 and IL-17A can stimulate *MUC5B* gene expression via the c-Jun kinase/extracellular signal-regulated kinase signaling pathway in normal human bronchial epithelial cells (Chen et al. 2003). However, whether IL-6 released from fibroblasts has the same function in promoting the release of MUC5B from AT2 cells remains to be further clarified.

Bleomycin is most commonly used to induce pulmonary fibrosis in mouse models and has recently been used in IPF-like organoids models (Suezawa et al. 2021). In our

organoid model, bleomycin stimulation increased *MUC5B* expression in organoids co-cultured with fibroblasts and promoted upregulation of the myofibroblasts marker *ACTA2* and fibrosis marker *CTHRC1*. This further demonstrates that AT2 cells transdifferentiate into MUC5B$^+$ AT2 cells in a pro-fibrotic microenvironment. Additionally, *DKK3*, a fibrosis-related factor, was also found to be upregulated after bleomycin treatment.

In summary, the co-culture model suggests that the interaction of fibroblasts with AT2 cells may lead to a vicious cycle in IPF progression. Additionally, the model can be used in many ways. Active ingredients can be tested with regard to cell differentiation and expression of secretory factors. Further studies with fibroblasts from a larger number of patients could show a pathological interaction of fibroblasts with AT2 cells.

4.2 Fibroblasts increase the epithelial barrier and AT2 differentiation in ALI culture

In an ALI mouse model, a regulatory loop was found between lung epithelial cells and the mesenchymal niche in a reciprocal manner to regulate the differentiation of both compartments. Co-culture with fibroblasts led to an increased epithelial barrier. scRNA-seq analysis showed that, in this model, the epithelial barrier is mainly established by club cells and pneumocytes. Co-culture with fibroblasts increased the expression of type 2 markers in pneumocytes, the activation of regulons mediating AT2 differentiation, and the trans-differentiation of club cells towards pneumocytes. Furthermore, lung epithelial cells promoted fibroblast secretion of growth factors that mediated epithelial regeneration.

Co-culture with fibroblasts led to increased expression of AT2 markers (e.g. *Cbr2*, *Sftpb* and *Cxcl15*) (Alysandratos et al. 2023; Strunz et al. 2020), in both pneumocyte and club cell populations . Furthermore, Etv5 regulon activity was increased in the AT2 and club cell populations, but not in the AT1 population. Etv5 has been shown to be essential for the maintenance of AT2 cells. Zhang et al. reported that Etv5 is expressed in AT2 cells in the lung and that deletion of Etv5 in AT2 cells results in reduced expression of AT2

markers and increased expression of AT1 markers *ex vivo* (Zhang et al. 2017). Thus, co-culture with fibroblasts leads to the activation of cellular programs that support AT2 differentiation and drive club cells toward AT2 cells.

Immunofluorescence staining showed that the vast majority of cells in the freshly isolated lung cells were SFTPC positive, CCSP positive and HOPX negative (a marker associated with AT2 regeneration and AT1 differentiation) (Jain et al. 2015; Ota et al. 2018). The isolated cells were mainly AT2 and club cells. In contrast, after four days on transwells, most of the $SFTPC^+$ cells were also positive for HOPX. In addition, the trajectory analysis of the pneumocyte cluster and the evaluation of cell type-specific markers showed that AT2 cells differentiate via immature AT1 cells to AT1 cells. Thus, the isolated AT2 cells differentiate to a significant extent towards AT1 cells in our model. For club cells, four days of ALI incubation was accompanied by HOPX expression in a proportion of club cells. scRNA-seq data also showed that club cells partially differentiated into AT2 marker-expressing cells, which was further enhanced in the presence of fibroblasts. These results are consistent with studies showing that club cells can differentiate into AT2-type cells and potentially contribute to lung regeneration, at least in mice (Lee et al. 2017). However, co-culture with fibroblasts also resulted in increased expression of *Scgb1a1*. This could also be an indication that a large proportion of club cells express certain alveolar markers during regeneration of the alveolar epithelium, but do not differentiate into “true” pneumocytes.

On the fibroblast side, co-culture with epithelial cells led to a further increased expression of the growth factors such as FGF7, FGF10 and EREG (Shiraishi et al. 2019) in the $Pdgfra^+/Serpinf1^+$ clusters. PDGFRα is widely expressed by alveolar and adventitial fibroblasts (Tsukui et al. 2020) and $PDGFR\alpha^+$ lung stromal cells have been shown to support the growth and differentiation of alveolospheres cultured in Matrigel (Barkauskas et al. 2013). Studies in mice further suggest that the interaction of AT2 cells with $Pdgfra^+$ mesenchymal cells is important in lung repair, but could also be deleterious in lung fibrosis (Li et al. 2018; Nabhan et al. 2018; Zepp et al. 2017). A cocktail of growth factors released by $Pdgfra^+$ fibroblasts therefore appear to

contribute to the improved epithelial barrier and maintenance of AT2 cells in our model. In addition, co-culture with epithelial cells increased activity of the JAK-STAT3, NK-κB pathway and Cebpb regulon in fibroblasts, which caused an increased expression of IL-6 (Nguyen et al. 2017). IL-6 has been described to be important for epithelial regeneration and lung diseases (Tadokoro et al. 2014; Zepp et al. 2017). Previous studies showed that high levels of IL-6 were found in IPF patients (Zhou et al. 2010) and animal models of pulmonary fibrosis (Pedroza et al. 2011), whereas other studies also showed IL-6 released by fibroblasts promote AT2 cell growth and self-renewal (Liang et al. 2016; Zepp et al. 2017). In this ALI model, cultivation of epithelial cells in the presence of recombinant IL-6 at low concentration resulted in an increased epithelial barrier at early time point and expression of AT2 markers. Therefore, low levels, not high levels, of IL-6 might be a factor supporting the maintenance of AT2 cells in our model. Further studies are needed to clarify to what extent IL-6 regulates AT2 cell maintenance and AT2 differentiation in AT1 cells.

Taken together, these two *in vitro* models show that interactions between mesenchymal and epithelial cells lead to the activation of signaling pathways, mediating coordinated alveolar epithelial regeneration or aberrant differentiation.

4.3 DKK3 is produced by fibroblasts and mediates experimental pulmonary fibrosis

The single-cell data from the ALI experiments showed that DKK3, a protein that mediates renal fibrosis, is strongly produced by fibroblasts and basal cells. This raises the question of to what extent DKK3 regulates the differentiation of pneumocytes and fibroblasts and whether DKK3 mediates pulmonary fibrosis. Therefore, this work examined to what extent the deficiency of DKK3 affects the differentiation of pneumocytes in the ALI model and to what extent DKK3-deficient fibroblasts differ from WT fibroblasts.

ALI cultures established with pneumocytes from *Dkk3*-deficient mice developed reduced transepithelial resistance. In addition, the expression of pneumocyte markers

such as *Sftpc*, *Hopx* and *Aqp5* was greatly reduced, indicating that DKK3 regulates the differentiation of pneumocytes. However, more in-depth single-cell analysis showed that no difference in the phenotype of the different cell populations between WT and DKK3ko cultures. For example, there was no differential gene regulation in the pneumocyte or club cell population in a DKK3-dependent manner. Like WT pneumocytes, DKK3-deficient pneumocytes formed a continuum from AT2 cells via immature AT1 cells to AT1 cells. Rather, it was shown that the ratios of the various cell populations differed between DKK3ko and WT cultures. The proportion of pneumocytes, particularly immature AT1 and AT1 cells, decreased significantly in DKK3ko cultures, whereas club cells increased. The different ratios of the cell populations to each other could explain the results of the classic semi-quantitative RT-PCR. It is unclear why the ratios of the individual cell populations differed. It could be that even in the preparation of the lung epithelial cells there were relatively less pneumocytes and more club cells in cells from DKK3ko animals. It is possible that the deficiency of DKK3 in the ALI model leads to increased proliferation of respiratory epithelial cells and differentiation of club cells. This could also be due to the fact that the lung cells were isolated from a DKK3-deficient lung, which is an indirect effect. Therefore, changes in epithelial cells were observed before and after 4 days of ALI culture. Cytospins staining and semi-quantitative RT-PCR results both showed that *Sftpc* expression was decreased accompanied by increased expression of type 1 markers (e.g. *Hopx*, *Aqp5*) in wild-type epithelial cells after 4 days of ALI culture, whereas expression of type 1 markers was not increased in DKK3ko epithelial cells. There was no difference in the expression of the club cell marker (*scgb1a1*) between wild-type and DKK3ko epithelial cells. This suggests that DKK3 may have a role in regulating the differentiation of AT2 cells to AT1 cells in regeneration. DKK3, as a protein members of the DKK family, is a modulator of the Wnt/β-catenin pathway (Niehrs 2006). The Wnt pathway is a key factor in modulating the AT2 to AT1 differentiation (Frank et al. 2016; Zacharias et al. 2018). This also indicates DKK3 might regulate AT2 to AT1 differentiation through Wnt/β-catenin pathway.

In accordance with the single cell data, DKK3-expressing fibroblasts were also found in the human and murine lungs. Experiments with a bleomycin-dependent fibrosis model showed that DKK3-expressing cells are numerous in fibrotic lesions. Moreover, the global knockout of *Dkk3* was associated with a drastically reduced loss of lung function 21 days post bleomycin-treatment. However, seven days after bleomycin administration, there was no difference in pulmonary inflammation between WT and DKK3ko mice (data not shown in this work). This indicates that DKK3 mediates lung regeneration in the fibrosis model, but has no function in the early action of bleomycin and the associated inflammation. Further experiments are needed to determine the mechanisms by which DKK3 mediate fibrotic lung damage and which cells produce DKK3. Single cell analyses with mouse lungs can show, for example, the phenotype of the DKK3-expressing fibroblasts and DKK3-dependent cell-cell interactions. Such analyses could be used to derive hypotheses about the cellular mechanisms by which DKK3 regulates cell differentiation, which could then be tested in other (cell culture) models. Such experiments could, for example, shed light on whether DKK3 regulates the proliferation and differentiation of pneumocytes in the damaged lung via common pathways such as WNT signaling (Niehrs 2006). In addition, mouse experiments in which DKK3 is inducible depleted in specific cell types such as fibroblasts would be useful. Such experiments help to avoid unspecific effects of a global knockout.

4.4 Concluding remarks

The results presented in this thesis show that the interaction between fibroblasts and lung epithelial cells is important for alveolar regeneration and disease progression. In the human alveolar organoids model, patient-derived fibroblasts are phenotypically highly similar to IPF-like fibroblasts. Co-culture with these fibroblasts leads to a dramatic loss of SFTPC expression and is accompanied by the appearance of MUC5B in organoids. MUC5B is abundantly expressed in honeycomb cysts and is one of the characteristic structures of pulmonary fibrosis. Moreover, bleomycin treatment exacerbated MUC5B and DKK3 expression in human AT2 organoids co-cultured with fibroblasts. In the ALI model, primary fibroblasts promote lung epithelial cell

regeneration by increasing the expression of AT2 markers in pneumocytes and club cell populations, as well as by supporting AT2 differentiation and driving club cells towards AT2 cells through the EVT5 regulon. Conversely, lung epithelial cells induce increased expression of IL-6 and other differentiation factors (e.g. FGFs) in fibroblasts through activation of signaling pathways such as JAK-STAT3, NK-κB and regulon of Cebpb. A low concentration of recombinant IL-6 enhanced epithelial barrier formation and the expression of AT2 and club cell markers in epithelial cells. DKK3 can promote renal fibrosis. In this study, DKK3 was found to be expressed in basal cells and fibroblasts in the ALI model. DKK3 may have a regulatory role in the differentiation of AT2 cells to AT1 cells. In lung tissue from IPF patients and in the bleomycin-induced mouse fibrosis model, cells expressing DKK3 were significantly more abundant at the site of fibrotic lesions. *Dkk3* knockout mice alleviate bleomycin-induced pulmonary fibrosis.

Today's cell culture models with differentiated epithelia make a valuable contribution to understanding the interaction between epithelial and mesenchymal cells during lung regeneration. The models established in this work make it possible to gain a deeper understanding of pathological processes. In further studies, the models can be used, for example, to elucidate disease mechanisms using a larger number of patient-obtained fibroblasts. In addition, the models are well suited to identify disease-associated targets as well as testing innovative active ingredients and drugs with regard to their effect and toxicity. DKK3 has been identified as one important factor in regulating the interaction between fibroblasts and lung epithelial cells during regeneration and fibrosis in the lung.

5. REFERENCE

Adams, Taylor S., Jonas C. Schupp, Sergio Poli, Ehab A. Ayaub, Nir Neumark, Farida Ahangari, Sarah G. Chu, et al. 2020. 'Single-Cell RNA-Seq Reveals Ectopic and Aberrant Lung-Resident Cell Populations in Idiopathic Pulmonary Fibrosis'. *Science Advances* 6 (28): eaba1983. https://doi.org/10.1126/sciadv.aba1983.

Alysandratos, Konstantinos-Dionysios, Carolina Garcia-de-Alba, Changfu Yao, Patrizia Pessina, Jessie Huang, Carlos Villacorta-Martin, Olivia T. Hix, et al. 2023. 'Culture Impact on the Transcriptomic Programs of Primary and IPSC-Derived Human Alveolar Type 2 Cells'. *JCI Insight* 8 (1): e158937. https://doi.org/10.1172/jci.insight.158937.

Armanios, Mary Y., Julian J.-L. Chen, Joy D. Cogan, Jonathan K. Alder, Roxann G. Ingersoll, Cheryl Markin, William E. Lawson, et al. 2007. 'Telomerase Mutations in Families with Idiopathic Pulmonary Fibrosis'. *The New England Journal of Medicine* 356 (13): 1317–26. https://doi.org/10.1056/NEJMoa066157.

Ashcroft, T, J M Simpson, and V Timbrell. 1988. 'Simple Method of Estimating Severity of Pulmonary Fibrosis on a Numerical Scale.' *Journal of Clinical Pathology* 41 (4): 467–70.

Ballester, Beatriz, Javier Milara, and Julio Cortijo. 2019. 'Mucins as a New Frontier in Pulmonary Fibrosis'. *Journal of Clinical Medicine* 8 (9): 1447. https://doi.org/10.3390/jcm8091447.

Barkauskas, Christina E., Michael J. Cronce, Craig R. Rackley, Emily J. Bowie, Douglas R. Keene, Barry R. Stripp, Scott H. Randell, Paul W. Noble, and Brigid L. M. Hogan. 2013. 'Type 2 Alveolar Cells Are Stem Cells in Adult Lung'. *The Journal of Clinical Investigation* 123 (7): 3025–36. https://doi.org/10.1172/JCI68782.

Basil, Maria C., Fabian L. Cardenas-Diaz, Jaymin J. Kathiriya, Michael P. Morley, Justine Carl, Alexis N. Brumwell, Jeremy Katzen, et al. 2022. 'Human Distal Airways Contain a Multipotent Secretory Cell That Can Regenerate Alveoli'. *Nature* 604 (7904): 120–26. https://doi.org/10.1038/s41586-022-04552-0.

Baumgartner, K. B., J. M. Samet, C. A. Stidley, T. V. Colby, and J. A. Waldron. 1997. 'Cigarette Smoking: A Risk Factor for Idiopathic Pulmonary Fibrosis'. *American Journal of Respiratory and Critical Care Medicine* 155 (1): 242–48. https://doi.org/10.1164/ajrccm.155.1.9001319.

Bucher, U., and L. Reid. 1961. 'Development of the Intrasegmental Bronchial Tree: The Pattern of Branching and Development of Cartilage at Various Stages of Intra-Uterine Life'. *Thorax* 16 (3): 207–18. https://doi.org/10.1136/thx.16.3.207.

Chen, Yin, Philip Thai, Yu-Hua Zhao, Ye-Shih Ho, Mary M. DeSouza, and Reen Wu. 2003. 'Stimulation of Airway Mucin Gene Expression by Interleukin (IL)-17 through IL-6 Paracrine/Autocrine Loop'. *The Journal of Biological Chemistry* 278 (19): 17036–43. https://doi.org/10.1074/jbc.M210429200.

Choi, Jinwook, Jong-Eun Park, Georgia Tsagkogeorga, Motoko Yanagita, Bon-Kyoung

Koo, Namshik Han, and Joo-Hyeon Lee. 2020. 'Inflammatory Signals Induce AT2 Cell-Derived Damage-Associated Transient Progenitors That Mediate Alveolar Regeneration'. *Cell Stem Cell* 27 (3): 366-382.e7. https://doi.org/10.1016/j.stem.2020.06.020.

Christenson, Stephanie A., Benjamin M. Smith, Mona Bafadhel, and Nirupama Putcha. 2022. 'Chronic Obstructive Pulmonary Disease'. *Lancet (London, England)* 399 (10342): 2227–42. https://doi.org/10.1016/S0140-6736(22)00470-6.

Ebisudani, Toshiki, Shinya Sugimoto, Kei Haga, Akifumi Mitsuishi, Reiko Takai-Todaka, Masayuki Fujii, Kohta Toshimitsu, et al. 2021. 'Direct Derivation of Human Alveolospheres for SARS-CoV-2 Infection Modeling and Drug Screening'. *Cell Reports* 35 (10): 109218. https://doi.org/10.1016/j.celrep.2021.109218.

El-Hashash, Ahmed H. K., Denise Al Alam, Gianluca Turcatel, Orquidea Rogers, Xue Li, Saverio Bellusci, and David Warburton. 2011. 'Six1 Transcription Factor Is Critical for Coordination of Epithelial, Mesenchymal and Vascular Morphogenesis in the Mammalian Lung'. *Developmental Biology* 353 (2): 242–58. https://doi.org/10.1016/j.ydbio.2011.02.031.

Evans, Christopher M., Tasha E. Fingerlin, Marvin I. Schwarz, David Lynch, Jonathan Kurche, Laura Warg, Ivana V. Yang, and David A. Schwartz. 2016. 'Idiopathic Pulmonary Fibrosis: A Genetic Disease That Involves Mucociliary Dysfunction of the Peripheral Airways'. *Physiological Reviews* 96 (4): 1567–91. https://doi.org/10.1152/physrev.00004.2016.

Federico, Giuseppina, Michael Meister, Daniel Mathow, Gunnar H. Heine, Gerhard Moldenhauer, Zoran V. Popovic, Viola Nordström, et al. 2016. 'Tubular Dickkopf-3 Promotes the Development of Renal Atrophy and Fibrosis'. *JCI Insight* 1 (1): e84916. https://doi.org/10.1172/jci.insight.84916.

Frank, David B., Tien Peng, Jarod A. Zepp, Melinda Snitow, Tiffaney L. Vincent, Ian J. Penkala, Zheng Cui, et al. 2016. 'Emergence of a Wave of Wnt Signaling That Regulates Lung Alveologenesis by Controlling Epithelial Self-Renewal and Differentiation'. *Cell Reports* 17 (9): 2312–25. https://doi.org/10.1016/j.celrep.2016.11.001.

Franks, Teri J., Thomas V. Colby, William D. Travis, Rubin M. Tuder, Herbert Y. Reynolds, Arnold R. Brody, Wellington V. Cardoso, et al. 2008. 'Resident Cellular Components of the Human Lung: Current Knowledge and Goals for Research on Cell Phenotyping and Function'. *Proceedings of the American Thoracic Society* 5 (7): 763–66. https://doi.org/10.1513/pats.200803-025HR.

Guha, Arjun, Aditya Deshpande, Aradhya Jain, Paola Sebastiani, and Wellington V. Cardoso. 2017. 'Uroplakin 3a+ Cells Are a Distinctive Population of Epithelial Progenitors That Contribute to Airway Maintenance and Post-Injury Repair'. *Cell Reports* 19 (2): 246–54. https://doi.org/10.1016/j.celrep.2017.03.051.

H, Katsura, Sontake V, Tata A, Kobayashi Y, Edwards Ce, Heaton Be, Konkimalla A, et al. 2020. 'Human Lung Stem Cell-Based Alveolospheres Provide Insights into SARS-CoV-2-Mediated Interferon Responses and Pneumocyte Dysfunction'. *Cell Stem Cell* 27 (6). https://doi.org/10.1016/j.stem.2020.10.005.

Habermann, Arun C., Austin J. Gutierrez, Linh T. Bui, Stephanie L. Yahn, Nichelle I. Winters, Carla L. Calvi, Lance Peter, et al. 2020. 'Single-Cell RNA Sequencing Reveals Profibrotic Roles of Distinct Epithelial and Mesenchymal Lineages in Pulmonary Fibrosis'. *Science Advances* 6 (28): eaba1972. https://doi.org/10.1126/sciadv.aba1972.

Hancock, Laura A., Corinne E. Hennessy, George M. Solomon, Evgenia Dobrinskikh, Alani Estrella, Naoko Hara, David B. Hill, et al. 2018. 'Muc5b Overexpression Causes Mucociliary Dysfunction and Enhances Lung Fibrosis in Mice'. *Nature Communications* 9 (1): 5363. https://doi.org/10.1038/s41467-018-07768-9.

Hislop, A. A., J. S. Wigglesworth, and R. Desai. 1986. 'Alveolar Development in the Human Fetus and Infant'. *Early Human Development* 13 (1): 1–11. https://doi.org/10.1016/0378-3782(86)90092-7.

Hoffmann, Karen, Benedikt Obermayer, Katja Hönzke, Diana Fatykhova, Zeynep Demir, Anna Löwa, Luiz Gustavo Teixeira Alves, et al. 2022. 'Human Alveolar Progenitors Generate Dual Lineage Bronchioalveolar Organoids'. *Communications Biology* 5 (1): 875. https://doi.org/10.1038/s42003-022-03828-5.

Hogan, Brigid L. M., Christina E. Barkauskas, Harold A. Chapman, Jonathan A. Epstein, Rajan Jain, Connie C. W. Hsia, Laura Niklason, et al. 2014. 'Repair and Regeneration of the Respiratory System: Complexity, Plasticity, and Mechanisms of Lung Stem Cell Function'. *Cell Stem Cell* 15 (2): 123–38. https://doi.org/10.1016/j.stem.2014.07.012.

Horowitz, Jeffrey C., and Victor J. Thannickal. 2006. 'Epithelial-Mesenchymal Interactions in Pulmonary Fibrosis'. *Seminars in Respiratory and Critical Care Medicine* 27 (6): 600–612. https://doi.org/10.1055/s-2006-957332.

Hung, Chi, Geoffrey Linn, Yu-Hua Chow, Akio Kobayashi, Kristen Mittelsteadt, William A. Altemeier, Sina A. Gharib, Lynn M. Schnapp, and Jeremy S. Duffield. 2013. 'Role of Lung Pericytes and Resident Fibroblasts in the Pathogenesis of Pulmonary Fibrosis'. *American Journal of Respiratory and Critical Care Medicine* 188 (7): 820–30. https://doi.org/10.1164/rccm.201212-2297OC.

Irvin, Charles G., and Jason H. T. Bates. 2003. 'Measuring the Lung Function in the Mouse: The Challenge of Size'. *Respiratory Research* 4 (1): 4. https://doi.org/10.1186/rr199.

Jain, Rajan, Christina E. Barkauskas, Norifumi Takeda, Emily J. Bowie, Haig Aghajanian, Qiaohong Wang, Arun Padmanabhan, et al. 2015. 'Plasticity of Hopx(+) Type I Alveolar Cells to Regenerate Type II Cells in the Lung'. *Nature Communications* 6 (April): 6727. https://doi.org/10.1038/ncomms7727.

Kadur, Preetish, Vishwaraj Sontake, Aleksandra Tata, Yoshihiko Kobayashi, Lauren Macadlo, Kenichi Okuda, Ansley S. Conchola, et al. 2022. 'Human Distal Lung Maps and Lineage Hierarchies Reveal a Bipotent Progenitor'. *Nature* 604 (7904): 111–19. https://doi.org/10.1038/s41586-022-04541-3.

Kathiriya, Jaymin J., Chaoqun Wang, Minqi Zhou, Alexis Brumwell, Monica Cassandras, Claude Jourdan Le Saux, Max Cohen, et al. 2022. 'Human Alveolar

Type 2 Epithelium Transdifferentiates into Metaplastic KRT5+ Basal Cells'. *Nature Cell Biology* 24 (1): 10–23. https://doi.org/10.1038/s41556-021-00809-4.

Kim, Geun Ho An, Ji-Young Kim, Roya Rasaei, Woo Jin Kim, Xiong Jin, Dong-Hun Woo, et al. 2021. 'Human Pluripotent Stem-Cell-Derived Alveolar Organoids for Modeling Pulmonary Fibrosis and Drug Testing'. *Cell Death Discovery* 7 (1): 48. https://doi.org/10.1038/s41420-021-00439-7.

Kim, Carla F. Bender, Erica L. Jackson, Amber E. Woolfenden, Sharon Lawrence, Imran Babar, Sinae Vogel, Denise Crowley, Roderick T. Bronson, and Tyler Jacks. 2005. 'Identification of Bronchioalveolar Stem Cells in Normal Lung and Lung Cancer'. *Cell* 121 (6): 823–35. https://doi.org/10.1016/j.cell.2005.03.032.

Kobayashi, Yoshihiko, Aleksandra Tata, Arvind Konkimalla, Hiroaki Katsura, Rebecca F. Lee, Jianhong Ou, Nicholas E. Banovich, Jonathan A. Kropski, and Purushothama Rao Tata. 2020. 'Persistence of a Regeneration-Associated, Transitional Alveolar Epithelial Cell State in Pulmonary Fibrosis'. *Nature Cell Biology* 22 (8): 934–46. https://doi.org/10.1038/s41556-020-0542-8.

Krupnik, V. E., J. D. Sharp, C. Jiang, K. Robison, T. W. Chickering, L. Amaravadi, D. E. Brown, et al. 1999. 'Functional and Structural Diversity of the Human Dickkopf Gene Family'. *Gene* 238 (2): 301–13. https://doi.org/10.1016/s0378-1119(99)00365-0.

Le, Thanh-Thuy T., Harry Karmouty-Quintana, Ernestina Melicoff, Thanh-Truc T. Le, Tingting Weng, Ning-Yuan Chen, Mesias Pedroza, et al. 2014. 'Blockade of IL-6 Trans Signaling Attenuates Pulmonary Fibrosis'. *The Journal of Immunology Author Choice* 193 (7): 3755–68. https://doi.org/10.4049/jimmunol.1302470.

Lederer, David J., and Fernando J. Martinez. 2018. 'Idiopathic Pulmonary Fibrosis'. *The New England Journal of Medicine* 378 (19): 1811–23. https://doi.org/10.1056/NEJMra1705751.

Lee, Jae Ha, Ji Hoon Jang, Jin Han Park, Hang-Jea Jang, Chan Sun Park, Sunggun Lee, Seong-Ho Kim, Ji Yeon Kim, and Hyun Kuk Kim. 2021. 'The Role of Interleukin-6 as a Prognostic Biomarker for Predicting Acute Exacerbation in Interstitial Lung Diseases'. *PLOS ONE* 16 (7): e0255365. https://doi.org/10.1371/journal.pone.0255365.

Lee, J.-P. Myong, H.-R. Kim, C. K. Rhee, H.-K. Yoon, and J.-W. Koo. 2016. 'Incidence and Prevalence of Idiopathic Interstitial Pneumonia and Idiopathic Pulmonary Fibrosis in Korea'. *The International Journal of Tuberculosis and Lung Disease: The Official Journal of the International Union Against Tuberculosis and Lung Disease* 20 (7): 978–84. https://doi.org/10.5588/ijtld.16.0003.

Lee, Tuomas Tammela, Matan Hofree, Jinwook Choi, Nemanja Despot Marjanovic, Seungmin Han, David Canner, et al. 2017. 'Anatomically and Functionally Distinct Lung Mesenchymal Populations Marked by Lgr5 and Lgr6'. *Cell* 170 (6): 1149-1163.e12. https://doi.org/10.1016/j.cell.2017.07.028.

Li, Ksenija Bernau, Nathan Sandbo, Jing Gu, Sebastian Preissl, and Xin Sun. 2018. 'Pdgfra Marks a Cellular Lineage with Distinct Contributions to Myofibroblasts in Lung Maturation and Injury Response'. *ELife* 7 (September): e36865.

https://doi.org/10.7554/eLife.36865.

Li, Feng, Jinxi He, Jun Wei, William C. Cho, and Xiaoming Liu. 2015. 'Diversity of Epithelial Stem Cell Types in Adult Lung'. *Stem Cells International* 2015: 728307. https://doi.org/10.1155/2015/728307.

Liang, Jiurong, Yanli Zhang, Ting Xie, Ningshan Liu, Huaiyong Chen, Yan Geng, Adrianne Kurkciyan, et al. 2016. 'Hyaluronan and TLR4 Promote Surfactant-Protein-C-Positive Alveolar Progenitor Cell Renewal and Prevent Severe Pulmonary Fibrosis in Mice'. *Nature Medicine* 22 (11): 1285–93. https://doi.org/10.1038/nm.4192.

Lipphardt, Mark, Hassan Dihazi, Noo Li Jeon, Sina Dadafarin, Brian B. Ratliff, David W. Rowe, Gerhard A. Müller, and Michael S. Goligorsky. 2019. 'Dickkopf-3 in Aberrant Endothelial Secretome Triggers Renal Fibroblast Activation and Endothelial-Mesenchymal Transition'. *Nephrology, Dialysis, Transplantation: Official Publication of the European Dialysis and Transplant Association - European Renal Association* 34 (1): 49–62. https://doi.org/10.1093/ndt/gfy100.

Liu, Quan-Wen, Yan-Min Ying, Jia-Xin Zhou, Wen-Jie Zhang, Zhao-Xiao Liu, Bing-Bing Jia, Hao-Cheng Gu, et al. 2022. 'Human Amniotic Mesenchymal Stem Cells-Derived IGFBP-3, DKK-3, and DKK-1 Attenuate Liver Fibrosis through Inhibiting Hepatic Stellate Cell Activation by Blocking Wnt/β-Catenin Signaling Pathway in Mice'. *Stem Cell Research & Therapy* 13 (1): 224. https://doi.org/10.1186/s13287-022-02906-z.

Martinez, Fernando J., Harold R. Collard, Annie Pardo, Ganesh Raghu, Luca Richeldi, Moises Selman, Jeffrey J. Swigris, Hiroyuki Taniguchi, and Athol U. Wells. 2017. 'Idiopathic Pulmonary Fibrosis'. *Nature Reviews. Disease Primers* 3 (October): 17074. https://doi.org/10.1038/nrdp.2017.74.

Moeller, Antje, Kjetil Ask, David Warburton, Jack Gauldie, and Martin Kolb. 2008. 'The Bleomycin Animal Model: A Useful Tool to Investigate Treatment Options for Idiopathic Pulmonary Fibrosis?' *The International Journal of Biochemistry & Cell Biology* 40 (3): 362–82. https://doi.org/10.1016/j.biocel.2007.08.011.

Montoro, Daniel T., Adam L. Haber, Moshe Biton, Vladimir Vinarsky, Brian Lin, Susan E. Birket, Feng Yuan, et al. 2018. 'A Revised Airway Epithelial Hierarchy Includes CFTR-Expressing Ionocytes'. *Nature* 560 (7718): 319–24. https://doi.org/10.1038/s41586-018-0393-7.

Morrisey, Edward E., and Brigid L. M. Hogan. 2010. 'Preparing for the First Breath: Genetic and Cellular Mechanisms in Lung Development'. *Developmental Cell* 18 (1): 8–23. https://doi.org/10.1016/j.devcel.2009.12.010.

Mulugeta, Surafel, Shin-Ichi Nureki, and Michael F. Beers. 2015. 'Lost after Translation: Insights from Pulmonary Surfactant for Understanding the Role of Alveolar Epithelial Dysfunction and Cellular Quality Control in Fibrotic Lung Disease'. *American Journal of Physiology. Lung Cellular and Molecular Physiology* 309 (6): L507-525. https://doi.org/10.1152/ajplung.00139.2015.

Nabhan, Ahmad N., Douglas G. Brownfield, Pehr B. Harbury, Mark A. Krasnow, and Tushar J. Desai. 2018. 'Single-Cell Wnt Signaling Niches Maintain Stemness of Alveolar Type 2 Cells'. *Science (New York, N.Y.)* 359 (6380): 1118–23.

https://doi.org/10.1126/science.aam6603.

Nguyen, Hung N., Erika H. Noss, Fumitaka Mizoguchi, Christine Huppertz, Kevin S. Wei, Gerald F. M. Watts, and Michael B. Brenner. 2017. 'Autocrine Loop Involving IL-6 Family Member LIF, LIF Receptor, and STAT4 Drives Sustained Fibroblast Production of Inflammatory Mediators'. *Immunity* 46 (2): 220–32. https://doi.org/10.1016/j.immuni.2017.01.004.

Niehrs, C. 2006. 'Function and Biological Roles of the Dickkopf Family of Wnt Modulators'. *Oncogene* 25 (57): 7469–81. https://doi.org/10.1038/sj.onc.1210054.

Olajuyin, Ayobami Matthew, Xiaoju Zhang, and Hong-Long Ji. 2019. 'Alveolar Type 2 Progenitor Cells for Lung Injury Repair'. *Cell Death Discovery* 5 (1): 1–11. https://doi.org/10.1038/s41420-019-0147-9.

Ong, Hui Xin, Claire L. Jackson, Janice L. Cole, Peter M. Lackie, Daniela Traini, Paul M. Young, Jane Lucas, and Joy Conway. 2016. 'Primary Air-Liquid Interface Culture of Nasal Epithelium for Nasal Drug Delivery'. *Molecular Pharmaceutics* 13 (7): 2242–52. https://doi.org/10.1021/acs.molpharmaceut.5b00852.

Ootani, A., S. Toda, K. Fujimoto, and H. Sugihara. 2000. 'An Air-Liquid Interface Promotes the Differentiation of Gastric Surface Mucous Cells (GSM06) in Culture'. *Biochemical and Biophysical Research Communications* 271 (3): 741–46. https://doi.org/10.1006/bbrc.2000.2673.

Ota, Chiharu, John-Poul Ng-Blichfeldt, Martina Korfei, Hani N. Alsafadi, Mareike Lehmann, Wioletta Skronska-Wasek, Martina M De Santis, Andreas Guenther, Darcy E. Wagner, and Melanie Königshoff. 2018. 'Dynamic Expression of HOPX in Alveolar Epithelial Cells Reflects Injury and Repair during the Progression of Pulmonary Fibrosis'. *Scientific Reports* 8 (1): 12983. https://doi.org/10.1038/s41598-018-31214-x.

Pan, Huaqin, Gail H. Deutsch, Susan E. Wert, Namasivayam Ambalavanan, Charles Ansong, Maryanne E. Ardini-Poleske, Jacqueline Bagwell, et al. 2019. 'Comprehensive Anatomic Ontologies for Lung Development: A Comparison of Alveolar Formation and Maturation within Mouse and Human Lung'. *Journal of Biomedical Semantics* 10 (1): 18. https://doi.org/10.1186/s13326-019-0209-1.

Parekh, Kalpaj R., Janna Nawroth, Albert Pai, Shana M. Busch, Christiana N. Senger, and Amy L. Ryan. 2020. 'Stem Cells and Lung Regeneration'. *American Journal of Physiology. Cell Physiology* 319 (4): C675–93. https://doi.org/10.1152/ajpcell.00036.2020.

Parker, Matthew W., Daniel Rossi, Mark Peterson, Karen Smith, Kristina Sikström, Eric S. White, John E. Connett, Craig A. Henke, Ola Larsson, and Peter B. Bitterman. 2014. 'Fibrotic Extracellular Matrix Activates a Profibrotic Positive Feedback Loop'. *The Journal of Clinical Investigation* 124 (4): 1622–35. https://doi.org/10.1172/JCI71386.

Pedroza, Mesias, Daniel J. Schneider, Harry Karmouty-Quintana, Julie Coote, Stevan Shaw, Rebecca Corrigan, Jose G. Molina, et al. 2011. 'Interleukin-6 Contributes

to Inflammation and Remodeling in a Model of Adenosine Mediated Lung Injury'. *PloS One* 6 (7): e22667. https://doi.org/10.1371/journal.pone.0022667.

Plasschaert, Lindsey W., Rapolas Žilionis, Rayman Choo-Wing, Virginia Savova, Judith Knehr, Guglielmo Roma, Allon M. Klein, and Aron B. Jaffe. 2018. 'A Single-Cell Atlas of the Airway Epithelium Reveals the CFTR-Rich Pulmonary Ionocyte'. *Nature* 560 (7718): 377–81. https://doi.org/10.1038/s41586-018-0394-6.

Rackley, Craig R., and Barry R. Stripp. 2012. 'Building and Maintaining the Epithelium of the Lung'. *The Journal of Clinical Investigation* 122 (8): 2724–30. https://doi.org/10.1172/JCI60519.

Raghu, Ganesh, Harold R. Collard, Jim J. Egan, Fernando J. Martinez, Juergen Behr, Kevin K. Brown, Thomas V. Colby, et al. 2011. 'An Official ATS/ERS/JRS/ALAT Statement: Idiopathic Pulmonary Fibrosis: Evidence-Based Guidelines for Diagnosis and Management'. *American Journal of Respiratory and Critical Care Medicine* 183 (6): 788–824. https://doi.org/10.1164/rccm.2009-040GL.

Reynolds, Susan D., and Alvin M. Malkinson. 2010. 'Clara Cell: Progenitor for the Bronchiolar Epithelium'. *The International Journal of Biochemistry & Cell Biology* 42 (1): 1–4. https://doi.org/10.1016/j.biocel.2009.09.002.

Richeldi, Luca, Harold R. Collard, and Mark G. Jones. 2017. 'Idiopathic Pulmonary Fibrosis'. *Lancet (London, England)* 389 (10082): 1941–52. https://doi.org/10.1016/S0140-6736(17)30866-8.

Rock, Jason R., and Brigid L. M. Hogan. 2011. 'Epithelial Progenitor Cells in Lung Development, Maintenance, Repair, and Disease'. *Annual Review of Cell and Developmental Biology* 27: 493–512. https://doi.org/10.1146/annurev-cellbio-100109-104040.

Rosas, Ivan O., Paul F. Dellaripa, David J. Lederer, Dinesh Khanna, Lisa R. Young, and Fernando J. Martinez. 2014. 'Interstitial Lung Disease: NHLBI Workshop on the Primary Prevention of Chronic Lung Diseases'. *Annals of the American Thoracic Society* 11 Suppl 3 (Suppl 3): S169-177. https://doi.org/10.1513/AnnalsATS.201312-429LD.

Seibold, Max A., Anastasia L. Wise, Marcy C. Speer, Mark P. Steele, Kevin K. Brown, James E. Loyd, Tasha E. Fingerlin, et al. 2011. 'A Common MUC5B Promoter Polymorphism and Pulmonary Fibrosis'. *The New England Journal of Medicine* 364 (16): 1503–12. https://doi.org/10.1056/NEJMoa1013660.

Selman, M., T. E. King, A. Pardo, American Thoracic Society, European Respiratory Society, and American College of Chest Physicians. 2001. 'Idiopathic Pulmonary Fibrosis: Prevailing and Evolving Hypotheses about Its Pathogenesis and Implications for Therapy'. *Annals of Internal Medicine* 134 (2): 136–51. https://doi.org/10.7326/0003-4819-134-2-200101160-00015.

Selman, Moisés, Carlos López-Otín, and Annie Pardo. 2016. 'Age-Driven Developmental Drift in the Pathogenesis of Idiopathic Pulmonary Fibrosis'. *The European Respiratory Journal* 48 (2): 538–52. https://doi.org/10.1183/13993003.00398-2016.

Shiraishi, Kazushige, Shigeyuki Shichino, Satoshi Ueha, Takuya Nakajima, Shinichi Hashimoto, Satoshi Yamazaki, and Kouji Matsushima. 2019. 'Mesenchymal-Epithelial Interactome Analysis Reveals Essential Factors Required for Fibroblast-Free Alveolosphere Formation'. *IScience* 11 (January): 318–33. https://doi.org/10.1016/j.isci.2018.12.022.

Strunz, Maximilian, Lukas M. Simon, Meshal Ansari, Jaymin J. Kathiriya, Ilias Angelidis, Christoph H. Mayr, George Tsidiridis, et al. 2020. 'Alveolar Regeneration through a Krt8+ Transitional Stem Cell State That Persists in Human Lung Fibrosis'. *Nature Communications* 11 (1): 3559. https://doi.org/10.1038/s41467-020-17358-3.

Suezawa, Takahiro, Shuhei Kanagaki, Keita Moriguchi, Atsushi Masui, Kazuhisa Nakao, Masayasu Toyomoto, Koji Tamai, et al. 2021. 'Disease Modeling of Pulmonary Fibrosis Using Human Pluripotent Stem Cell-Derived Alveolar Organoids'. *Stem Cell Reports* 16 (12): 2973–87. https://doi.org/10.1016/j.stemcr.2021.10.015.

Tadokoro, Tomomi, Yang Wang, Larry S. Barak, Yushi Bai, Scott H. Randell, and Brigid L. M. Hogan. 2014. 'IL-6/STAT3 Promotes Regeneration of Airway Ciliated Cells from Basal Stem Cells'. *Proceedings of the National Academy of Sciences of the United States of America* 111 (35): E3641-3649. https://doi.org/10.1073/pnas.1409781111.

Taskar, Varsha S., and David B. Coultas. 2006. 'Is Idiopathic Pulmonary Fibrosis an Environmental Disease?' *Proceedings of the American Thoracic Society* 3 (4): 293–98. https://doi.org/10.1513/pats.200512-131TK.

Tsukui, Tatsuya, Kai-Hui Sun, Joseph B. Wetter, John R. Wilson-Kanamori, Lisa A. Hazelwood, Neil C. Henderson, Taylor S. Adams, et al. 2020. 'Collagen-Producing Lung Cell Atlas Identifies Multiple Subsets with Distinct Localization and Relevance to Fibrosis'. *Nature Communications* 11 (1): 1920. https://doi.org/10.1038/s41467-020-15647-5.

Ushakumary, Mereena George, Matthew Riccetti, and Anne-Karina T. Perl. 2021a. 'Resident Interstitial Lung Fibroblasts and Their Role in Alveolar Stem Cell Niche Development, Homeostasis, Injury, and Regeneration'. *STEM CELLS Translational Medicine* 10 (7): 1021–32. https://doi.org/10.1002/sctm.20-0526.

———. 2021b. 'Resident Interstitial Lung Fibroblasts and Their Role in Alveolar Stem Cell Niche Development, Homeostasis, Injury, and Regeneration'. *Stem Cells Translational Medicine* 10 (7): 1021–32. https://doi.org/10.1002/sctm.20-0526.

Vasilescu, Dragoş M., Zhiyun Gao, Punam K. Saha, Leilei Yin, Ge Wang, Beatrice Haefeli-Bleuer, Matthias Ochs, Ewald R. Weibel, and Eric A. Hoffman. 2012. 'Assessment of Morphometry of Pulmonary Acini in Mouse Lungs by Nondestructive Imaging Using Multiscale Microcomputed Tomography'. *Proceedings of the National Academy of Sciences of the United States of America* 109 (42): 17105–10. https://doi.org/10.1073/pnas.1215112109.

Volckaert, Thomas, Erik Dill, Alice Campbell, Caterina Tiozzo, Susan Majka, Saverio Bellusci, and Stijn P. De Langhe. 2011. 'Parabronchial Smooth Muscle Constitutes an Airway Epithelial Stem Cell Niche in the Mouse Lung after

Injury'. *The Journal of Clinical Investigation* 121 (11): 4409–19. https://doi.org/10.1172/JCI58097.

Waters, David W., Kaj E. C. Blokland, Prabuddha S. Pathinayake, Janette K. Burgess, Steven E. Mutsaers, Cecilia M. Prele, Michael Schuliga, Christopher L. Grainge, and Darryl A. Knight. 2018. 'Fibroblast Senescence in the Pathology of Idiopathic Pulmonary Fibrosis'. *American Journal of Physiology - Lung Cellular and Molecular Physiology* 315 (2): L162–72. https://doi.org/10.1152/ajplung.00037.2018.

Weibel, E. R., and D. M. Gomez. 1962. 'Architecture of the Human Lung. Use of Quantitative Methods Establishes Fundamental Relations between Size and Number of Lung Structures'. *Science (New York, N.Y.)* 137 (3530): 577–85. https://doi.org/10.1126/science.137.3530.577.

Wolf, Lisa, Christian Herr, Julia Niederstraßer, Christoph Beisswenger, and Robert Bals. 2017. 'Receptor for Advanced Glycation Endproducts (RAGE) Maintains Pulmonary Structure and Regulates the Response to Cigarette Smoke'. *PloS One* 12 (7): e0180092. https://doi.org/10.1371/journal.pone.0180092.

Wolf, Lisa, Sandra Sapich, Anja Honecker, Christopher Jungnickel, Frederik Seiler, Markus Bischoff, Bodo Wonnenberg, et al. 2016. 'IL-17A-Mediated Expression of Epithelial IL-17C Promotes Inflammation during Acute Pseudomonas Aeruginosa Pneumonia'. *American Journal of Physiology. Lung Cellular and Molecular Physiology* 311 (5): L1015–22. https://doi.org/10.1152/ajplung.00158.2016.

Wu, Huijuan, and Nan Tang. 2021. 'Stem Cells in Pulmonary Alveolar Regeneration'. *Development (Cambridge, England)* 148 (2): dev193458. https://doi.org/10.1242/dev.193458.

Yu, Wenjie, Xiao Li, Steven Eliason, Miguel Romero-Bustillos, Ryan J. Ries, Huojun Cao, and Brad A. Amendt. 2017. 'Irx1 Regulates Dental Outer Enamel Epithelial and Lung Alveolar Type II Epithelial Differentiation'. *Developmental Biology* 429 (1): 44–55. https://doi.org/10.1016/j.ydbio.2017.07.011.

Zacharias, William J., David B. Frank, Jarod A. Zepp, Michael P. Morley, Farrah A. Alkhaleel, Jun Kong, Su Zhou, Edward Cantu, and Edward E. Morrisey. 2018. 'Regeneration of the Lung Alveolus by an Evolutionarily Conserved Epithelial Progenitor'. *Nature* 555 (7695): 251–55. https://doi.org/10.1038/nature25786.

Zepp, Jarod A., William J. Zacharias, David B. Frank, Christina A. Cavanaugh, Su Zhou, Michael P. Morley, and Edward E. Morrisey. 2017. 'Distinct Mesenchymal Lineages and Niches Promote Epithelial Self-Renewal and Myofibrogenesis in the Lung'. *Cell* 170 (6): 1134-1148.e10. https://doi.org/10.1016/j.cell.2017.07.034.

Zhai, Chun-Gang, Ye-Yang Xu, Yuan-Yuan Tie, Ya Zhang, Wen-Qiang Chen, Xiao-Ping Ji, Yang Mao, et al. 2018. 'DKK3 Overexpression Attenuates Cardiac Hypertrophy and Fibrosis in an Angiotensin-Perfused Animal Model by Regulating the ADAM17/ACE2 and GSK-3β/β-Catenin Pathways'. *Journal of Molecular and Cellular Cardiology* 114 (January): 243–52. https://doi.org/10.1016/j.yjmcc.2017.11.018.

Zhang, Zhen, Kim Newton, Sarah K. Kummerfeld, Joshua Webster, Donald S. Kirkpatrick, Lilian Phu, Jeffrey Eastham-Anderson, et al. 2017. 'Transcription Factor Etv5 Is Essential for the Maintenance of Alveolar Type II Cells'. *Proceedings of the National Academy of Sciences of the United States of America* 114 (15): 3903–8. https://doi.org/10.1073/pnas.1621177114.

Zhou, Yang, Jayasimha N. Murthy, Dewan Zeng, Luiz Belardinelli, and Michael R. Blackburn. 2010. 'Alterations in Adenosine Metabolism and Signaling in Patients with Chronic Obstructive Pulmonary Disease and Idiopathic Pulmonary Fibrosis'. *PloS One* 5 (2): e9224. https://doi.org/10.1371/journal.pone.0009224.

6. LIST OF FIGURES

7. LIST OF TABLES

8. LIST OF PUBLICATIONS

Mutual regulation of transcriptomes between pneumocytes and fibroblasts mediates alveolar regeneration in air-liquid interface cultures

Yao Y, Miethe S, Kattler K, Walter J, Schneider-Daum N, Herr C, Garn H, Ritzmann F, Bals R, Beisswenger C. in review

DKK3 promotes lung fibrosis by modulation of pneumocyte differentiation

Yao Y, Ritzmann F, Herr C, Miethe S, Wyatt A, Scheller A, Garn H, Boehm U, Fliser D, Langer F, Speer T, Beisswenger C, Bals R. in preparation

Patents:

The DKK3 data is part of an ongoing patent process. The data will be published once the patent process has been completed.

Human bronchospheres – A mirror of bronchiolar surfaces?

Yao Y*, Sprott R*, Ritzmann F, Grißmer A, Langer F, Herr C, Meier C, Bals R, Beisswenger C, Tschernig T * contributed equally

Transl. Res. Anat. 26 (2022),100169. DOI: 10.1016/j.tria.2022.100169

Flagellin shifts 3D bronchospheres towards mucus hyperproduction

Ritzmann F, Sprott R, Langer F, Yao Y, Herr C, Kohl Y, Tschernig T, Bals R, Beisswenger C

Respir Res. 2020 Aug 26;21(1):222. DOI: 10.1186/s12931-020-01486-x.

Exosomal circPACRGL promotes progression of colorectal cancer via the miR-142-3p/miR-506-3p- TGF-β1 axis

Shang A, Gu C, Wang W, Wang X, Sun J, Zeng B, Chen C, Chang W, Ping Y, Ji P, Wu J, Quan W, Yao Y, Zhou Y, Sun Z, Li D

Mol. Cancer 2020, 19, 117. DOI: 10.1186/s12943-020-01235-0

PLAC8 inhibits oral squamous cell carcinogenesis and epithelial-mesenchymal transition via the Wnt/β-catenin and PI3K/Akt/GSK3β signalling pathways

Wu J, Wang X, Shang A, Vella G, Sun Z, Ji P, Yang D, Wan A, Yao Y[#], Li D[#]

[#] contributed equally

Oncology Letters, 2020,20(5):1-1. DOI: 10.3892/ol.2020.11989

9. CONFERENCE PAPERS

Oral presentations

Fibroblasts drive the differentiation of murine pneumocytes in air-liquid interface cultures

Program of the Herbsttagung of the German Respiratory Society (DGP) Section Cell Biology, Hannover (2021)

Fibroblasts drive the differentiation of murine pneumocytes in air-liquid interface cultures

Congress of the German Society for Pneumology and Respiratory Medicine, Leipzig (2022)

Poster

Single cell analysis of murine lung epithelial cells cultured in air-liquid interface cultures

Congress of the German Society for Pneumology and Respiratory Medicine, Marburg (2022)

10. ACKNOWLEDGEMENTS

I would like to thank my supervisor Prof. Dr. Dr. Robert Bals for giving me this opportunity to start and finish my PhD in his working group, where I spent a wonderful 4 years and was well supervised.

I would also like to thank Prof. Dr. Christoph Beisswenger for his excellent scientific guidance in the completion of this work and for his multifaceted support on every conceivable issue.

In addition, I would like to thank all the current and former members of our awesome laboratory, especially those who have been by my side almost from day one. Thank you to Dr. Felix Ritzmann, Dr. Christian Herr, Dr. Mariza Bortolanza, Dr. Giovanna Vella, Anja Honecker, Andreas Kamyschnikow, Victoria Weinhold, Susanne Reinhold, Michelle Brand, Isabell Theisohn, Chunmao Wang for the wonderful atmosphere and the good cooperation.

I also have to thank all the new friends I have made in Homburg, Qing Liu, Qinghua Luo, Wenqiang Quan, Xiaoyu Cai, Anqi sheng, Xianshu Bai, Renping Zhao, Lipao Fang, Qilin Guo…...thank you for your company over the last 4 years, it has enriched my life.

The biggest thanks go to my parents. Without your support it would not have been possible.

I thank the Academy.

11. CURRICULUM VITAE

The curriculum vitae was removed from the electronic version of the doctoral thesis for reasons of data protection.